IMPROVING THE PERFORMANCE OF SUPERABSORBENT POLYMERS AS INTERNAL CURING AGENTS IN CONCRETE: EFFECTS OF NOVEL COMPOSITE HYDROGELS ON MICROSTRUCTURE AND HYDRATION OF CEMENTITIOUS SYSTEMS

by

Baishakhi Bose

A Dissertation

Submitted to the Faculty of Purdue University

In Partial Fulfillment of the Requirements for the degree of

Doctor of Philosophy

School of Materials Engineering

West Lafayette, Indiana

August 2021

THE PURDUE UNIVERSITY GRADUATE SCHOOL

STATEMENT OF COMMITTEE APPROVAL

Dr. Kendra A. Erk, Chair

School of Materials Engineering

Dr. John A. Howarter

School of Materials Engineering

Dr. Jan Olek

School of Civil Engineering

Dr. Jeffrey P. Youngblood

School of Materials Engineering

Approved by:

Dr. David F. Bahr

To Baba and Ma

ACKNOWLEDGMENTS

First, I would like to express my gratitude towards my advisor, Professor. Kendra Erk, who has not only taught me the technical aspects of research in these past years, but also provided continuous support for my professional growth. Her patience and conviction in me are what helped me achieve the big and small milestones in my PhD. journey. My graduate school experience was truly an all-encompassing fulfilling one thanks to her.

I am fortunate to have gotten various opportunities to interact with my committee outside of my research projects. I am grateful to Prof. Howarter for providing me with the opportunity to be a part of the SURF program, which offered me with multitudes of avenues to grow as a mentor. The SURF program provided me with a platform to develop my leadership skills and this would not have been possible without Prof. Howarter. I am thankful to Prof. Youngblood for always supporting me in whatever aspects that needed his guidance during my role as a TGA superuser at the Soft Materials Characterization lab. I am also grateful to Prof. Olek for always providing me with time whenever I wanted his feedback on my research. Also, the knowledge I gathered from his courses were immensely helpful in conducing my research.

I am also grateful to all the Soft Materials Mechanics group members: Dr. Matt Krafcik, Dr. Travis Thornell, Dr. Anna Walter, Dr. Jerome Nash, Dr. Eduard Caicedo-Casso, Dr. Jessica Sargent, Dr. Cole Davis, Ryan Szeto, and Caitlin Adams, for their willingness to help me in my journey in the world of polymer science. I would also like to thank all the undergraduates who worked with me and provided me with an opportunity to mentor and learn with them (Zuha, Edwin, Jonathan, Ethan, Lauren, Pattiya). Thanks to Dr. Matt Korey, Dr. Reza Moini and Dr. Raikhan Tokpatayeva for always being there whenever I needed guidance. I would also like to thank Robert Hershberger for his assistance and acknowledge Pankow Lab in the Lyles School of Civil Engineering for the use of the facilities. Thanks to the friends I made at Bangladesh Students Association and the women I got to work with at the Women in Engineering Program, and the graduate assistants I worked with in the SURF team who all made these past few years memorable. My sincere gratitude to Darshini Render, who has provided me with advice and support that gave me the confidence to not just to carry out my responsibilities at the SURF program, but also pursue my professional goals. I am forever grateful to her and Prof. Howarter for all the beautiful

memories I have of the SURF program and the opportunities to meet and work with collaborating partners at various departments at Purdue.

Last, but not the least, this journey would not have been possible without my family's support. I would like to thank my husband, Dr. Shoumya Nandy Shuvo, who introduced me to the world of materials engineering. Thank you for being a patient listener and always encouraging my professional and personal growth. Lastly, I would like to thank my parents, without whose immense support and sacrifices throughout the years, this milestone would not have been possible. My mother's quiet confidence in me, and my father's unrelenting support in everything I do provided me with the confidence to pursue this journey. Thank you for always having my back.

TABLE OF CONTENTS

LIST OF TABLES 9
LIST OF FIGURES 10
SYMBOLS 14
ABBREVIATIONS 15
ABSTRACT 17
1. INTRODUCTION 19
1.1 High performance concrete 19
1.2 Internal curing in concrete 20
1.3 Use of superabsorbent polymers to internally cure concrete 20
1.4 Composite silica-containing polyacrylamide hydrogels as internal curing agents 23
1.5 Composite retarding admixture-containing polyacrylamide hydrogels 24
1.6 Internal curing of conventional concrete 26
2. MATERIALS AND METHODOLOGY 28
2.1 Study on composite silica-containing polyacrylamide as internal curing agents 28
2.1.1 Silica characterization 30
2.1.2 Composite silica-containing hydrogels synthesis 31
2.1.3 Creation and characterization of composite silica-containing polyacrylamide hydrogels 33
Scanning Electron Microscopy of synthesized hydrogels 34
Thermogravimetric analysis of synthesized hydrogels 34
Gravimetric absorption tests of synthesized hydrogels 34
2.1.4 Batch mixing of cement paste 35
2.1.5 Characterization of cement paste 37
Density and Absorption of Cement Paste 37
Non-evaporable water content of cement paste 38
Backscattered electron microscopy of cement paste 39
Compressive strength of cement paste 40
Thermogravimetric analysis of cement paste 41
Electrical resistivity of cement paste 41

Isothermal calorimetry of cement paste 41
2.1.6 Batch mixing of mortar 42
2.1.7 Characterization of mortar 43
Compressive and flexural strength of mortar 43
Autogenous shrinkage of mortar 44
2.2 Study on composite retardation admixture containing polyacrylamide 45
2.2.1 Creation and characterization of composite retarding admixture-containing polyacrylamide hydrogels 45
Fourier-Transform Infrared Spectroscopy (FTIR) of synthesized hydrogels 47
2.2.2 Batch mixing and characterization of cement paste 48
2.3 Study on commercial SAPs to inform the design of internally cured concrete bridge decks and pavement patches 49
2.3.1 Characterization of SAP 50
2.3.2 Batch mixing of mortar and cement paste 51
2.3.3 Characterization of cement paste and mortar 52
Isothermal calorimetry of cement paste 52
Non-evaporable water content of cement paste 53
Autogenous shrinkage of mortar 53
Backscattered electron microscopy of cement paste and mortar 53
3. CHARACTERIZATION OF COMPOSITE SILICA-CONTAINING HYDROGEL PARTICLES 55
3.1 Microstructural analysis of hydrogel particles 55
3.2 Thermogravimetric analysis of hydrogel particles 56
3.3 Absorption capacity of hydrogel particles 58
4. INFLUENCE OF COMPOSITE SILICA-CONTAINING POLYACRYLAMIDE HYDROGEL ON CEMENTITIOUS SYSTEMS 61
4.1 Specific gravity and absorption of cement paste 61
4.2 Non-evaporable water content of cement paste 62
4.3 Microstructural Analysis 63
4.4 Compressive strength of cement paste 72
4.5 Thermogravimetric Analysis 78

4.6 Electrical Resistivity of Cement Paste 79
4.7 Isothermal Calorimetry of Cement Paste 81
4.8 Compressive and Flexural Strength of Mortar 84
4.9 Autogenous shrinkage of mortar 88
4.10 Conclusion 89
5. INFLUENCE OF COMPOSITE RETARDING ADMIXTURE- CONTAINING HYDROGEL PARTICLES ON CEMENTITIOUS SYSTEMS 92
5.1 Characterization of composite retarding admixture-containing hydrogel particles 92
5.1.1 Absorption capacity of hydrogel particles 92
5.1.2 Thermogravimetric analysis of hydrogel particles 93
5.1.3 FTIR analysis of hydrogel particles 95
5.2 Isothermal calorimetry of cement paste containing composite hydrogel particles 97
5.3 Conclusion 102
6. EARLY AGE PERFORMANCE OF COMMERCIALLY AVAILABLE SAPS IN CEMENTITIOUS MATERIALS 103
6.1 Characterization of SAP particles 103
6.2 Characterization of mortar 105
6.2.1 Autogenous shrinkage of mortar 105
6.2.2 Backscattered electron microscopy of mortar 107
6.3 Characterization of cement paste 109
6.3.1 Isothermal calorimetry analysis 109
6.3.2 Non-evaporable water content 114
6.3.3 Backscattered electron microscopy 115
6.4 Conclusion 118
REFERENCES 119

LIST OF TABLES

Table 1: Zeta potential measurements of SF and NS. 31

Table 2: Hydrogel compositions for composite Si-containing hydrogel study. 32

Table 3: Properties of the cement used for Si-containing hydrogel study. 36

Table 4: Mixture proportions for cement pastes (WRA in % by weight of cement). 37

Table 5: Mixture proportions for mortar (WRA in % by weight of cement). 43

Table 6: Hydrogel compositions for composite retarding admixture-containing polyacrylamide hydrogel synthesis. 46

Table 7: Mixture proportions for cement pastes for retardation admixture containing hydrogel study. 49

Table 8: Composition of the ordinary Portland cement and slag used in this study. 50

Table 9: Composition of mortar mixtures. 51

Table 10: Mixture proportions for cement pastes. 52

Table 11: Average size of composite silica-containing hydrogels. 55

Table 12: Average maximum length of SAP-induced voids from cement paste microstructure analysis. 67

Table 13: Impact of crosslink density decrease on hydration product growth in hydrogel-induced voids, void size, and 28 days compressive strength. 76

LIST OF FIGURES

Figure 1: Two-dimensional slice of concrete mixture containing hydrogel particles and cement grains: (a) immediately after concrete mixing and placement; (b) after a few minutes to hours (before final setting of cement) when the hydrogel particle has swollen to its maximum capacity; and (c) after a few days when substantial amount of cement is hydrated, and the hydrogel particles have partially deswollen. 21

Figure 2: A schematic representations (not to scale) of the hydrogel particles in dry and hydrated state in (a) macroscale; (b) nanoscale at a high crosslink density without the presence of silica; (c) nanoscale at a low crosslink density without the presence of silica; and (d) with silica particles confined within the network of a low crosslink density particle. 29

Figure 3: XRD pattern of the (a) silica fume (SF) (b) nanosilica (NS) used in this study. 30

Figure 4: Synthesized dry hydrogel particles for composite Si-containing hydrogel study. Each vial contains 1.10 ± 0.01 g. 34

Figure 5: Calculation of area fraction of hydrated product growth in hydrogel-induced void using ImageJ. (a) A deswollen hydrogel void. (b) Hydrogel void showing the perimeter of the void and hydrated products deposition/growth. (c) Separate outline of each area of hydration product growth within the hydrogel void. 40

Figure 6: Micrograph of cement paste with hydrogel particle void. (a) Deswollen hydrogel void. (b) Relevant features of the hydrogel voids highlighted. (c) Measured maximum diameter of the hydrogel particle. 40

Figure 7: Experimental setup used for determination of (a) compressive strength and (b) flexural strength. 44

Figure 8: Synthesized dry hydrogel particles for the composite retarding admixture-containing polyacrylamide study. 47

Figure 9: Chemical structure of (a) acrylamide, (b) citric acid and (c) sucrose showing the functional group present in the structures. 48

Figure 10. Scanning electron micrograph of (a) SF-10-2, and (b) NS-10-2, showing the angular morphology of the hydrogel particles. 56

Figure 11: Thermogravimetric analysis of polyacrylamide hydrogel particles with a crosslinker dosage of 2% by weight of monomer. 57

Figure 12: Thermogravimetric analysis of polyacrylamide hydrogel particles with a crosslinker dosage of 0.5% by weight of monomer. 57

Figure 13. Absorption capacity of hydrogel particles as a function of immersion time in RO water. 59

Figure 14. Absorption capacity of hydrogel particles as a function of immersion time in pore solution. 59

Figure 15: Absorption capacity of hydrogel particles as a function of immersion time in pore solution from 1 minute to 3 days. 60

Figure 16: Oven dry (OD) specific gravity and absorption of cement paste samples at 7 and 28 days. For clarity, hatched bars and cross-hatched bars represent samples containing low crosslink density hydrogel particles and high crosslink density hydrogel particles, respectively. 62

Figure 17: Non-evaporable water content (Wn) of the cement pastes at 28 days. For clarity, hatched bars represent samples containing low crosslink density hydrogel particles and cross-hatched bars represent samples containing high crosslink density hydrogel particles. 63

Figure 18: Microstructure analysis of pastes cured with high crosslink density hydrogel particles. (a) (c) and (e) Area of hydrogel particle voids filled with hydration products as a function of cement paste composition. Micrographs (3-day cured) of hydrogel particle voids in cement paste internally cured with (b) C.35-AM-2 with 35% of the void filled, (d) SF-10-2 with 89% of the void filled, and (f) NS-10-2 with 93% of the void filled. 64

Figure 19: Microstructure analysis of pastes cured with low crosslink density hydrogel particles. (a) (c) and (e) Area of hydrogel particle voids filled with hydration products as a function of cement paste composition. Micrographs (3-day cured) of hydrogel particle voids in cement paste internally cured with (b) C.35-AM-0.5 with 40% of the void filled, (d) SF-10-0.5 with 80% of the void filled, and (f) NS-10-0.5 with 89% of the upper-right hand corner void filled. 65

Figure 20: Maximum Diameter of Hydrogel-induced voids as a function of cement paste composition. 3 days aged cement paste internally cured with (a) C.35-AM-2 and C.35-AM-0.5, (b) SF-10-2 and SF-10-0.5, (c) NS-10-2 and NS-10-0.5 were used for analysis and plotting the histogram. Arrows show the average maximum diameter of 30 imaged voids for that particular sample. 66

Figure 21: (a) Micrograph of cement paste with the hydrogel-induced voids contained significant growth of hydrated product, obscuring the original dimensions of the swollen hydrogel particles. (b) Visible edges of the hydrogel-induced voids were marked off and the diameter in several directions were measured to obtain the maximum diameter. 68

Figure 22: Compressive strength of cement pastes at various ages. (a) Control pastes at different w/c without hydrogel particles; (b) pastes internally cured with high crosslink density hydrogel particles; and (c) pastes internally cured with low crosslink density hydrogel particles. 75

Figure 23: Compressive strength of cement pastes at various ages internally cured with 0.5% crosslinked hydrogel particles of different size ranges: "-75" denotes dry particles within 45-75 μm and "-114" denotes dry particles within 75-114 μm. 77

Figure 24: Calcium hydroxide content (%) of cement paste at 7 and 28 days. For clarity, cross-hatched bars represent samples containing high crosslink density hydrogel particles and hatched bars represent samples containing low crosslink density hydrogel particles. 78

Figure 25: Variation of electrical resistivity of cement paste samples with the age of the sample. 80

Figure 26: Hydration heat release rate from cement paste (24 hours) with composite silica-containing polyacrylamide hydrogel. For clarity, dashed lines represent cement paste with low

crosslinked hydrogel particles while solid lines represent cement paste with high crosslinked hydrogel particles. For easier visualization, the first 6 hours after mixing are zoomed in. 82

Figure 27: Cumulative heat of cement paste (48 hours) with composite silica-containing polyacrylamide hydrogel. For clarity, blue and red dashed curves represent cement paste with low crosslinked hydrogel particles while solid blue and red curves represent cement paste with high crosslinked hydrogel particles..... 84

Figure 28: Compressive strength of mortar at 1, 7 and 28 days. The hatched bars denote mortars with composite silica-containing polyacrylamide hydrogel particles. The pink and green bars denote mortars with hydrogel particles with a crosslink density of 0.5% and 2% by weight of monomer, respectively. 85

Figure 29: Flexural strength of mortar at 1 and 28 days. The hatched bars denote mortar containing composite silica-containing polyacrylamide hydrogel particles. The pink and green bars denote mortars with hydrogel particles with a crosslink density of 0.5% and 2% by weight of monomer, respectively. 87

Figure 30: Autogenous shrinkage of mortar internally cured with composite Si-containing hydrogel particles. 89

Figure 31: Absorption capacity of hydrogel particles as a function of immersion time in RO water. 93

Figure 32: Thermogravimetric analysis of composite retarding admixture-containing hydrogel particles. 95

Figure 33: FTIR spectra of synthesized hydrogel particles. Black arrows show peaks due to functional groups associated with acrylamides. Teal and pink arrows show peaks due to the presence of functional groups characteristic of CA and sucrose, respectively.. 96

Figure 34: Isothermal calorimetry of cement paste showing the effect of CA and PAM (a) Hydration heat release rate (until 24 hours) and (b) cumulative heat (until 72 hours). 98

Figure 35: Isothermal calorimetry of cement paste showing the effect of sucrose and PAM (a) Hydration heat release rate (until 24 hours) and (b) cumulative heat (until 72 hours). 101

Figure 36: SEM images of the (a) LA and (b) HA dry SAP particles used in the experiments. 103

Figure 37: Absorption capacity of (a) LA and (b) HA SAP particles as a function of immersion time in pore solution. For clarity, square, triangle, and round symbols denote Buzzi Unicem, Lehigh and St. Mary's Type I cement, respectively. Absorption capacity of the LA and HA SAP particles are plotted using dashed and dotted lines, respectively..... 104

Figure 38: Autogenous shrinkage of Buzzi Type I and Type III mortars with a w/c of 0.42. For easier visualization of the Type I mortars, the right-side plot is zoomed in. 106

Figure 39: Autogenous shrinkage of Buzzi Type I mortars with a w/c of 0.35. 107

Figure 40: Representative SEM images of 28-day mortar samples (w/c 0.42): (a) B Type I_No SAP_0.5_0.42, (b) B Type I_LA_0.5_0.42, (c) B Type I_HA_0.5_0.42. The arrows in (a) indicate

microcracks formed in the matrix of the mortar. The red outlines in in (b) and (c) indicate the outer edges of deswollen SAP particles. 108

Figure 41: SEM image of a SAP-induced void in 28-day mortar sample B Type I_HA_0.5_0.42 (a) with two spots highlighted for EDX analysis (1 and 2); (b) the SAP void outlined in red and the portlandite growth inside the void highlighted in cyan. 109

Figure 42: Isothermal calorimetry analysis of cement paste showing the effect of Type I and Type III cement from the same source on (a) heat flow (24 hours) and (b) total heat (72 hours). 110

Figure 43: Isothermal calorimetry analysis of cement paste showing the effect of three different sources of Type I cement on (a) heat flow (24 hours) and (b) total heat (72 hours). 112

Figure 44: Isothermal calorimetry analysis of cement paste showing the effect of partial replacement of cement by slag on (a) heat flow (24 hours) and (b) total heat (72 hours). 113

Figure 45: Isothermal calorimetry analysis of cement paste showing the effect of WRA on cement paste (a) heat flow (24 hours) and (b) total heat (72 hours)..... 114

Figure 46: Non-evaporable water content (Wn) of the cement pastes at 7 days at a w/c of 0.42. For clarity, hatched bars represent samples containing HA SAP particles and cross-hatched bars represent samples containing LA SAP particles. 115

Figure 47: Microstructure analysis of 7-days old pastes cured with LA and HA SAP particles. Buzzi Type I cement was used for (a), (c) and (e), while St. Mary's Type I cement was used for (b), (d) and (f). Scale bar in each micrograph represents 400 µm. 4% and 83% of the SAP voids are filled with hydration products in (c) and (d), respectively, while 14% and 18% of the SAP void are filled with hydration products in the upper-right SAP voids in (e) and (f), respectively. 116

Figure 48: Microstructure analysis of pastes cured with LA and HA SAP particles. (a) and (b) Area of SAP particle voids filled with hydration products as a function of cement paste composition. 117

SYMBOLS

ε	Linear strain
L	liter
M	Molar concentrations
Q	Swelling Ratio
T	Temperature
W_n	Non-evaporable water content

ABBREVIATIONS

ACI	American Concrete Institute
AM	Acrylamide
ASTM	American Society for Testing and Materials
BSE	Backscattered Electron
bwoc	by weight of cement
C	Calcium oxide (lime) (CaO)
C_2S	Dicalcium silicate ($2CaO \cdot SiO_2$)
C_3S	Tricalcium silicate ($3CaO \cdot SiO_2$)
CA	Citric acid ($C_6H_8O_7$)
CH	Calcium hydroxide ($Ca(OH)_2$)
C-S-H	Calcium silicate hydrate
DI	Deionized
FTIR	Fourier-Transform Infrared Spectroscopy
HPC	High performance concrete
LOI	Loss On Ignition
MBAM	N,N'-methylenebisacrylamide
mL	Milliliters
NaOH	Sodium hydroxide
NaS_2O_5	Sodium metabisulfate

NaS_2O_8	Sodium persulfate
NS	Nanosilica
OD	Oven dry
OPC	Ordinary Portland cement
PAA	Poly(acrylic acid)
PAM	Polyacrylamide
RH	Relative Humidity
RO	Reverse osmosis
rpm	Rotations per minute
S	Silica (SiO_2)
SAP	Superabsorbent polymers
SCM	Supplementary Cementitious Materials
SEM	Scanning Electron Microscopy
SF	Silica Fume
SSD	Saturated surface dry
TDS	Total Dissolved Solids
TGA	Thermogravimetric Analysis
w/c	water-to-cement ratio
WRA	Water Reducing Admixture
XRD	X-ray diffraction

ABSTRACT

Superabsorbent polymer (SAP) hydrogel particles have been used as internal curing agents in concrete mixes as they are capable of absorbing and subsequently releasing large amounts of water. This reduces autogenous shrinkage during early stages of hydration. The size, shape, and composition of the hydrogel particles can be controlled during the synthesis, hence providing the opportunity to custom synthesize these internal curing agents to elicit desired structure-property relationships. Utilization of optimized dosage and formulation of SAP has the potential to improve the microstructure, durability, and strength of internally cured concrete.

The first study focuses on the synthesis and application of novel composite hydrogel particles as internal curing agents in cementitious mixes. Composite polyacrylamide hydrogel particles containing two different amorphous silica–either nanosilica or silica fume–were used to investigate whether the internal curing performance of hydrogel particles could be enhanced. The dosage and type of silica, crosslinker amount were varied to identify the composite polyacrylamide hydrogel particle composition that provides optimum benefits to internally cured cementitious systems. The synthesized hydrogels were characterized by means of absorption capacity tests, compositional and size analysis. The beneficial impacts of the addition of composite hydrogels on cement paste microstructure are highlighted, including the preferential formation of cement hydration products (such as portlandite) within the hydrogel-induced voids that appeared to be influenced by the composition of the hydrogel particles. The interrelationship between extent of hydration, size of hydrogel voids, and void-filling with hydration products was found to strongly influence mechanical strength and is thus an important structure-property relationship to consider when selecting hydrogels for internal curing purposes. This study informs the design of composite hydrogel particles to optimize performance in cementitious mixes. Additionally, it provides a novel means of incorporating other commonly used admixtures in concrete without facing common challenges related to dispersion and health hazards.

The second study focuses on the utilization of two retarding admixture-citric acid and sucrose-to custom synthesize composite polyacrylamides to investigate whether the composite hydrogels could delay hydration of cement paste. Isothermal calorimetry analysis results showed that composite sucrose-containing polyacrylamide hydrogel particles were successfully able to retard main hydration peak of cement paste, beyond the retardation capabilities of the pure

polyacrylamide hydrogels. Thus, this study provides avenues of exploring the utilization of common admixtures to formulate novel composite hydrogels that imparts specific properties to cementitious systems.

In another study, SAP formulated by admixture industries were used to investigate the feasibility of internal curing of bridge decks and pavement patches with SAP particles. The microstructure and early age hydration properties of SAP-cured cementitious systems were studied. Mitigation of microcracks in the matrix, along with portlandite growth in SAP voids, were observed in SAP-cured mortars. Presence of SAP also mitigated autogenous shrinkage and improved early age hydration as observed by isothermal calorimetry analysis. This thesis highlights some of the beneficial impacts of SAP-cured cementitious systems, and the potential to harness those benefits in large-scale applications of SAP-cured concrete.

1. INTRODUCTION

The following chapter contains text and a figure adapted with permission from Kendra A. Erk and Baishakhi Bose, "Using Polymer Science to Improve Concrete: Superabsorbent Polymer Hydrogels in Highly Alkaline Environments" in *Gels and Other Soft Amorphous Solids*, American Chemical Society Symposium Series - Vol. 1296, 333-356. Copyright 2018. American Chemical Society. https://doi.org/10.1021/bk-2018-1296.ch017.

1.1 High performance concrete

Concrete, the largest volume building material in use worldwide, is produced at levels twice that of steel, aluminum, and wood combined; and due to its versatility, accessibility, low price and high durability, it provides shelter for an estimated 70% of the world's population [1], [2]. Compared to other building materials, including steel, it possesses high compressive strength and excellent resistance to corrosive fluids, assuring its ubiquity in construction for long into the future. However, conventional concrete can be easily adulterated, leading to poor quality mixtures subject to shrinkage and cracks as well as structures requiring frequent repair and replacement. Indeed, the amazing devastation following the 7.0-magnitude earthquake in Haiti in 2010 was directly linked to the poor quality concrete used for housing and other buildings [3]. In addition, the frequent repair and replacement required for conventional concrete has a significant environmental impact, as concrete production accounts for 8% of global CO_2 emissions [4],[5]. The growing demand for concrete with better quality in terms of strength and durability while ensuring low carbon footprint has led to the development of high performance concrete (HPC).

HPC has a very dense microstructure to ensure an optimum particle packing and a water-cement ratio so low that all the water is consumed during the hydration reaction (*i.e.*, cement curing) [6]. The dense microstructure engenders a strong and durable structure [7] with reduced impact on the environment [8]. The main disadvantage of HPC is the autogenous (volumetric) shrinkage that is encountered during the early stages of curing, eventually resulting in the formation of cracks, increased porosity, and an overall reduction in strength [9]. Shrinkage increases in magnitude as result of incomplete hydration of cement due to the scarcity of water[10],[11]. to fuel curing, causing the mixture to self-desiccate. A compressive stress develops in the system, driven by the negative capillary pressure within the aqueous fluid in the mixture (termed "pore fluid") and ultimately leading to collapse of the cement structure [10],[12]. The lack of water inside the system

can be offset by use of internal curing agents that effectively replenish the water reservoir from inside the mixture and aid in cement hydration.

1.2 Internal curing in concrete

Previous researchers have reported attainment of higher degrees of hydration, reduced shrinkage and cracking potentials when internally curing cementitious systems, as compared to traditional curing regimes [13]. These advantages make internal curing a practical means of improving the long-term performance of concrete infrastructures. Two common methods of internal curing of concrete includes the use of lightweight aggregate (LWA) and superabsorbent polymers (SAP). LWA poses some challenges in its practical implementation. At least 20% of the fine aggregate needs to be replaced by LWA [14]. Furthermore, prewetting of the aggregates is necessary before it is used in concrete production, which introduces variability in total water content of the mix [15]. Another source of variability in field implementation of LWA is that the length of prewetting is variable and can take up to 48 hours [14], [16]. In general, the process of LWA prewetting is vulnerable to inconsistencies in implementation, leading to unpredictable values of the total water to binder ratios (w/b).

Superabsorbent polymer (SAP) hydrogel particles provide an effective method of internal curing[10], [17]–[19] because the hydrogel particles can absorb and release large amounts of water to fuel the hydration reaction [20]. Compared to LWA, SAPs are required in very low dosages (0.2% by weight of binder) and can be used in their dry form without any pre-wetting. Although presoaking of SAP can yield better workability, addition of SAP in dry state ensures better dispersion of the SAP particles in the cementitious matrix [21]. Additionally, it is possible to control the chemical composition, size and shape of the SAP particles used for internal curing. This provides an exciting opportunity to fine-tune the chemistry of the SAP particles to meet the criteria of their intended target performance as internal curing agents in cementitious systems.

1.3 Use of superabsorbent polymers to internally cure concrete

As mentioned above, HPC is prone to self-desiccation and shrinkage [9], [22], due to the low water-to-cement (w/c) ratio used in its production. To mitigate the scarcity of water in HPC, SAP particles have been successfully used in previous research as internal curing agents [10], [17],

[20], [23], [24]. SAPs can absorb large amounts of water during mixing of concrete and release the water as the concrete ages, facilitating hydration reactions. Use of SAPs has been proven to be effective in preventing self-desiccation [10], mitigating autogenous shrinkage [17], [25]–[29], sealing cracks [30]–[32], improving resistance to freeze-thaw attack [33],[34], improving the microstructure [35] from the additional hydration, thereby enhancing strength and durability of the concrete.

Figure 1 is an illustration of the phenomena occurring in concrete containing hydrogel particles from the time it is cast to the time when the cement has reasonably hardened. As hydrogel is used to ensure proper hydration of the cement matrix, the interaction between the cement paste and hydrogel particles is of primal significance; the coarse aggregate and fine aggregate have been omitted for the sake of simplicity. Also, it is presumed that a similar process of hydration would occur in mortar and concrete samples.

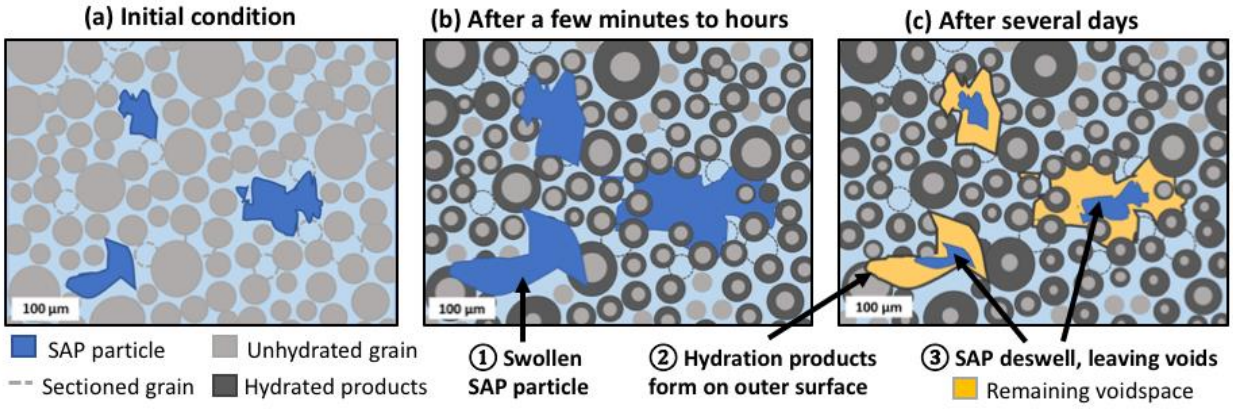

Figure 1: Two-dimensional slice of concrete mixture containing hydrogel particles and cement grains: (a) immediately after concrete mixing and placement; (b) after a few minutes to hours (before final setting of cement) when the hydrogel particle has swollen to its maximum capacity; and (c) after a few days when substantial amount of cement is hydrated, and the hydrogel particles have partially deswollen.

Initially, the cement grains start to hydrate from the water available in the mixture, causing the hydration products to form an outer layer on the grains (illustrated in Figure 1b). This causes a retardation in the process of hydration as the unhydrated core of the cement grains will have reduced access to water. Meanwhile, the hydrogel particles begin to swell and increase in volume, also drawing water available within the mixture (see Figure 1b). As the cement curing proceeds,

water is extracted from the hydrogel particles to fuel the hydration reactions, driven by osmotic pressure gradients in the system and facilitated by the formation of capillary networks in the cement matrix. Eventually the hydrogel particles deswell (as shown in Figure 1c) from a combination of two factors: the extraction of water by the cement paste and the intrusion of cations from the pore solution into the polymer network. Even after a few days (or years, for some types of cement), hydration reactions are still incomplete, and there are always some unreacted cement grains in the cement paste (C_2S takes a long time to undergo hydrolysis).

It is possible that the cement grains in close vicinity to the hydrogel particles may undergo faster and greater amounts of hydration than those further away, especially if there is an inhomogeneity in the dispersion of the hydrogel particles throughout the cement paste. Over time, hydration products form on the outer surfaces of the voids that remain from the deswelled hydrogel particles. Since the hydration reactions of C_3S start immediately after water is added to the dry cement grains, it would take a few minutes to hours for the hydration products to form. Meanwhile, depending on the composition of the hydrogel particles and the availability of water, it might take a few minutes to hours to reach its maximum absorption capacity. The deswelling of the hydrogel particles leaves behind voids in the hardened cement paste, which can aid in enhancing the durability, density and freeze-thaw resistance in concrete [36].

The introduction of SAPs into concrete introduces its own sets of challenges. The dosing and size of the hydrogel-based particles must be carefully monitored to ensure that the mechanical strength of the bulk concrete is not compromised by large voids left behind by the dehydrated SAPs. Furthermore, the rheological properties of fresh mortar are governed by the chemical structure of the SAPs [37]. The timing of water release is also of paramount importance: desorption during the acceleration period of the cement paste aids in mitigating autogenous shrinkage and improvement in hydration [38].

Additionally, SAPs are not chemically inert. SAPs used in cementitious composites are primarily composed of poly(acrylic acid-acrylamide) [37], [39], [40]. Multivalent cations – which are abundant in the alkaline pore solution of freshly mixed concrete – have been shown to induce rapid dehydration (deswelling) of swollen hydrogel particles [18],[20],[41],[42]. In particular, complete collapse of polymer networks comprised primarily of acrylic acid (sodium acrylate) has been observed [25], as the carboxylic acid groups in these networks become anionic in alkaline environments and able to complex with free cations [43]. Thus, SAPs containing acrylic acid are

prone to premature water release in cementitious environments, potentially causing an increase in effective w/c and decreasing the compressive strength of mortar [19]. Desorption of acrylic acid-rich SAPs has been observed in previous studies to occur within few minutes in free swelling experiments [25] and reduces the effectiveness of the internal curing if it occurs during the dormant period.

By determining these key structure-property-performance relationships through careful experimental study, the chemical composition of the hydrogel network can be successfully designed to create hydrogel particles that have a desired sorption behavior and can trigger the growth of specific inorganic phases within cement microstructure, leading to the development of next-generation high performance concrete materials.

1.4 Composite silica-containing polyacrylamide hydrogels as internal curing agents

Considering the sensitivity of acrylic acid to pore solution composition, the first part of this dissertation focuses on acrylamide-based hydrogel particles which are not strongly ionized in alkaline environments and thus are expected to display more desirable, stable swelling behavior in cementitious mixtures. Acrylamide-rich SAPs have previously been shown to be more resistant to changes in pore solution chemistry [44] and have also displayed inorganic phase growth within the voids which remained in the cement microstructure after SAP dehydration [35][45]. This "void-filling" phenomenon was even more pronounced for hydrogel particles containing only acrylamide [46]. Also, a greater percentage of acrylamide in the hydrogel was observed to promote adhesion to the cement matrix, which further appeared to facilitate desorption of the hydrogel particles due to capillary effects [47], [48].

Supplementary cementitious materials (SCMs) have recently grown in popularity as a strategy to reduce the carbon footprint caused by the cement industry while improving the strength and durability of HPC. Both silica fume (SF) [49], [50] and nanosilica (NS) [51]–[53] have been used for partial replacement of cement or in conjunction with cement as binder material in cement-composites. In addition to fostering pozzolanic reactions, NS also acts as a filler material to improve microstructure [54]. The high surface area of NS promotes nucleation of calcium silicate hydrate (C-S-H) [55], which presumably leads to higher compressive strengths. However, there are some issues when incorporating these fine-grained SCMs into cement-composites. For example, particles are subject to agglomeration at higher dosages and may reduce mixture

workability [55]. Additionally, the fineness of the particles may create inhalation hazards during processing and exacerbate respiratory issues in workers, although amorphous silica has not been conclusively proven to cause pulmonary sicknesses [56].

Several research studies have been conducted previously in presence of both SAP particles and silica (in the form of NS or SF) to improve performance of internally cured cementitious systems[57]–[61]. Mechanical strength of SAP-cured mortar containing NS was comparable to reference mortar without SAP [62]–[64]. Another study showed that inclusion of SAP reduced shrinkage when added to concrete containing NS, while maintaining slump [65]. Addition of SAP to SF-containing mixes showed that autogenous shrinkage was effectively reduced and more than half of the volume of SAP-induced voids were filled with portlandite [66]. It is important to note that in these previous studies, SAP and silica were separately incorporated into the cementitious mixtures; as described here, the present study investigates the effects of directly combining SAP and silica.

A novel method of incorporating amorphous NS into poly(acrylic acid-acrylamide) hydrogel particles to form a "composite" hydrogel has already been reported by Erk and Krafcik et al. [67][68]. Cement pastes internally cured with acrylamide-rich composite hydrogels particles displayed greater growth of hydration products in SAP-induced voids compared with pastes containing conventional (silica-free) SAPs as well as those containing acrylic acid-rich composite hydrogel particles. Another study conducted by Davis et al. showed that the absorption capacity and the growth of products inside SAP-induced voids can be enhanced by decreasing the crosslink density of the polyacrylamide particle [46]. Thus, polyacrylamide-silica composite hydrogel particles appear to have an advantage over conventional SAPs by promoting pozzolanic reactions in vicinity of the SAP-induced voids while continuing to facilitate internal curing. Also, as the NS is physically confined within the polymer network during synthesis of the composite hydrogel, NS inhalation risks during concrete batching and casting are expected to be minimized.

1.5 Composite retarding admixture-containing polyacrylamide hydrogels

The second part of this dissertation focuses on creation and characterization of the performance of novel composite hydrogel particles incorporating a retarding admixture. This work is intended to provide alternative composite hydrogel formulations by custom design of SAP particles to better suit the needs of niche applications.

Retarders are a type of chemical admixtures used in cementitious systems to increase the amount of time the mixture is workable. This allows for longer transportation time, placing and finishing of concrete. In presence of organic retarders, an increased level of CH supersaturation and lengthening of the induction period has been observed [69], thereby successfully delaying hydration of cementitious systems. Sucrose is a common admixture that is used as a retarder in Portland cement hydration, while citric acid is also used for the same purpose in specific applications [70].

Several studies have used sucrose in the past to investigate its impact on retardation of cement hydration [71]–[75]. When compared to other sugars, sucrose has been reported to have greater retarding effect [76], with the retardation effect prevalent for up to several months [73]. The greater retarding effect when compared to other sugars had been attributed to the fact that the disaccharide structure of sucrose lends itself with capabilities of stronger stearic hinderance [77]. The mechanism by which sucrose impacts cement hydration is not yet fully understood. Researchers have postulated that sucrose poisons the nucleation sites for hydration products growth [70], [73]. As dissolution of cement continues, number of nucleation sites increases, which eventually outnumbers the sucrose molecules available to poison the sites. This causes a spurt in hydration reactions after the retardation period, which is attributed to the increased calcium ion concentration in the pore solution [73].

Citric acid influences the retardation by delaying the dissolution of the clinker grains. Potassium ion from pore solution forms complexes with the citrate, thereby precipitating potassium citrate on the clinker surface, which forms a protective barrier that delays further dissolution [78]. It is also possible that, that the citrate ions could form complexes with calcium ion from pore solution, thus precipitating calcium citrate, and removing calcium ions from the system. Zuo et al. showed that although citric acid retards the early stages of hydration, it accelerates the later stages [79]. Singh et al. reported that low dosage of citric acid could cause an acceleration of the hydration reactions since at smaller concentrations, the dispersion effect is more dominant than the poisoning of nucleation sites due to citrate adsorption [80]. This has interesting implications for the use of citric acid in the composite hydrogel synthesis since optimizing the dosage of citric acid in the synthesis procedure would be necessary to ensure retardation effect is significant. Previous research studies conducted on cementitious systems in the presence of both SAP particles and citric acid have shown that presence of citric acid (CA) improves the efficiency

of SAP in mortar macro-crack healing [81]. Thus, addition of citric acid could provide additional benefits to the composite hydrogel performance, other than delaying hydration of cement paste.

To the author's knowledge, no previous attempt has been made to incorporate citric acid or sucrose directly within polyacrylamide hydrogel synthesis procedure for the intended purpose of internal curing of cementitious systems. However, in a previous study, synthesis of citric acid/acrylamide copolymeric hydrogel was conducted using gamma irradiation method, in the absence of an initiator and a crosslinking agent [82]. In the current study, solution polymerization method was utilized to synthesize polyacrylamide hydrogels in the presence of initiators and crosslinking agents; and the retarding admixture (citric acid or sucrose) was directly incorporated in the polyacrylamide hydrogel synthesis procedure. The findings from this present study can be utilized in places where elevated temperature, longer transportation distances or placement times might warrant the use of hydrogels that contribute towards retardation of cement hydration.

1.6 Internal curing of conventional concrete

The benefits of utilization of SAP in concrete has been shown in several studies conducted in research laboratories worldwide [10], [17], [20], [23]–[29], [30]–[35]. Such studies have fueled the interest of admixture companies and construction industry in the United States to utilize SAP to harness its potential benefits in bridge and pavement construction. As such, the third part of this dissertation focuses on the utilization of SAPs provided by admixture industries to internally cure cement paste and investigate its microstructural and hydration properties.

The introduction of SAP as an additive in concrete allows for numerous possibilities since the uptake and release of water and thus the hydration and local microstructural development can be influenced by controlling the SAP composition. However, one of the reason for limited practical implementation of SAP in construction is that most studies involving SAP only investigated concrete mixtures with a low (0.15 to 0.35) w/c values [19], [35], [37], [43], [66], [67]. This is because SAP has been found to be efficient in mitigating autogenous shrinkage [10], [26], [28], [83], which is most prevalent in water-starved concrete systems. Few studies have focused on the use of SAP in mixtures with w/c of 0.42 or higher [23]. The present study focuses on the utilization of SAPs formulated by two different admixture companies to internally cure cementitious systems at a w/c of 0.42. The microstructure and hydration of the cement paste internally cured with the SAPs were studied. Findings from this study can be utilized in the future to develop

recommendations to identify suitable SAP formulations for internally cured concrete bridge decks and pavement patches.

2. MATERIALS AND METHODOLOGY

Select figures and text in the following chapter have been adapted with permissions from Baishakhi Bose, Cole R. Davis, Kendra A. Erk, "Microstructural refinement of cement paste internally cured by polyacrylamide composite hydrogel particles containing silica fume and nanosilica," Cement and Concrete Research, Volume 143, 2021, 106400, ISSN 0008-8846, https://doi.org/10.1016/j.cemconres.2021.106400.

2.1 Study on composite silica-containing polyacrylamide as internal curing agents

The goal of this study was to measure the effect of dosage and type of silica and the crosslink density of the polyacrylamide network on the performance of polyacrylamide composite hydrogel particles as internal curing agents. Two types of amorphous silica (SiO_2) were chosen for this study – NS and SF – keeping in mind the most common SCMs used in the concrete industry. Each different type of hydrogel was synthesized at two different crosslink densities. Figure 2 shows a schematic of the polyacrylamide network with and without silica particles, with a relatively high and low density of crosslinks before and after hydration. The absorption behavior of composite hydrogel particles was characterized using gravimetric absorption tests. Experiments were then performed on cement paste internally cured by composite hydrogel particles to determine the impact on hydration density, porosity, inorganic phase development, and compressive strength. Furthermore, experiments were performed on mortar to see if the autogenous shrinkage could be mitigated without compromising the compressive and flexural strength of mortar.

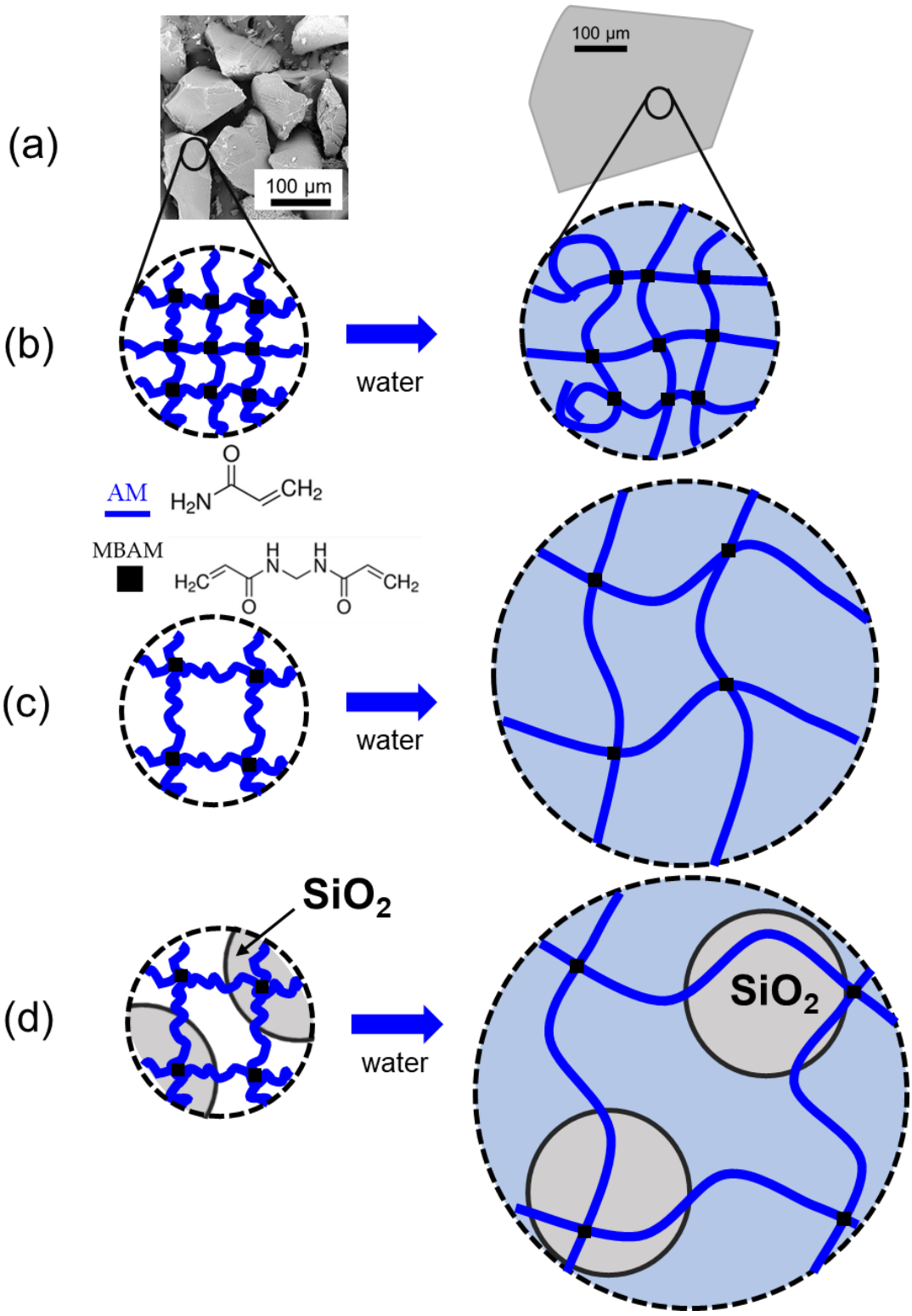

Figure 2: A schematic representations (not to scale) of the hydrogel particles in dry and hydrated state in (a) macroscale; (b) nanoscale at a high crosslink density without the presence of silica; (c) nanoscale at a low crosslink density without the presence of silica; and (d) with silica particles confined within the network of a low crosslink density particle.

2.1.1 Silica characterization

Two sources of amorphous silicon dioxide (SiO_2; silica) were utilized in this study. Silica nanoparticles (NS) with a reported diameter of 60-70 nm were purchased from U.S. Research Nanomaterials, Inc. (Houston, TX). Silica fume (SF) with a reported diameter of 150 nm was purchased from Norchem, Inc. (Beverly, OH). X-ray diffraction (XRD) was performed on the as-received SF and NS particles using a Siemens D500 diffractometer (30 mA, 50 kV) at 0.02°/s scanning rate in (10–40)° 2θ range (Siemens AG, Germany). Samples were prepared by loosely packing the silica particles into a metal sample holder pressed to a paper surface in order to avoid preferential orientation of the particles.

As shown in

Figure 3, the XRD patterns indicated that both NS and SF are highly amorphous as the overall intensity of the signal was extremely low with a broad reflex, centered at about 22°. For SF, a peak at 2θ ~ 35.5° was obtained due to the presence of silica carbide [84]. Crystalline silica would have given a pattern with two high-intensity peaks about the 2θ at 20.8° and 26.6°, respectively [85].

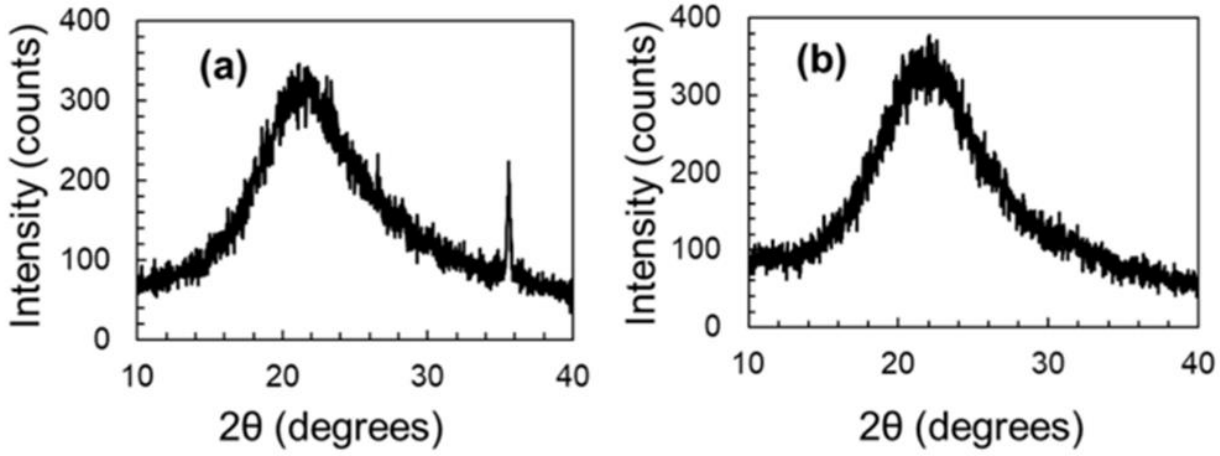

Figure 3: XRD pattern of the (a) silica fume (SF) (b) nanosilica (NS) used in this study.

A Zetasizer Nano ZS (Malvern Instruments, Malvern, United Kingdom) was used to measure the zeta potential of dilute suspensions of silica dispersed in deionized (DI) water. For each type of silica, two samples were created at different values of pH, 7.1 ± 0.1 and 9.8 ± 0.1, through the progressive addition of a 2M NaOH solution and measured with an electronic pH

meter. Measurements at pH > 10 were not possible with the existing Zetasizer configuration. Silica particles were added to the solution at a concentration of 0.1 wt.%, sonicated with a Branson Digital sonicator at 25% amplitude for 2 minutes, and allowed to equilibrate at 25°C for 6.5 hours prior to testing. Three measurements were performed for each sample and averaged to report the zeta potential.

The zeta potential measurements are given in Table 1. These results suggest that the amorphous silica particles have a negative surface charge due to the dissociation of terminal silanol groups and subsequent formation of surface hydroxyl (-OH) groups [86]. Also, the zeta potential values indicated that both forms of silica will be stable at the highly alkaline pH that is usually common in cementitious mixtures as aqueous dispersions with zeta potentials less than -30mV are considered to be stable [87].

Table 1: Zeta potential measurements of SF and NS.

Form of silica	pH	Zeta Potential (mV)
Silica Fume (SF)	7.1 ± 0.1	- 28.6 ± 0.7
	9.8 ± 0.1	- 41.3 ± 0.6
Nanosilica (NS)	7.1 ± 0.1	- 26.1 ± 2.4
	9.8 ± 0.1	- 41.6 ± 1.4

2.1.2 Composite silica-containing hydrogels synthesis

Hydrogel particles were synthesized following the solution polymerization method. Acrylamide (AM, monomer), N,N'-methylenebisacrylamide (MBAM, crosslinker), sodium metabisulfate (NaS_2O_5), sodium persulfate (NaS_2O_8), were all purchased from Sigma-Aldrich (St. Louis, MO) and used without further purification. Deionized (DI) water used for the synthesis of hydrogels was collected from a Barnstead Nanopure Infinity system (Barnstead Thermolyne Corporation, Ramsey, MN). DI water used had a resistivity of >18 Mohm cm.

Crosslinking solutions were prepared by adding 0.3 g of MBAM to 20 mL of DI water. Initiator solutions were prepared by adding 0.3g of NaS_2O_5 and NaS_2O_8 to 10 mL of DI water, separately (initiator dosage was fixed at 1% by monomer weight). Fresh batches of crosslinking and initiator solutions were prepared for each batch of hydrogel synthesis. The reagents used and their proportion in each variation of hydrogel are summarized in Table 2. Two dosages of silica and crosslinker were investigated: a silica dosage of 1 and 10% by weight of monomer and

crosslinker dosage of 0.5 and 2% by weight of monomer. In Table 2, composite hydrogels are labelled as "X-Y-Z" to indicate composition, where "X" is either NS or SF, "Y" is the dosage of silica (1 or 10), and "Z" is the dosage of crosslinker (0.5 or 2).

Table 2: Hydrogel compositions for composite Si-containing hydrogel study.

Hydrogel	**AM (g)**	**Water (mL)**	**Crosslinking Solution (mL)**	**Silica (g)**
AM-2	3.0	7.0	4.0	-
SF-1-2	3.0	7.0	4.0	0.030
SF-10-2	3.0	7.0	4.0	0.300
NS-1-2	3.0	7.0	4.0	0.030
NS-10-2	3.0	7.0	4.0	0.300
AM-0.5	3.0	7.0	1.0	-
SF-10-0.5	3.0	7.0	1.0	0.300
NS-10-0.5	3.0	7.0	1.0	0.300

The hydrogel synthesis was adapted from Krafcik et al. [67]. To minimize the absorption of water on the silica, particles were placed inside 20 mL glass scintillation vials, covered with aluminum foil, and kept in a vacuum oven at 23°C for 8 hours. Particles were then stored in a desiccator prior to use. The required amount of water and silica (as per dosage requirement, see Table 2) were added to a centrifuge tube and ultrasonication was performed to disperse the particles. A Branson Digital sonicator equipped with a tapered microtip for low volumes (3 mm tip for 1-10 mL, Sigma-Aldrich) was used to sonicate the suspensions at 35% amplitude for 2 minutes and then at 40% amplitude for 3 minutes.

The hydrogel synthesis reaction was conducted in 20 mL glass scintillation vials. The water-silica suspensions were added to the vials first. AM monomer and the prepared crosslinking (MBAM) solution in required amount (see Table 2) was added to the vials and stirred for 5 minutes. Then, 0.5 mL of each of the freshly prepared initiator solutions were added to the vial, and the vial was capped and placed in a temperature-controlled oil bath set at 60°C until gelation was observed (typically within 10 minutes). It is worth mentioning that following the current procedure for hydrogel synthesis, attempt to increase the dosage of silica beyond 10% by weight of monomer prevented gelation (sample-spanning percolation of the polymer network, [88]) from occurring.

Following gelation, the reaction product – a bulk hydrogel – was removed from the vial and immersed in DI water for 24 hours at 23°C to remove any unreacted reagents. The hydrogels containing silica differed in appearance compared with the silica-free hydrogels. Hydrogels containing NS were more opaque compared to pure AM hydrogels while hydrogels containing SF were shades of grey, with the intensity of grey increasing with SF dosage. TDS measurements of the DI "wash" water were nearly identical before and after hydrogel immersion. This, along with the variation in color of the synthesized hydrogels, provides evidence of the silica being physically confined in the polymer network even when hydrogels were swollen and immersed in fresh water. Also, no visible sedimentation of silica aggregates was observed in the synthesis vials or wash beakers.

2.1.3 Creation and characterization of composite silica-containing polyacrylamide hydrogels

Bulk hydrogels were dried in an oven at 80 ± 1°C for 10 hours and then ground into first a coarse powder using an electric grinder and then into finer particle size using a mortar and pestle. Hydrogel particles were then sieved into different size fractions by vibrating a set of standard ASTM sieves on a mechanical vibrator table for 30 minutes at 1725 rpm. Particles retained on the sieves with mesh size of 45, 75, and 114 μm were added to a scintillation vial in equal weight proportions, mixed, and then capped to form a representative sample of each hydrogel type with particle size ranging from 45 to 150 μm. To prevent any moisture uptake from the atmosphere, the vials of representative samples were kept sealed under laboratory conditions at 23°C, away from direct exposure to sunlight or moisture. This representative sample of hydrogel particle size was used for all the tests in this study except select compressive strength of cement paste using different sized hydrogels. The synthesized hydrogel particles in their dry form are shown in Figure 4. The synthesized hydrogels were characterized using scanning electron microscopy, thermogravimetric analysis, and gravimetric absorption tests.

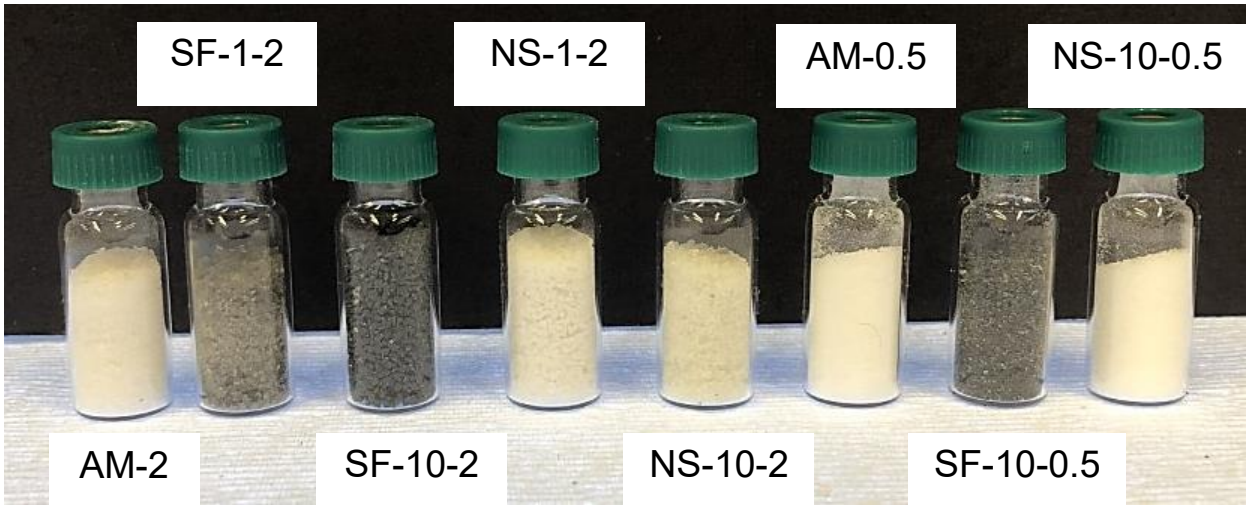

Figure 4: Synthesized dry hydrogel particles for composite Si-containing hydrogel study. Each vial contains 1.10 ± 0.01 g.

Scanning Electron Microscopy of synthesized hydrogels

Hydrogel particles were imaged using a NanoScience Instruments Phenom Desktop scanning electron microscope (Thermo Fisher Scientific, Waltham, MA), (uncoated sample, 15 kV).

Thermogravimetric analysis of synthesized hydrogels

A 2050 Thermogravimetric Analyzer manufactured by TA Instruments (New Castle, DE) was utilized to study the degradation of the synthesized hydrogels. A small amount of representative sample of 6 ± 1 mg hydrogel particles was placed in a platinum crucible and studied under nitrogen atmosphere at a heating rate of 10°C/min.

Gravimetric absorption tests of synthesized hydrogels

The tea-bag method [89],[90] was employed to quantify the absorption capacity of the hydrogel particles in both reverse osmosis (RO) water and pore solution. Previous researchers have used synthetic or extracted pore solution to characterize absorption behavior of SAPs [25], [91], [92]. SAP absorption capacity studied using tea-bag tests have been found to be an overestimation

of the amount of water that would be absorbed when placed in cement mixes [93][94], however it serves as a simple, reproducible test to estimate the absorption capacity of SAPs.

In this study, pore solution was prepared by adding tap water to cement at a water-to-cement ratio of 10 and stirring, covered, for 4 hours. The solution was poured through a Büchner funnel under vacuum with a 589/3 Whatman filter paper (diameter of 150 mm) to remove the cement particles. The filtered solution was kept covered in a plastic container to minimize carbonation effects. Fresh pore solution was prepared for each batch of gravimetric absorption tests.

For both solutions (RO and pore solution), 200 mL of liquid was added to a beaker and a teabag was fully immersed into the solution for 30 seconds. The teabag was allowed to drip dry and then weighed to obtain the wet mass of the bag, m_{bag}. Then, 0.2 g of dry hydrogel particles (m_{dry}) were added to the wet teabag. The teabag was then immersed into the solution and removed at regular time intervals for weighing (m_{wet}). In the case of pore solution, the beakers were covered with aluminum foil in between measurements to minimize carbonation. Absorption tests were conducted in triplicate. The swelling ratio, Q (grams of absorbed fluid per grams of dry hydrogel particles), was calculated using the following formula:

$$Q = \frac{m_{wet} - m_{bag} - m_{dry}}{m_{dry}}$$

2.1.4 Batch mixing of cement paste

Ordinary Type I Portland cement (ASTM C150) obtained from Buzzi Unicem (Greencastle, IN) was used. This was the first batch of Buzzi Unicem cement used for this dissertation and the properties of the cement from the manufacturer's mill certificate are reported in Table 3 which varies slightly from the second batch of Buzzi Unicem that was used in subsequent studies (see Table 8). Mixture proportions for the mixing of cement paste are given in Table 4. Tap water was used for mixing and the admixture used was Glenium 3030 NS full-range water reducer (WRA) supplied by BASF (Cleveland, Ohio). Hydrogel dosage (0.2% by weight of cement) and WRA amount were kept constant (see Table 4).

Five control samples (denoted as "C.XX" in Table 4) were investigated for the compressive strength study. The first three control samples, C.35, C.35-AM-2 and C.35-AM-0.5, have w/c of

0.35, the same w/c that was used for all pastes internally cured with composite hydrogel particles. The other two controls, C.30 and C.40, were created to provide upper and lower bounds of comparison with the internally cured pastes. These bounds were chosen based on the maximum equilibrium absorption capacity that was observed in this study for NS-10-0.5 sample. Some researchers will add extra "curing" water to SAP-containing mixtures (e.g., 5%) to maintain mixture workability [42]. Here, no additional "curing" water was added to the mixture and given the relatively low absorption capacity of acrylamide-based SAPs observed at 24 hours compared with commercial SAPs, there was no detectible change in workability of mixtures with and without hydrogel particles.

Table 3: Properties of the cement used for Si-containing hydrogel study.

		wt. (%)
Oxide Composition	SiO_2	19.58
	Al_2O_3	5.17
	Fe_2O_3	2.84
	CaO	63.78
	MgO	2.40
	Na_2O	0.70*
	K_2O	--
	SO_3	3.06
Phase Composition	C_3S	58.1
	C_2S	7.7
	C_3A	8.2
	C_4AF	8.0
Blaine Fineness (m^2/kg)	--	381

*Reported as Na_2O equivalent in the mill certificate.

Table 4: Mixture proportions for cement pastes (WRA in % by weight of cement).

Sample Name	Cement (g)	Water (g)	Hydrogel particles (g)	WRA (%)
C.35	100	35	--	0.70
C.35-AM-2	100	35	0.2	0.70
C.35-AM-0.5	100	35	0.2	0.70
C.30	100	30	--	0.70
C.40	100	40	--	0.70
SF-1-2	100	35	0.2 [a]	0.70
SF-10-2	100	35	0.2 [b]	0.70
NS-1-2	100	35	0.2 [a]	0.70
NS-10-2	100	35	0.2 [b]	0.70
SF-10-0.5	100	35	0.2 [b]	0.70
NS-10-0.5	100	35	0.2 [b]	0.70

[a] containing 0.0004% silica by weight of cement
[b] containing 0.004% silica by weight of cement

Dry cement and dry hydrogel particles (if applicable) were added to a mixing cup and hand mixed for 30 seconds. Water and WRA were added simultaneously, and the mixture was hand-mixed for 60 seconds, scraped from the sides of the container, allowed to rest for 30 seconds, and then mixed for another 60 seconds before pouring into cylindrical molds each of 1" diameter and 2" height. The molds used for this study were developed by Davis et al.[46]. Molds were sealed and kept in an environmental chamber at 23 ± 0.1°C and 50% relative humidity for 24 hours. The paste samples were then demolded and stored in the environmental chamber (23 ± 0.1°C and 50% relative humidity) until testing. Samples utilized for electrical resistivity tests were placed in saturated lime water until testing after demolding. Care was taken to ensure that the level of saturated lime water remained constant for the duration of test period.

2.1.5 Characterization of cement paste

Density and Absorption of Cement Paste

Density measurements were conducted on cement paste samples to evaluate if the voids left behind by the hydrogel particles introduced significant porosity so as to affect bulk density. After the 7- and 28-day compressive strength tests, pieces from the paste sample were collected to conduct density measurements. The specimens (3 for each cement paste sample) were dried in an

oven for 3 days at 110 ± 5 °C until constant mass was obtained. The specimens were immersed in DI water at temperature of 23 ± 1°C for 24 ± 4 hours. Specimens were then dried on a large piece of absorbent cloth and the mass of each specimen was measured (in saturated surface dry condition, (*B*)). The specimens were again immersed in water and its apparent mass measured, (*C*). The specimens were dried in the oven for 24 hours at 110 ± 5 °C and the oven dried mass was measured (*A*). The oven dried (OD) specific gravity and the absorption (in percentage) in terms of *A*, *B* and *C* are given by the following equations:

$$Oven\ dried\ specific\ gravity = \frac{A}{(B - C)}$$

$$Absorption\ (\%) = \frac{(B - A)}{A}\ x\ 100$$

Non-evaporable water content of cement paste

Internal curing water held by SAPs may increase the degree of hydration [95]. This test is a commonly used method to provide an indication of the hydration of cementitious materials [96]. A small piece from the 28-day cement paste sample (cast and stored in the manner described in Section 2.1.4) was immersed in isopropanol for 24 hours, ground and sieved using a sieve with mesh size of 250 µm. About 3 g of the ground cement paste was dried for 24 h in an oven at 105°C. Then, the samples were ignited in a muffle furnace at 1050°C for 3 h. The mass of the samples was measured using a balance with a 0.0001 g resolution and was used to calculate the non-evaporable water content using the following equation:

$$W_n = \frac{m_{105} - m_{1050}}{m_{1050}} - LOI$$

where W_n is the non-evaporable water content (g/g cement paste), m_{105} is the dry mass (g), m_{1050} is the ignited mass (g), and *LOI* is the loss on ignition of cement, which is 2.19% according to the mill certificate provided by the manufacturer. The test was run in triplicate and average values were reported.

Backscattered electron microscopy of cement paste

Cement paste prepared using the method described in Section 2.1.4 were used for electron microscopy imaging. Microstructure analysis was performed on 3 days old cement paste. Cured cylinders were immersed in isopropanol for 24 hours to stop hydration, cut into manageable pieces with a diamond saw, vacuum dried for 72 hours at (23 ± 5) °C, and then vacuum impregnated with epoxy. The epoxy coated cement paste samples were then dried at (60 ± 5) °C for 48 hours. Then, a fresh section of each epoxy coated sample was exposed by cutting with a diamond saw and polished. The samples were then carbon coated and imaged using a NanoScience Instruments Phenom Desktop SEM. At least 30 random hydrogel particles' voids were imaged for further microstructural analysis using ImageJ to quantify the portions of the hydrogel particles' voids filled with some product of hydration. Details regarding the procedure implemented to calculate area fraction of the hydrogel void filled with hydration products can be found in Figure 5. The perimeter of the void was first marked to find the total area of the void and the shaded regions (Figure 5b) shown demonstrates the areas where hydrated products have deposited/grown. Each area with product growth was separately marked off at the perimeter (Figure 5c) and the area within was calculated, totaled, and divided by the total area of the void from Figure 5(b) to obtain the area fraction of the hydrated product growth in the hydrogel particle void. 30 such hydrogel particle voids were analyzed for each type of internally cured cement paste composition.

The largest diameter for 30 voids within select paste samples was also measured to compare the hydrogel-induced void size between different cement paste samples. Figure 6 illustrates the maximum diameter calculation process from a micrograph of a hydrogel void that is labeled with all the relevant features: original dimension of the hydrogel at the time of set, open void space, dehydrated hydrogel, and hydration product growth. Figure 6(a) shows the microstructure features within the local vicinity of the void clearly indicated the dimensions of the original swollen hydrogel particles, including visible cracks marked by the arrow. In Figure 6(b), open void space, layers of dehydrated hydrogel and hydration product growth/deposit inside the void are highlighted along with the perimeter of the original swollen hydrogel particle at the time of set.

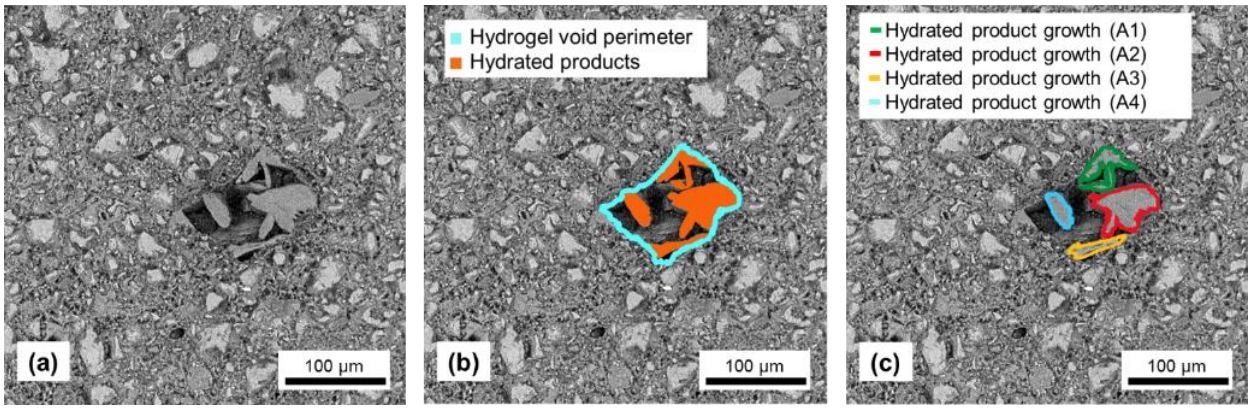

Figure 5: Calculation of area fraction of hydrated product growth in hydrogel-induced void using ImageJ. (a) A deswollen hydrogel void. (b) Hydrogel void showing the perimeter of the void and hydrated products deposition/growth. (c) Separate outline of each area of hydration product growth within the hydrogel void.

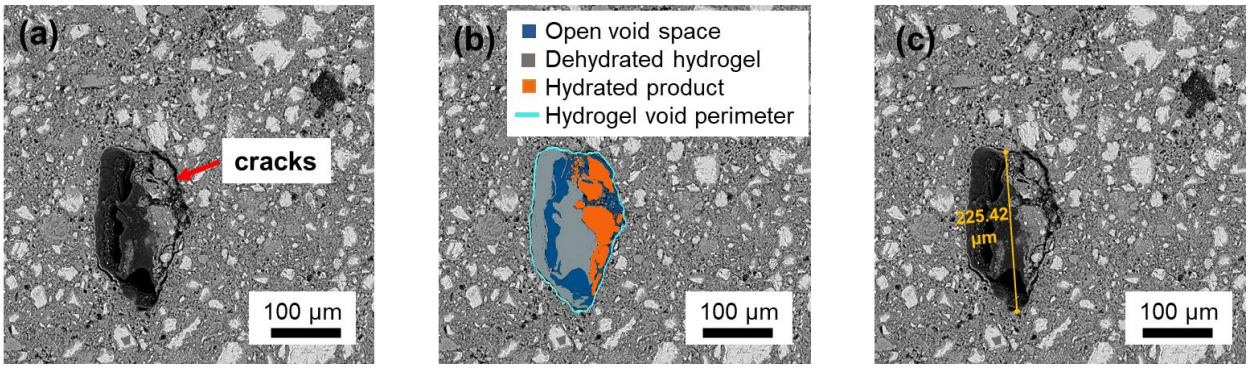

Figure 6: Micrograph of cement paste with hydrogel particle void. (a) Deswollen hydrogel void. (b) Relevant features of the hydrogel voids highlighted. (c) Measured maximum diameter of the hydrogel particle.

Compressive strength of cement paste

Compressive strength tests of cement paste were conducted on cement paste samples aged 3, 7, and 28 days using an Insight 820.300-SL machine with a load capacity of 300 kN (MTS Systems Corp., Eden Prairie, MN) at a constant strain rate of 1 mm/min. For each sample, three specimens were tested and the average compressive strength along with the standard deviation were calculated.

Thermogravimetric analysis of cement paste

Cement paste samples were used to quantify content of calcium hydroxide (CH) in 7- and 28-day samples by thermogravimetric analysis (TGA). Paste samples were taken out of the environmental chamber at the specified days, hydration stopped by immersing in isopropanol for 24 hours and then ground into powder using a mortar and pestle. Care was taken to ensure the powder used for TGA analysis did not originate from the surface of the cylindrical paste sample to eliminate any potential effects of moisture condensation. The powder was sieved through No. 200 (75 μm) sieve and then dried in a vacuum oven at 23°C for 3 days until constant mass was obtained. A small sample of powder (15 to 25 mg in size) was used for TGA measurements using a 2050 Thermogravimetric Analyzer manufactured by TA Instruments (New Castle, DE) with platinum crucibles. Analysis was performed in a nitrogen gas atmosphere, with a temperature range of 23 °C to 1000 °C at a heating rate of 10 °C/min.

Electrical resistivity of cement paste

The electrical resistivity of cementitious materials provides an indirect indication of porosity. It is a non-destructive means of investigating microstructural characteristics which in turn can aid in understanding the uptake and transportation of ions as the paste ages [97]. Cement paste samples were removed from the environmental chamber at specified days and the resistance of the samples was measured following procedure described by Spragg et al.[98] . The sponges were wetted in a freshly prepared saturated calcium hydroxide solution prior to each measurement, and the resistance of the top and bottom sponge was accounted for.

A separate study of the control samples (without any hydrogels) left in a controlled temperature environment without any curing water and another set in lime water was performed to ensure that there is no significant difference in electrical resistivity of samples if submerged in saturated lime water.

Isothermal calorimetry of cement paste

A TA Instruments TAM Air isothermal calorimeter (New Castle, DE) was used to measure hydration kinetics for freshly mixed paste. Cement paste samples prepared for isothermal

calorimetry analysis were mixed using a Renfert Twister vacuum mixer (Charles, IN) using the same proportions described in Table 4. DI water was used for the preparation of cement paste samples for isothermal calorimetry analysis, instead of tap water. Since paste samples was mixed outside of the calorimeter, the initial reactions due to aluminate phases dissolution were not recorded. 12 ± 3 mg of paste was added to glass ampoules, which were immediately sealed, weighed, and placed into the calorimeter for 48 hours. The bath temperature of the calorimeter was maintained at (23 ± 0.02)°C. For each type of paste composition, three ampoules were tested, and average results reported to ensure consistency of results.

2.1.6 Batch mixing of mortar

The proportions of cement to sand in all mortar mixtures were 1:2.75 by weight. The cement and WRA used was the same as that mentioned in Section 2.1.4. Locally available natural siliceous sand was used to prepare mortars. The sand utilized in this study was oven dried and sieved to pass through a No. 4 (4.75 mm) sieve. Prior to mixing, water in the amount needed to bring the oven-dried sand to SSD condition (ASTM C128-15) [99] was added to the sand. The required amount of WRA was added to the mixing water and stirred with a spoon to pre-dissolve it prior to addition of the water to the mix. The WRA added was varied to achieve a target flow of 110% ± 10% at 15 minutes after the addition of water to cement. The value of flow was determined using ASTM C1437-20 [100].

Each mortar was mixed using a 5L capacity mortar mixer (Hobart N50, Ohio, USA) with the batch volume equal to 1L. The SSD condition sand was placed in the mixing bowl and stirred for ten seconds and then mixed at a medium speed (281 rpm) for two minutes. Cement, hydrogel particles (if used for the mix) and the mixing water (with WRA pre-dissolved in it) were added to the bowl. The materials in the bowl were then stirred for 10 seconds followed by mixing for two minutes at medium speed (281 rpm). Once the mixing was completed, the sides of the bowl were scraped with the mixing paddle. The mixture proportions of the mortar mixes are given in Table 5.

Table 5: Mixture proportions for mortar (WRA in % by weight of cement).

Sample Name	Cement (g)	Sand (g)	Water (g)	Hydrogel particles (g)	WRA (%)
C.35	450	1238	175	--	2.5
C.35-AM-2	450	1238	175	0.9	3.0
C.35-AM-0.5	450	1238	175	0.9	4.0
SF-10-2	450	1238	175	0.9	4.0
SF-10-0.5	450	1238	175	0.9	4.5

2.1.7 Characterization of mortar

Compressive and flexural strength of mortar

Compressive strength and flexural strength values were determined for all mortar mixtures according ASTM C109/C109M-20b [101] and ASTM C348-20 [102], respectively. Compressive strength of the mortar specimens was recorded at 1, 7 and 28 days while flexural strength was determined at 1 and 28 days. All specimens were cured at 23 ± 0.1°C and 50 ± 0.1% relative humidity (RH) until the time of testing. This curing regime is different from that stated in ASTM C109, and it was implemented to eliminate chances of external curing. The experimental setups for strength characterization of mortars are shown in Figure 7.

Figure 7: Experimental setup used for determination of (a) compressive strength and (b) flexural strength.

Autogenous shrinkage of mortar

The procedure adapted from ASTM-C1698 [103] was used to investigate autogenous shrinkage of the mortar. The procedure was adapted so that the recording of the data began immediately after casting. The corrugated tubes were placed in an environmentally controlled chamber at (23 ± 0.5)°C and (50 ± 1) % relative humidity for seven days. Electronic probes measured length change from both ends of each corrugated tube at a rate of 1 scan every 5 minutes. The tubes were weighed before placing them in the environmental chamber and after the completion of the experiment. This was done to ensure no significant mass loss occurred during the experimentation period. Linear autogenous strain, ε, was calculated with the following formula:

$$\varepsilon = \frac{\Delta L(t) - \Delta L(0)}{0.382 + \Delta L(0)} \times 10^{6}.$$

$\Delta L(t)$ is the length of the tube at time t and ΔL (0) is the length of the tube at the sample's time of final set. The final setting time of cement paste was estimated from isothermal calorimetry experiments.

2.2 Study on composite retardation admixture containing polyacrylamide

The goal of this study was to measure the effect of two different retarding admixtures-citric acid and sucrose- on the performance of polyacrylamide composite hydrogel particles as internal curing agents. Citric acid, (CA) (ACS reagent, ≥99.5%) (Sigma-Aldrich, St. Louis, MO) and sucrose (analytical reagent, Mallinckrodt, St. Louis, MO) were used without further purification in the synthesis process. Isothermal calorimetry of cement paste was conducted to investigate whether the presence of composite hydrogel particles caused any retarding effect on the hydration of the cement paste.

2.2.1 Creation and characterization of composite retarding admixture-containing polyacrylamide hydrogels

Hydrogel particles were synthesized following the solution polymerization method. Acrylamide (AM, monomer), N,N'-methylenebisacrylamide (MBAM, crosslinker), sodium metabisulfate (NaS_2O_5), sodium persulfate (NaS_2O_8), were all purchased from Sigma-Aldrich (St. Louis, MO) and used without further purification. Deionized (DI) water used for the synthesis of hydrogels was collected from a Barnstead Nanopure Infinity system (Barnstead Thermolyne Corporation, Ramsey, MN).

Crosslinking solutions were prepared by adding 0.3 g of MBAM to 20 mL of DI water (crosslinker dosage was fixed at 2% by monomer weight). Initiator solutions were prepared by adding 0.3g of NaS_2O_5 and NaS_2O_8 to 10 ml of DI water, separately (each initiator dosage was fixed at 1% by monomer weight). Neutralization solution were prepared by adding 15.72g of sodium hydroxide pellets in 40 mL DI water. Neutralizing solution was added to the synthesis of composite CA-containing hydrogels only. Fresh batches of neutralization, crosslinking and initiator solutions were prepared for each batch of hydrogel synthesis.

The reagents used and their proportion in each variation of hydrogel are summarized in Table 6. AM-2 denotes pure polyacrylamide hydrogel particles without any retarding admixture added in the synthesis process, at 2% crosslink density. The composite particles are denoted as X-

Y-Z (for example, CA-20-2 and S-20-2) where X, Y and Z represents the admixture type, admixture dosage by weight of monomer (%) and crosslink density, respectively. It is worth noting that following the procedure mentioned below, composite CA-containing polyacrylamide hydrogels with a dosage of 50% by weight of monomer of CA prevented gelation.

Table 6: Hydrogel compositions for composite retarding admixture-containing polyacrylamide hydrogel synthesis.

Hydrogel	**AM (g)**	**Retarding admixture (g)**	**Water (mL)**	**NaOH (mL)**
AM-2	3.0	--	7.0	--
CA-20-2	3.0	0.6	5.3	1.7
S-20-2	3.0	0.6	7.0	--

The hydrogel synthesis adapted from Zhu, et al.[40] is described below. The synthesis was carried out in 20 mL glass scintillation vials. Water was added to the vials first. Citric acid or sucrose (if present) was added to the vials and the resulting mixture was mixed utilizing a magnetic stirrer. In the vials containing citric acid, the prepared sodium hydroxide solution was added next in the amount prescribed in Table 6. Vials were allowed to cool for 5 minutes and then AM monomer and 4 mL of MBAM solution were added and stirred for an additional 5 minutes. Initiator solutions were added at 0.5 mL each and vials were capped and placed in a temperature-controlled oil bath set at 60°C until gelation was observed (within 8 minutes).

Following gelation, the reaction product – a bulk hydrogel – was removed from the vials after 24 hours. For the composite hydrogels containing either citric acid or sucrose, half of the bulk hydrogel obtained was immersed in DI water for 24 hours at 23°C to remove any unreacted reagents. This portion of the hydrogels were further denoted as “washed” (for example, CA-20-2-washed). For the other half of the bulk hydrogel, this step was skipped (sample denoted as “unwashed”). This was done to detect whether this step, which is typical for the polyacrylamide post-synthesis process, removes the retarding admixture from the synthesized composite polyacrylamide. After this process, the bulk hydrogels were dried and further processed in the manner described in Section 2.1.3 to obtain representative samples. Figure 8 shows the synthesized

dry hydrogel particles after they have been sieved to obtain a representative sample. Each vial contains 1.10 ± 0.01 g.

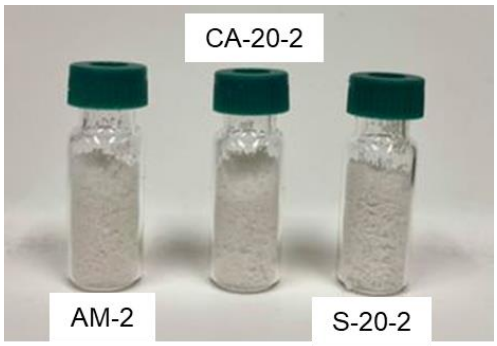

Figure 8: Synthesized dry hydrogel particles for the composite retarding admixture-containing polyacrylamide study.

The synthesized hydrogels were characterized using TGA, Fourier-transform infrared spectroscopy (FTIR) and gravimetric absorption tests (see Section 2.1.3 for details on TGA and gravimetric absorption tests procedure).

Fourier-Transform Infrared Spectroscopy (FTIR) of synthesized hydrogels

The functional groups of the synthesized hydrogels were characterized using FTIR. The functional groups present in acrylamide, citric acid and sucrose are shown in Figure 9. Approximately 3 mg of the representative sample of the hydrogel particles were used for the study. Attenuated total reflectance (ATR) Fourier-transform infrared spectra were collected by averaging 10 scans on a PerkinElmer Spectrum 100 FTIR spectrometer (Waltham, MA) by transmittance between 550 and 4000 cm^{-1} at a resolution of 0.5 cm^{-1} on ~3 mg of powder. Baseline correction was applied to every recorded spectral data.

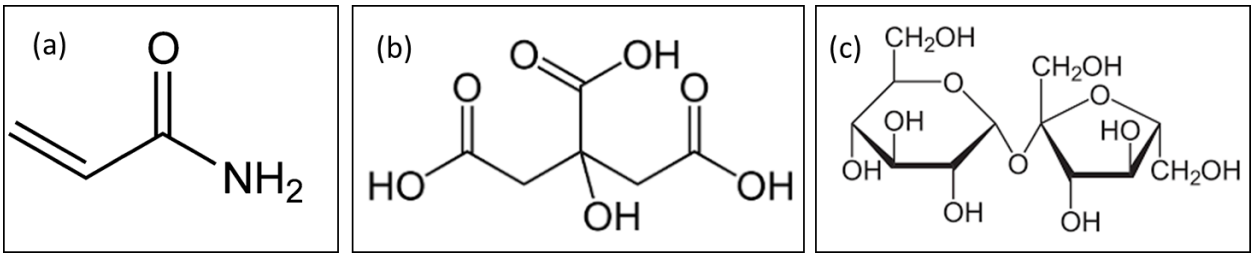

Figure 9: Chemical structure of (a) acrylamide, (b) citric acid and (c) sucrose showing the functional group present in the structures.

2.2.2 Batch mixing and characterization of cement paste

Ordinary Type I Portland cement (ASTM C150) obtained from Buzzi Unicem (Greencastle, IN) was used. Mixture proportions for the mixing of cement paste are given in Table 7. The composition of the Buzzi Unicem Type I cement used is given in Table 8. Hydrogel dosage (0.2% by weight of cement) was kept constant. No WRA was used for the preparation of cement paste so as to isolate the retardation effect of the composite hydrogels (if any) on the cement paste. Eight control samples (denoted as "C.XX" in Table 7) were investigated, having a w/c of 0.35, the same w/c that was used for all pastes internally cured with composite hydrogel particles. The C.35-CA_x and C.35-S_x samples were prepared so as to compare the effect of various dosage of addition of retarding admixtures to the cement paste to the incorporation of retarding admixture to the hydrogels, where x denotes the retarding admixture amount added to the mixture (by weight of cement). No additional "curing" water was added to the mixture to compensate for hydrogel absorption capacity.

Dry cement and dry hydrogel particles (if applicable) were added to a mixing cup and hand mixed for 30 seconds. Water was added and the mixture was mixed at 400 rpm using a Renfert Twister vacuum mixer (St. Charles, IL) for 60 seconds, scraped from the sides of the container, allowed to rest for 30 seconds. The paste was then mixed for another 60 seconds before being utilized for isothermal calorimetry measurements (see Section 2.1.5 for details on sample preparation for isothermal calorimetry). The pastes were studied for 3 days.

Table 7: Mixture proportions for cement pastes for retardation admixture containing hydrogel study.

Sample Name	Cement (g)	Water (g)	Retarding Admixture (g)	Hydrogel particles (g)
C.35	100	35	--	--
C.35-AM-2	100	35	--	0.2
C.35-$CA_{0.01}$	100	35	0.01	--
C.35-$CA_{0.1}$	100	35	0.10	--
C.35-$CA_{0.5}$	100	35	0.50	--
C.35-$S_{0.01}$	100	35	0.01	--
C.35-$S_{0.1}$	100	35	0.10	--
C.35-$S_{0.5}$	100	35	0.50	--
CA-20-2-washed	100	35	--	0.2[a]
CA-20-2-unwashed	100	35	--	0.2[a]
S-20-2-washed	100	35	--	0.2[b]
S-20-2-unwashed	100	35	--	0.2[b]

[a] containing 0.01% citric acid by weight of cement
[b] containing 0.01% sucrose by weight of cement

2.3 Study on commercial SAPs to inform the design of internally cured concrete bridge decks and pavement patches

The goal of this project was to utilize SAP formulations obtained from admixture industries to create internally cured concrete with improved hydration and mechanical properties for bridge decks and pavement patching applications. Two acrylic acid-based SAPs from industrial sources (BASF, Ohio, USA and SNF Floeger, France) were used in as-received form. Throughout this dissertation, these two SAPs are identified as “LA” (low absorption) and “HA” (high absorption), indicating their relative absorption capacity as determined through gravimetric absorption tests. The variables used in this study was: source of SAP, source of cement, type of cement, presence of slag, presence of WRA. The composition of the cement and slag used for this study is presented in Table 8. Three different sources of Type I cement were used: namely Buzzi Unicem (Greencastle, IN), Lehigh (Logansport, IN) and St. Mary’s (Charlevoix, MI) along with one Type III cement, i.e. Buzzi Unicem Type III Cement (Greencastle, IN). The slag used was NewCem Grade 100 by Lafarge Holcim (Chicago, IL). The Buzzi Unicem Type I cement used for this study was a second batch and the composition differs slightly from those presented in Table 3.

Table 8: Composition of the ordinary Portland cement and slag used in this study.

		B-Type I	B-Type III	L-Type I	S-Type I	Slag
		wt. (%)	wt. (%)	wt. (%)	wt. (%)	wt. (%)
Oxide Composition	SiO_2	19.5	19.62	19.8	19.7	--
	Al_2O_3	5.2	5.3	5.3	4.9	9.57
	Fe_2O_3	2.73	2.63	2.07	3.01	--
	CaO	63.42	63.58	62.7	62.3	--
	MgO	2.32	1.94	2.8	3.2	--
	Na_2O	0.65*	0.65*	0.12	0.13	--
	K_2O	--	--	0.11	0.96	--
	SO_3	3.25	4.06	2.62	4.03	0
Phase Composition	C_3S	60.2	58.8	50.8	52	--
	C_2S	9	11.9	17.2	17	--
	C_3A	8.9	9.6	10.3	8	--
	C_4AF	8.1	8	6.1	9	--
Blaine Fineness (m^2/kg)	--	412	593	418	376	5337

*Reported as Na_2O equivalent in the mill certificate.

2.3.1 Characterization of SAP

Scanning electron microscopy (SEM) and gravimetric absorption capacity tests were utilized to characterize the SAPs. The absorption capacity of the SAP particles was measured in cementitious pore solution by using gravimetric absorption tests [27], [89]. Gravimetric absorption capacity tests were carried out following the procedure described in Section 2.1.3.The pore solution was prepared by adding tap water to cement at a 1:10 ratio by weight and mixing these two materials for 30 seconds. The solution was then allowed to settle for 1 minute before decanting. Fresh pore solution was prepared for each batch of absorption tests. WRA, if used, was added in dosage of 0.7% by weight of cement to the decanted pore solution and the mixture was stirred for 30 seconds. In pore solution containing slag, 30% of the cement was replaced by slag.

2.3.2 Batch mixing of mortar and cement paste

The mortar and cement paste mixtures were prepared following the procedure described in Section 2.1.6 and Section 2.2.2, respectively. The following nomenclature was followed for naming the samples: X_Y_Z_A, where X, Y, Z, and A are cement type (Buzzi Unicem Type I or Type III), SAP type, WRA dosage (in % by weight of cement) and w/c, respectively. The mortar and cement paste composition of this study are given in Table 9 and Table 10, respectively. An extra water dosage in the amount of 1.46% by weight of sand was added to bring the oven dried sand to SSD condition.

Table 9: Composition of mortar mixtures.

Id.	Sample	Cement (g)	Sand (g)	Water (g)	SAP particles (g)	WRA (mL)
1	B Type I_No SAP_0.5_0.42	500	1375	230	--	2.5
2	B Type I_LA_0.5_0.42	500	1375	230	1	2.5
3	B Type I_HA_0.5_0.42	500	1375	230	1	2.5
4	B Type I_LA_1.45_0.42	500	1375	230	1	7.3
5	B Type I_HA_1.15_0.42	500	1375	230	1	5.8
6	B Type III_No SAP_0.5_0.42	500	1375	230	--	2.5
7	B Type III_LA_1.45_0.42	500	1375	230	1	7.3
8	B Type III_HA_1.15_0.42	500	1375	230	1	5.8
9	B Type I_No SAP_0.5_0.35	500	1375	195	--	2.5
10	B Type I_LA_1.45_0.35	500	1375	195	1	7.3
11	B Type I_HA_1.15_0.35	500	1375	195	1	5.8

DI water and tempered water was used during creation of cement pastes and mortar mixtures, respectively. WRA, if present, were pre-dissolved in the mixing water used for the mixtures. The WRA used for this study was MasterGlenium 7511 (BASF, Ohio, USA). A 0.5% by weight of cement dosage of WRA was used for preparation of some of the mortar mixtures (ID 1-3, 6, 9) as this was the amount of WRA that was needed to achieve a target flow of 110% ± 10% of the reference mortar at 0.42 w/c (Buzzi Type I_No SAP_0.5_0.42) at 10 minutes after the addition of water to cement. The value of flow was determined using ASTM C1437-20 [100]. Similarly, a WRA dosage of 1.45% and 1.15% by weight of cement was used for some mixtures containing LA and HA SAP, respectively as this was the amount that was needed for the

aforementioned SAP-containing mixes with Buzzi Unicem Type I cement to achieve a target flow of 110% ± 10% at a w/c of 0.42.

Table 10: Mixture proportions for cement pastes.

Sample Name	Cement (g)	Slag (g)	Water (g)	SAP particles (g)	WRA (mL)
B Type I+No SAP	100	--	42	--	--
B Type I+LA	100	--	42	0.2	--
B Type I+HA	100	--	42	0.2	--
L Type I+No SAP	100	--	42	--	--
L Type I+LA	100	--	42	0.2	--
L Type I+HA	100	--	42	0.2	--
S Type I+No SAP	100	--	42	--	--
S Type I+LA	100	--	42	0.2	--
S Type I+HA	100	--	42	0.2	--
B Type III+No SAP	100	--	42	--	--
B Type III+LA	100	--	42	0.2	--
B Type III+HA	100	--	42	0.2	--
B Type I+Slag+ No SAP	70	30	42	--	--
B Type I+ Slag+LA	70	30	42	0.2	--
B Type I+ Slag+HA	70	30	42	0.2	--
B Type I+No SAP+WRA	100	--	42	--	0.7
B Type I+LA+WRA	100	--	42	0.2	0.7
B Type I+HA+WRA	100	--	42	0.2	0.7
B Type III+No SAP+WRA	100	--	42	--	0.7
B Type III+LA+WRA	100	--	42	0.2	0.7
B Type III+HA+WRA	100	--	42	0.2	0.7

2.3.3 Characterization of cement paste and mortar

Isothermal calorimetry of cement paste

The cement paste samples were prepared in the manner described in Section 2.1.5 following the proportions mentioned in Table 10. The pastes were studied for 3 days.

Non-evaporable water content of cement paste

Select cement paste samples were prepared in the manner described in Section 2.1.5 following the proportions mentioned in Table 10. Only 7 days aged samples were used to investigate the non-evaporable water content.

Autogenous shrinkage of mortar

Mortar mixtures prepared in the manner described in Section 2.1.7 (see Table 9) were utilized to investigate the autogenous shrinkage of internally cured mortars. Data was recorded for 7 days.

Backscattered electron microscopy of cement paste and mortar

Mortar specimens prepared using the method described in Section 2.3.2 were used for scanning electron microscopy (SEM) imaging. 28-days old samples were used for microstructure analysis. After 28 days of curing at 23 ± 0.1°C and 50 ± 0.1% relative humidity (RH), the specimens were immersed in isopropanol for 48 hours to stop hydration, cut into manageable pieces with a glycol-cooled diamond saw, vacuum dried for 48 hours at (23 ± 5) °C, and then vacuum impregnated with epoxy. The epoxy embedded mortar mixtures were then dried at (60 ± 5) °C for 24 hours. Then, a fresh section of each epoxy coated sample was exposed by cutting with a diamond saw and polished. The samples were then carbon coated and imaged (in the backscattered mode) using a NanoScience Instruments Phenom Desktop SEM (Arizona, USA). For the mortar mixtures containing SAP particles, at least 30 random SAP voids were imaged and further analyzed using ImageJ software to quantify size of the voids. The analysis of the size of the voids involved measuring their diameter in several directions using ImageJ and then reporting the largest diameter of that particular void to compare the average size of SAP voids in the mortar mixtures (for more details regarding the SAP void size analysis procedure, refer to Bose et al. [104]).

In a further attempt to analyze the microstructure of the cementitious systems containing the two SAPs, cement paste from two different sources (B Type I and S Type I) were prepared using the procedure described in Section 2.3.2 and using a Renfert Twister vacuum mixer and DI water (instead of tap water). A 0.7% bwoc dosage of MasterGlenium 7511 (BASF, Ohio, USA),

was used as WRA in preparation of the cement paste samples. The paste samples were prepared for microstructure analysis following the same procedure described in the previous paragraph. 7 days old cement paste samples were imaged (in the backscattered mode) using a FEI Quanta 650 FEG (Hillsboro, OR) (coated sample, 15kV).

3. CHARACTERIZATION OF COMPOSITE SILICA-CONTAINING HYDROGEL PARTICLES

Following chapter contains text or figures adapted with permissions from Baishakhi Bose, Cole R. Davis, Kendra A. Erk, "Microstructural refinement of cement paste internally cured by polyacrylamide composite hydrogel particles containing silica fume and nanosilica," Cement and Concrete Research, Volume 143, 2021, 106400, ISSN 0008-8846, https://doi.org/10.1016/j.cemconres.2021.106400.

3.1 Microstructural analysis of hydrogel particles

Hydrogel particles were imaged using a NanoScience Instruments Phenom Desktop scanning electron microscope (Thermo Fisher Scientific, Waltham, MA), (uncoated sample, 15 kV). Average size of each composition of composite hydrogels were obtained by analyzing the SEM images of about 100 particles using ImageJ software. The average sizes of composite hydrogels are given in Table 11. Scanning electron micrograph of SF-10-2 and NS-10-2 are shown in Figure 10. Some silica particles are visible on Figure 10 in the form of bright white spots on the surface of the hydrogel particles.

Table 11: Average size of composite silica-containing hydrogels.

Hydrogel	Average particle size (µm)
AM-2	101
SF-10-2	97
NS-10-2	106
AM-0.5	94
SF-10-0.5	111
NS-10-0.5	102

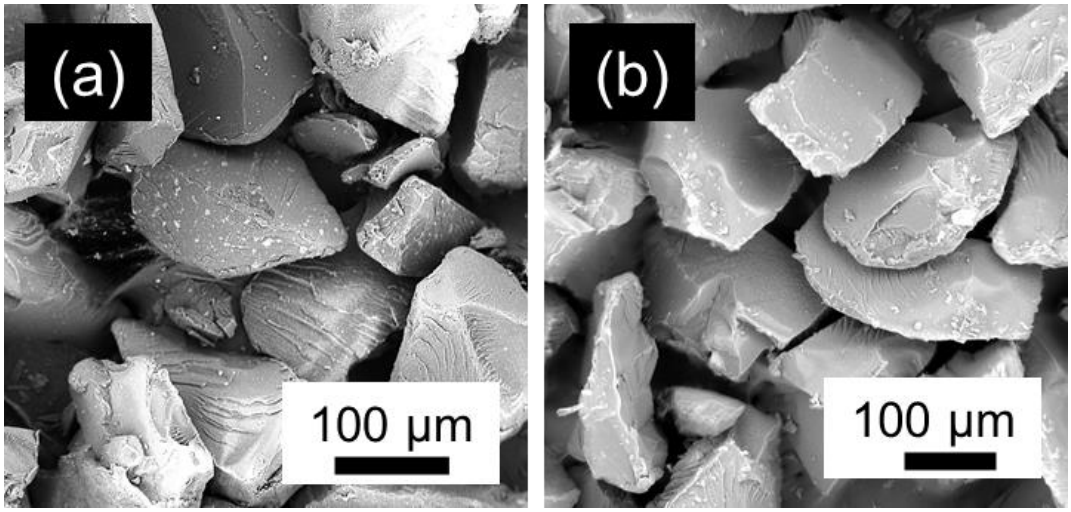

Figure 10. Scanning electron micrograph of (a) SF-10-2, and (b) NS-10-2, showing the angular morphology of the hydrogel particles.

3.2 Thermogravimetric analysis of hydrogel particles

Thermogravimetric analysis of the composite silica-containing polyacrylamide hydrogels with 2% and 0.5% crosslinker dosage are shown in Figure 11 and Figure 12, respectively. All six hydrogel particles sample displayed significant weight loss in three separate regions, which are characteristic of polyacrylamide degradation [105], [106]. At temperatures less than 220°C, the weight loss observed was attributed to evaporation of water. The second region of weight loss corresponded with the decomposition of the amide group to ammonia from 220-340°C. The third region of weight loss was in the range 340-430°C, which previous researchers attributed to chain scission of PAM. Due to significant amount of char left over in the sample pans at the end of the experiment, the residual weight loss gave an overestimation of the silica present in the polyacrylamide network.

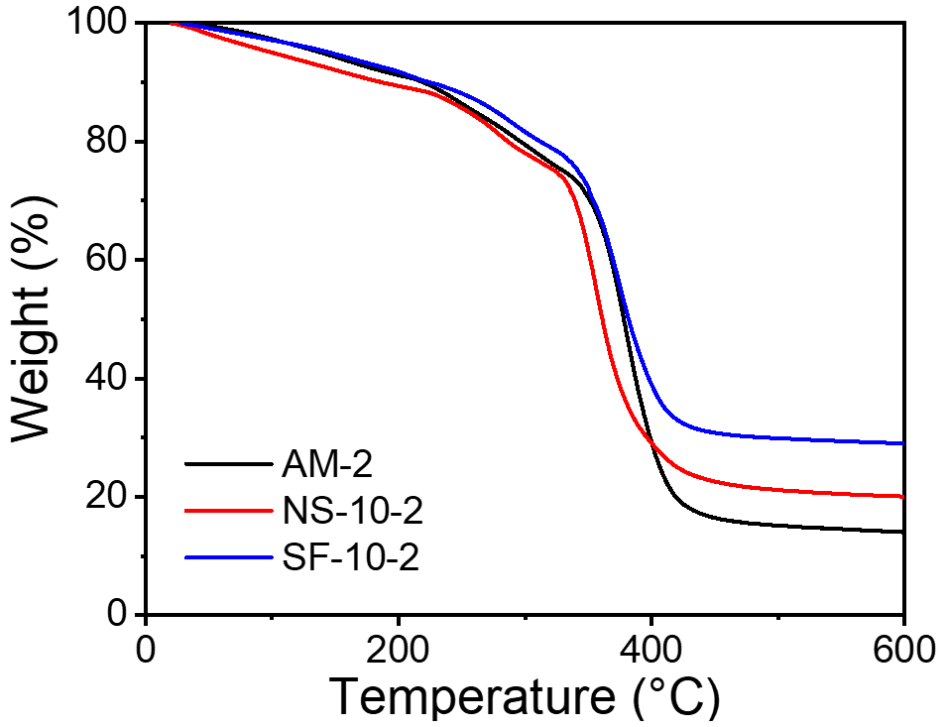

Figure 11: Thermogravimetric analysis of polyacrylamide hydrogel particles with a crosslinker dosage of 2% by weight of monomer.

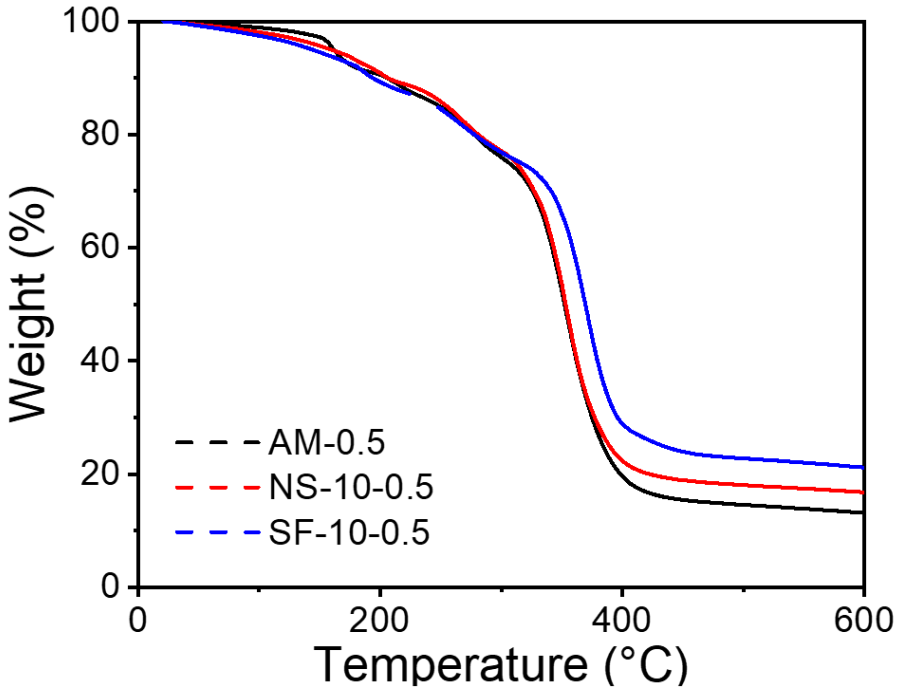

Figure 12: Thermogravimetric analysis of polyacrylamide hydrogel particles with a crosslinker dosage of 0.5% by weight of monomer.

3.3 Absorption capacity of hydrogel particles

Figure 13 and Figure 14 show the absorption capacities of hydrogel particles in RO water and pore solution, respectively. At a constant crosslink density of 2%, compared with pure (silica-free) AM particles, the addition of NS resulted in greater absorption in RO water, which at equilibrium (24 h) increased by 19% and 55% for NS dosages of 1% and 10%, respectively. To a lesser extent, addition of SF also increased the equilibrium absorption by 2% and 20% for SF dosages of 1% and 10%, respectively. Additionally, the decrease of crosslink density increased the absorption capacity by 110% for the pure (silica-free) AM particles, and similar trends were also observed for the silica-containing particles. For instance, an 80% increase in equilibrium absorption capacity of NS-10-0.5 was observed compared with NS-10-2. As expected, absorption capacities for each hydrogel sample were reduced in pore solution (Figure 14), as the ions in pore solution reduced the osmotic driving force for water absorption [43]. It is important to note that no residues of silica particles were observed in the beakers after the absorption tests, i.e., the NS and SF particles remained physically confined within the hydrogel particles even at maximum particle swelling.

The NS-10-0.5 hydrogel particles, with lower crosslink density and containing NS, displayed the greatest absorption capacity in both RO water and pore solution. Two factors contributed to this behavior. First, reducing the crosslink density of the hydrogel particles effectively doubled their measured absorption capacity. This is well-known behavior in polymer physics [88], illustrated in Figure 2, as the presence of chemical crosslinks in a polymer network reduces the overall flexibility (degrees of freedom) of the polymer molecules and thus hinders volumetric expansion. Consistent with past work by Davis et al. [46], the greater network restrictions and reduced absorption due to crosslinks manifest as large increases in the particles' compressive, shear, and elastic moduli [46]. Second, zeta potential measurements (Table 1) indicated the likelihood of water adsorption directly on to the silica particles driven by hydrogen bonding and dipole interactions of water molecules with surface hydroxyl groups [107]. As the silica particles were physically confined in the polymer network, such surface adsorption would manifest globally as an increase in absorption capacity. This idea is consistent with the greater increase in absorption observed for NS-containing hydrogel particles compared with SF, as the smaller NS particles displayed greater total surface area for water adsorption.

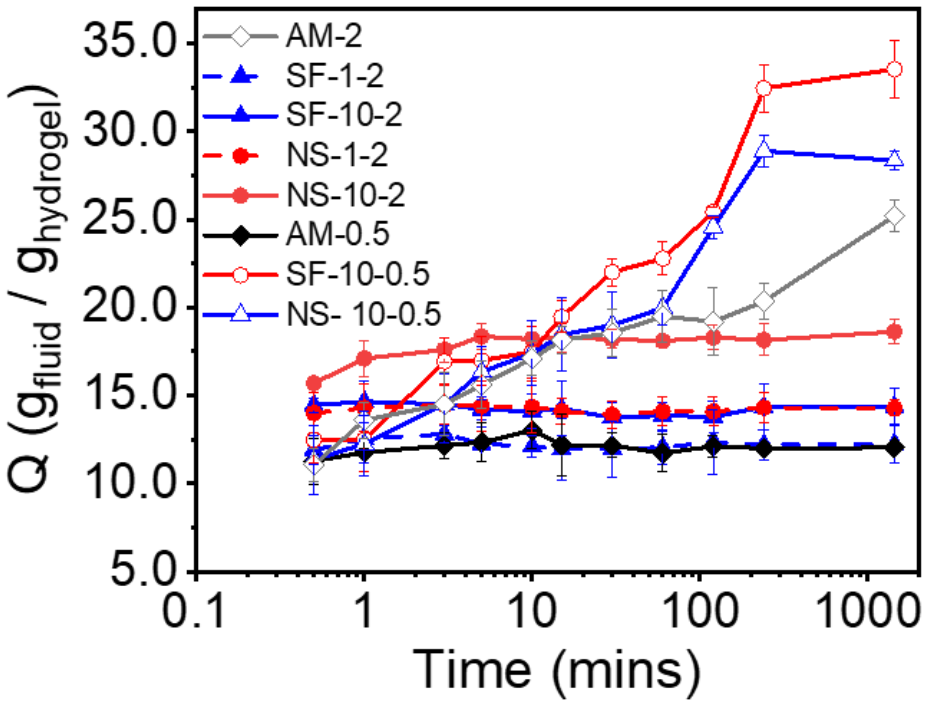

Figure 13. Absorption capacity of hydrogel particles as a function of immersion time in RO water.

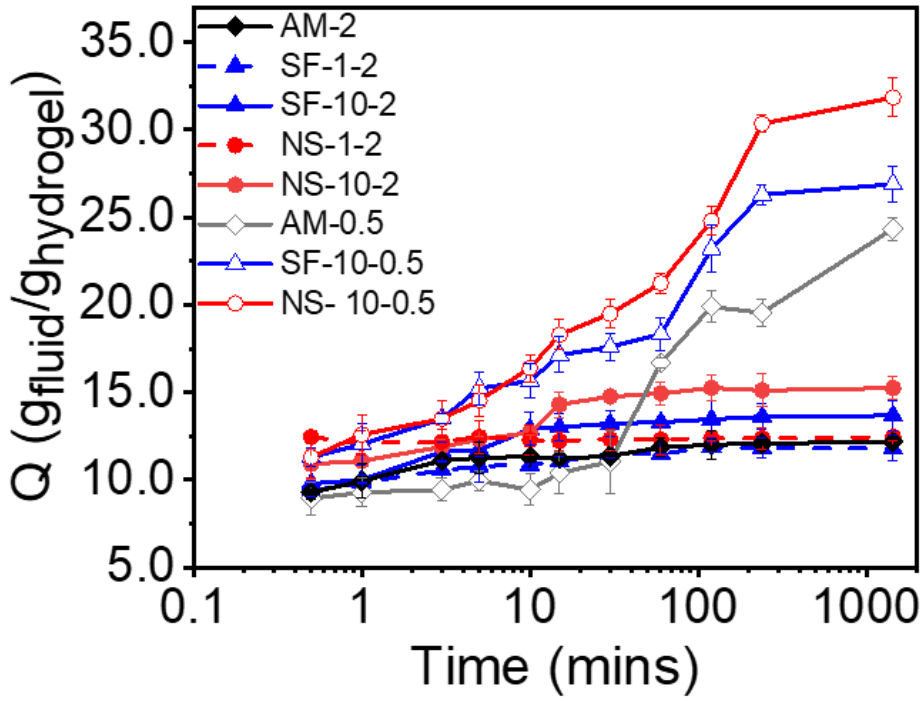

Figure 14. Absorption capacity of hydrogel particles as a function of immersion time in pore solution.

Compared to previous investigations [67] of the absorption behavior of poly(acrylic acid-acrylamide) hydrogel particles with and without NS, the polyacrylamide composite hydrogel particles studied here displayed lower absorption capacity in RO water and pore solution and were less sensitive to fluid composition, displaying similar equilibrium absorption values in both environments. In the previous investigation, hydrogel particles containing a high concentration of acrylic acid also displayed relatively fast desorption (rapid deswelling) during immersion in pore solution due to the interactions of the anionic segments in the polymer network with cations typically present in the pore solution. As expected, the acrylamide-based particles studied herein were much less sensitive to pore solution composition due to their low anionicity and thus did not display any significant desorption behavior even after 3 days of immersion in pore solution (Figure 15).

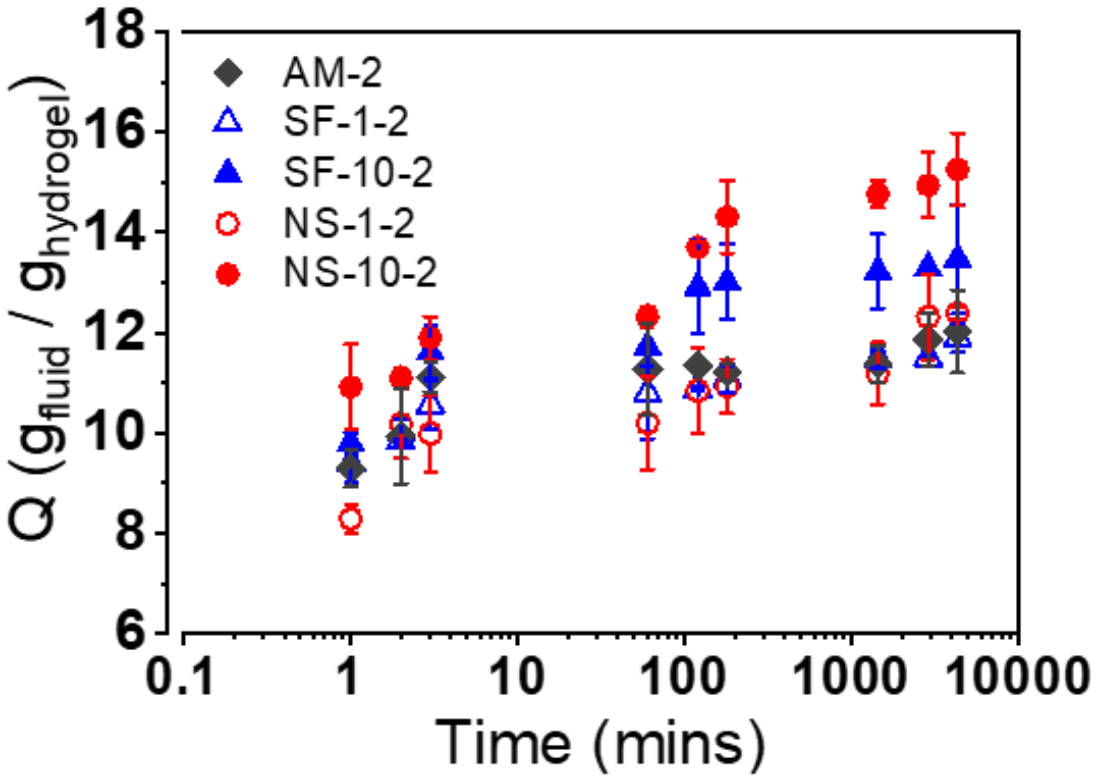

Figure 15: Absorption capacity of hydrogel particles as a function of immersion time in pore solution from 1 minute to 3 days.

4. INFLUENCE OF COMPOSITE SILICA-CONTAINING POLYACRYLAMIDE HYDROGEL ON CEMENTITIOUS SYSTEMS

The following chapter contain text or figures adapted with permissions from Baishakhi Bose, Cole R. Davis, Kendra A. Erk, "Microstructural refinement of cement paste internally cured by polyacrylamide composite hydrogel particles containing silica fume and nanosilica," Cement and Concrete Research, Volume 143, 2021, 106400, ISSN 0008-8846, https://doi.org/10.1016/j.cemconres.2021.106400.

4.1 Specific gravity and absorption of cement paste

The oven dried specific gravity (OD) and the absorption of the cement pastes samples are reported in Figure 16. A slight increase in specific gravity and consequent decrease in absorption of the cement pastes were observed with age. This was expected as over time, the cement paste hydrated, and porosity decreased; hence, the density increased, and the absorption subsequently decreased. Interestingly, the addition any hydrogel particles – high or low crosslink density, containing NS or SF – did not significantly change the density of the paste samples compared with the control paste (C.35), indicating that the hydrogel-induced voids did not significantly affect the bulk density of the paste samples at the chosen conventional dosage of 0.2% hydrogel particles by weight of cement.

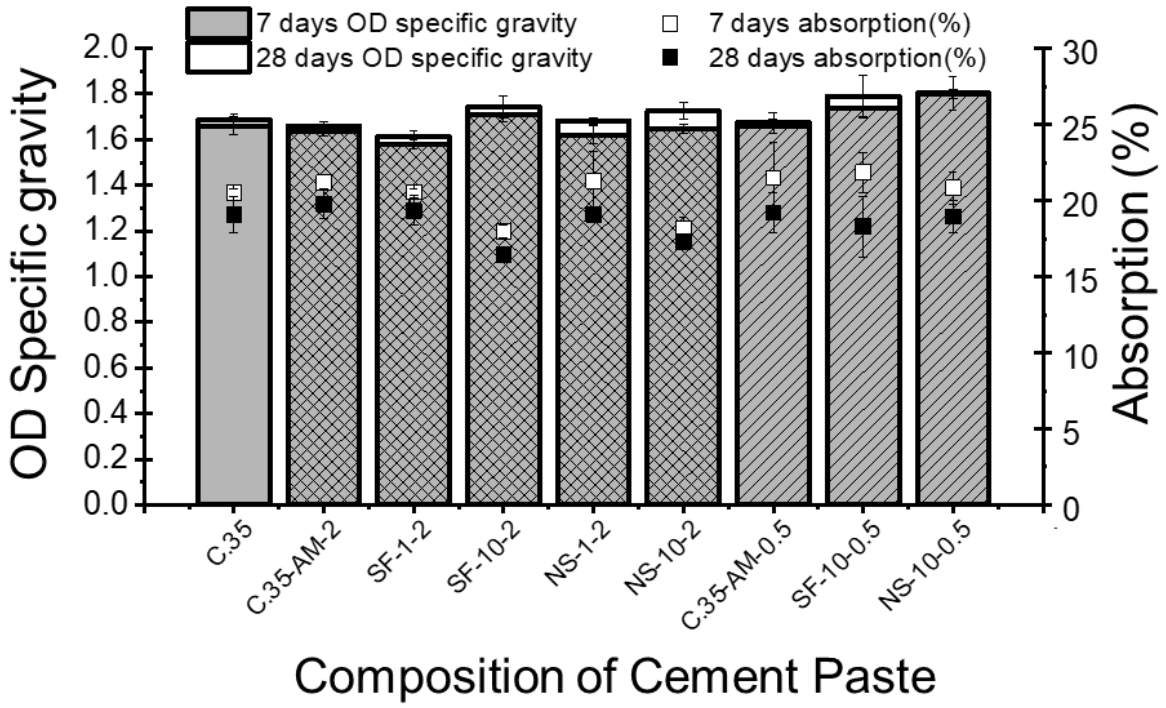

Figure 16: Oven dry (OD) specific gravity and absorption of cement paste samples at 7 and 28 days. For clarity, hatched bars and cross-hatched bars represent samples containing low crosslink density hydrogel particles and high crosslink density hydrogel particles, respectively.

4.2 Non-evaporable water content of cement paste

The non-evaporable water content (W_n) at 28 days is shown in Figure 17. It was evident that the addition of hydrogel particles increased the hydration of the cement paste samples, which is in agreement with previous research performed on cement paste containing hydrogel particles [96]. Also, for the high crosslink density particles, an improved degree of hydration for paste containing composite hydrogel particles compared to paste samples containing silica-free hydrogels. No significant improvement of hydration was observed when comparing paste containing hydrogel particles with low crosslink density.

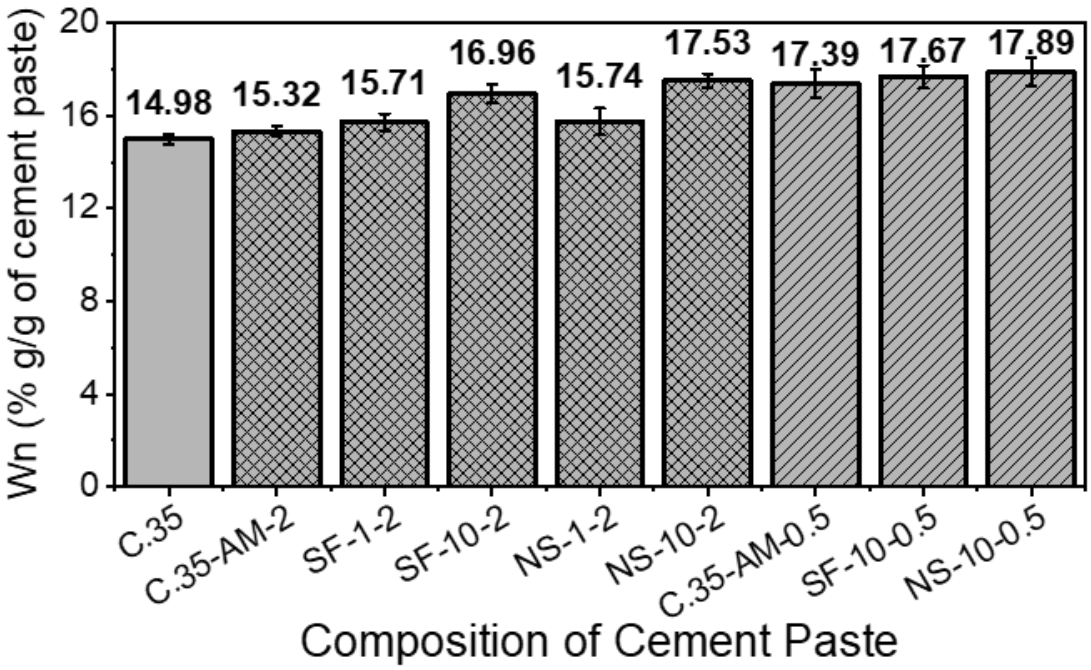

Figure 17: Non-evaporable water content (Wn) of the cement pastes at 28 days. For clarity, hatched bars represent samples containing low crosslink density hydrogel particles and cross-hatched bars represent samples containing high crosslink density hydrogel particles.

4.3 Microstructural Analysis

Scanning electron micrographs of internally cured cement pastes are shown in Figure 18 and Figure 19 for high and low crosslink density hydrogel particles, respectively. For each sample, the sizes of the hydrogel-induced voids and the amounts of hydration product observed within the voids were measured and are described below to ultimately determine the effects of hydrogel particle composition – crosslink density and the presence of silica – on the cement paste microstructure.

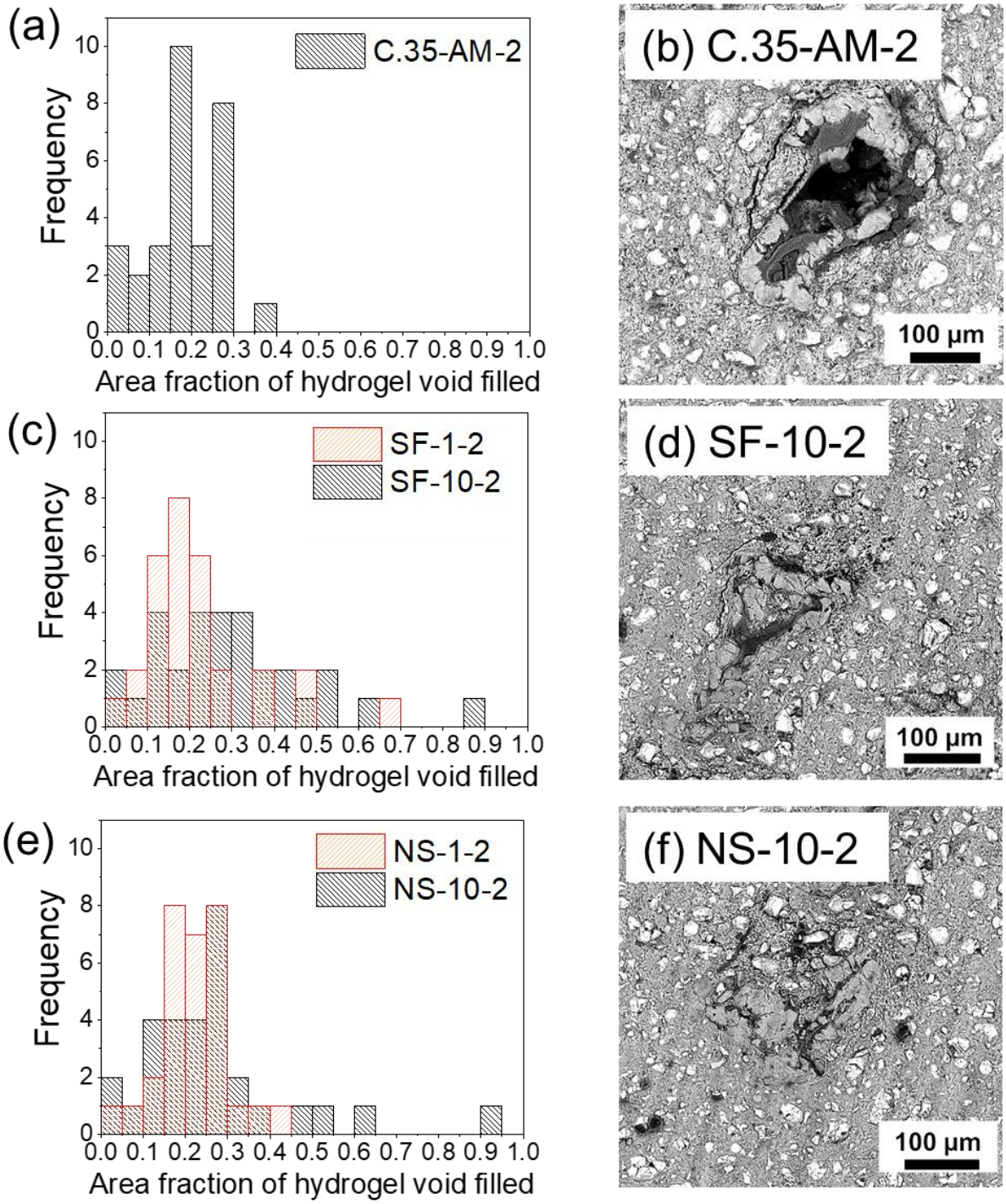

Figure 18: Microstructure analysis of pastes cured with high crosslink density hydrogel particles. (a) (c) and (e) Area of hydrogel particle voids filled with hydration products as a function of cement paste composition. Micrographs (3-day cured) of hydrogel particle voids in cement paste internally cured with (b) C.35-AM-2 with 35% of the void filled, (d) SF-10-2 with 89% of the void filled, and (f) NS-10-2 with 93% of the void filled.

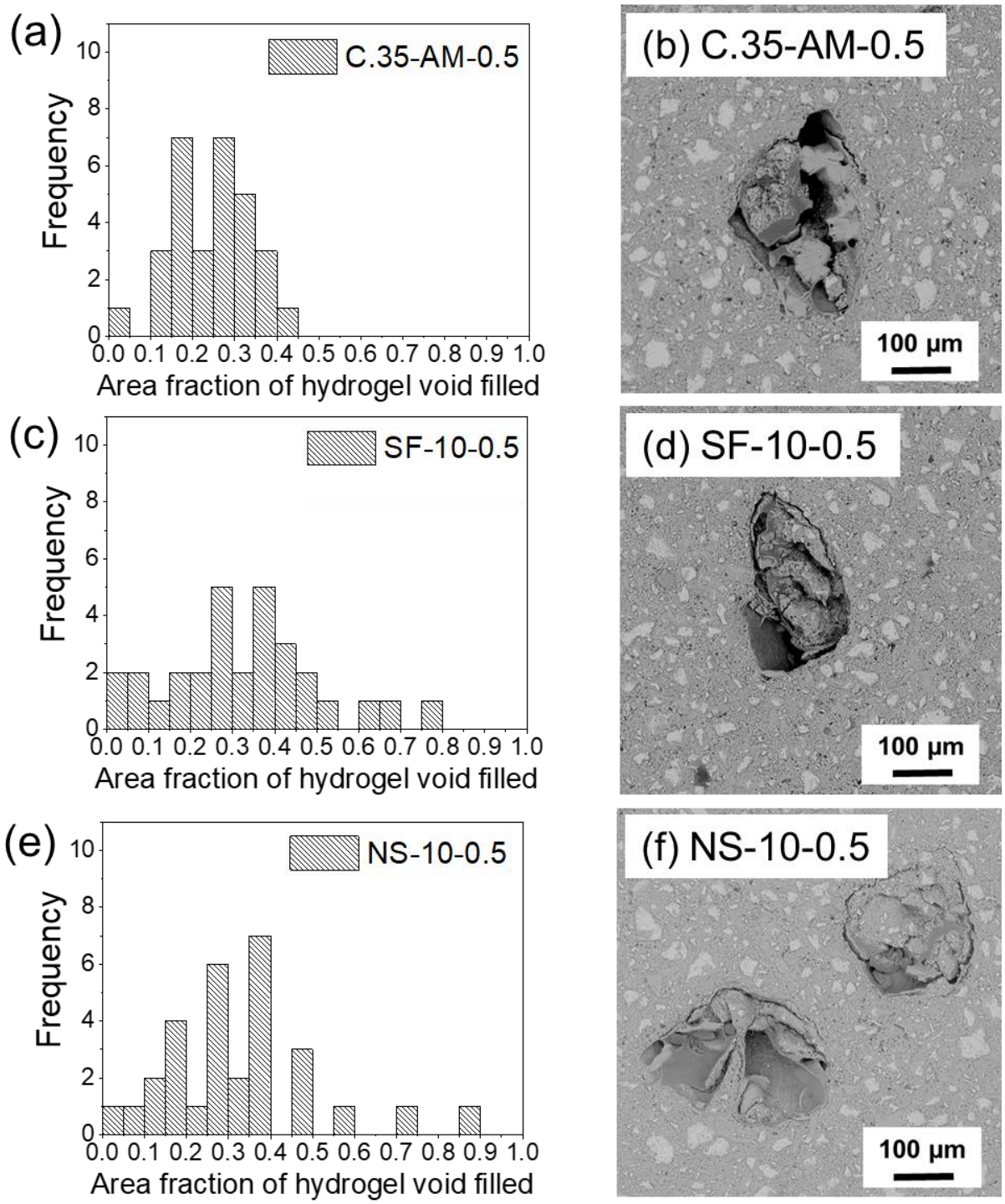

Figure 19: Microstructure analysis of pastes cured with low crosslink density hydrogel particles. (a) (c) and (e) Area of hydrogel particle voids filled with hydration products as a function of cement paste composition. Micrographs (3-day cured) of hydrogel particle voids in cement paste internally cured with (b) C.35-AM-0.5 with 40% of the void filled, (d) SF-10-0.5 with 80% of the void filled, and (f) NS-10-0.5 with 89% of the upper-right hand corner void filled.

The size of the hydrogel-induced voids in the cement microstructure is an important parameter to estimate for each hydrogel particle composition as the presence of voids beyond a critical size will reduce strength of hardened cementitious systems. Additionally, hydrogel particle absorption capacity results from the free absorption experiments (Figure 13 and Figure 14) cannot be directly applied to estimate void sizes in the microstructure. This is because during mixing and placement of cement, the hydrogel particles will likely experience physical confinement from the surrounding cement solids which can hinder the volumetric expansion of the hydrogel particles and ultimately reduce their capacity for fluid absorption.

To estimate the size of the hydrogel-induced voids within the cement microstructure, the maximum diameter was measured for 30 randomly selected voids in each sample. Histograms of all measurements are given in Figure 20. Table 12 reports the average values to allow for relative comparisons to be made between different hydrogel particle compositions. While some quantitative information was lost when comparing average size values instead of complete size distributions, these averages were treated here as rough estimates of particle sizes due to the measurement challenges described in the following paragraph.

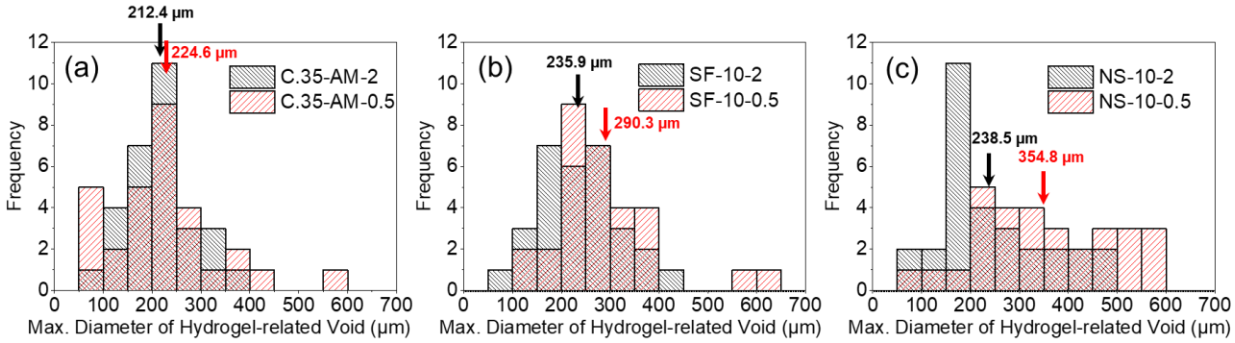

Figure 20: Maximum Diameter of Hydrogel-induced voids as a function of cement paste composition. 3 days aged cement paste internally cured with (a) C.35-AM-2 and C.35-AM-0.5, (b) SF-10-2 and SF-10-0.5, (c) NS-10-2 and NS-10-0.5 were used for analysis and plotting the histogram. Arrows show the average maximum diameter of 30 imaged voids for that particular sample.

Table 12: Average maximum length of SAP-induced voids from cement paste microstructure analysis.

Sample	Average maximum length of void (μm)
C.35-AM-2	212
SF-10-2	236
NS-10-2	239
C.35-AM-0.5	225
SF-10-0.5	290
NS-10-0.5	355

Example diameter measurements are provided in Figure 21 to illustrate that the maximum diameters sometimes included regions filled with hydration product, which was believed to form during/after particle dehydration. As such, these measured diameters provided a rough estimate of the size of the swollen hydrogel particles at the cement setting time. In some images (e.g., Figure 18b; Figure 19b, d, and f), microstructure features within the local vicinity of the void clearly indicated the dimensions of the original swollen hydrogel particles, including visible cracks, open void space, layers of dehydrated hydrogel, poorly consolidated hydration product (also see Figure 6). However, in other images (e.g., Figure 18d and f), such features were less visible when the hydrogel-induced voids contained significant growth of hydration product, partially obscuring the original dimensions of the swollen hydrogel particles. In these cases (< 9% of all analyzed images), maximum diameter was determined by marking off the visible edges of the hydrogel-induced voids and then measuring the diameter in several directions to obtain the maximum diameter (see labeled image in Figure 21, for more details).

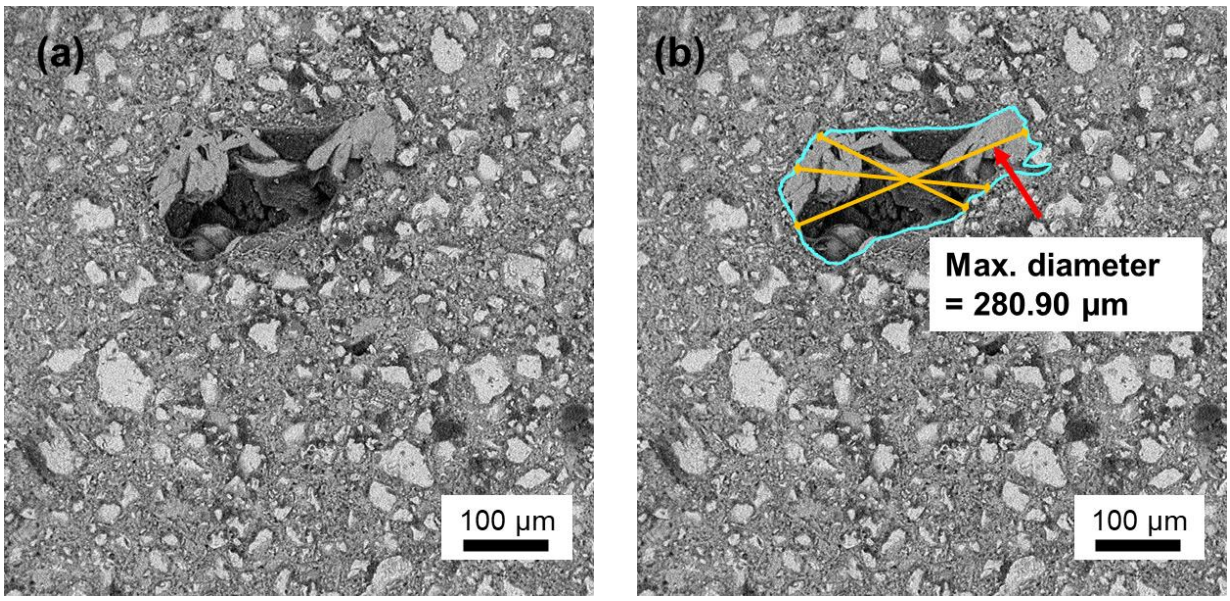

Figure 21: (a) Micrograph of cement paste with the hydrogel-induced voids contained significant growth of hydrated product, obscuring the original dimensions of the swollen hydrogel particles. (b) Visible edges of the hydrogel-induced voids were marked off and the diameter in several directions were measured to obtain the maximum diameter.

Despite these measurement challenges, some significant trends were observed from Table 12. Most notable was the relatively smaller swollen sizes displayed by the high crosslink density particles compared with the low crosslink density particles. In the free swelling experiments reported in Figure 13 and Figure 14, the high crosslink density particles only swelled to approximately half the capacity of the low crosslink density particles after 24 hours, an expected outcome due to the network restrictions imparted by the chemical crosslinks. In the cement pastes, however, the differences in swollen particle size reported in Table 12 were not as great due in part to the confinement of the swelling particles by the surrounding cement solids. This trend was also observed during a previous study conducted by Erk and coworkers on cement paste internally cured with spherical PAM [46]. Increases in swollen particle sizes were observed when silica was present in the hydrogel particles, again consistent with free swelling results in Figure 13 and Figure 14. For the high crosslink density particles containing silica, a small increase in swollen particle size was observed (e.g., 13% increase in size from C.35-AM-2 to NS-10-2) while greater increases were observed for low crosslink density particles containing silica (e.g., 58% increase in size from C.35-AM-0.5 to NS-10-0.5).

As seen in the micrographs in Figure 18 and Figure 19, one of the most striking features of the cement microstructures was the observed "filling" of the hydrogel-induced voids with hydration product. Based on elemental analysis conducted in a prior study [46], the hydration products are believed to be mostly CH with some amount of intermixed C-S-H.

To determine how the hydrogel particle composition affected the observed void-filling, the amounts (by area fraction) of hydration product observed within the hydrogel-induced voids were quantified for each internally cured paste. Details of these measurements, including representative images, are provided in supporting information (Figure 5). Of the 30 hydrogel-induced voids that were analyzed for paste containing high crosslink density particles (see histograms in Figure 18), the following numbers of voids were more than 30% filled: 1 void in C.35-AM-2; 5 voids in SF-1-2 and 13 voids in SF-10-2; 3 voids in NS-1-2 and 7 voids in NS-10-2. By comparison, of the 30 hydrogel voids analyzed for paste containing low crosslink density particles (see Figure 19), the following numbers of voids were more than 30% filled: 9 voids in C.35-AM-0.5; 16 voids in SF-10-0.5; and 15 voids in NS-10-0.5. Thus, more voids resulting from low crosslink density hydrogel particles containing silica were filled with hydration products compared to voids resulting from high crosslink density particles.

The greater filling of hydrogel-induced voids in SF-10-2 and NS-10-2 samples was in good agreement with the increased amount of non-evaporable water observed in Figure 17. In particular, the SF-10-2 composite hydrogel particles appeared to have the greatest impact on the microstructure of the cement paste, potentially indicating that desorption and reaction rates may depend on silica form. Increased non-evaporable water content for NS-10-0.5 when compared to NS-10-2 was also observed which is consistent with the larger amount of filled hydrogel voids in NS-10-0.5.

The differences in void-filling ability observed in Figure 18 and Figure 19 are most likely due to the different physical and chemical structures of the hydrogel particles, including the crosslink density and the presence of silica. The following paragraphs describe the hydrogel structure-property relationships that are hypothesized to directly impact the development of the cement microstructure.

The differences in absorption capacity (Figure 13 and Figure 14) of the high and low crosslink density hydrogel particles were significant and important to consider when analyzing the internally cured paste microstructures. The significantly higher absorption capacity of the low

crosslink density particles likely caused the hydrogels to retain more water in the paste mixture. In turn, greater amounts of water may have facilitated more hydration product growth inside the voids during early stages of hydration. It was also expected to take longer to fully expel the absorbed water; hence, this additional water present for longer time durations might have facilitated growth of more products in and around the hydrogel-induced voids. Additionally, it is noteworthy that the high-swelling low crosslink density hydrogel particles formed larger sized voids on average compared with the voids resulting from the low-swelling high crosslink hydrogels (see Table 12). Hence, the void-filling "activity" in the vicinity of the low crosslink density hydrogel particles appeared to be much greater than in the vicinity of the high crosslink particles, ultimately resulting in more total void space filled by hydration product in pastes cured with the low crosslink density hydrogel particles.

Besides dictating absorption capacity, the nanostructure of the hydrogel's internal polymer network may have played additional roles in the formation of hydration product. In particular, as illustrated in Figure 2, the high crosslink density hydrogels have higher polymer concentration and thus smaller mesh size (pore size) compared with the low crosslink density hydrogels. Inspired by existing hydrogel-based crystallization studies [108], the high crosslink density, small mesh size hydrogel particles were expected to more strongly hinder the nucleation and growth of hydration product within the hydrogel, by a combination of the following factors. First, the supersaturation threshold probably increased for the nucleation of inorganic phases including CH and C-S-H. This is supported by a study that found higher supersaturation levels are required for crystallization of calcium carbonate from solutions confined within gelatin-based hydrogels with smaller mesh size [109]. Second, the growth rate of the hydration products might have been significantly reduced due to slower diffusion of ions throughout the smaller mesh size of the hydrogel particle. As reported by Lopez-Bengaza et al., [110] and others [111], hindrance of ion diffusion in agarose hydrogels with small mesh size resulted in slower growth of calcium carbonate. Third, the smaller mesh size might have physically confined the growing inorganic phases, thereby limiting the product's overall size and morphology, especially as the latter is typically dictated by preferred crystallographic growth orientations. To summarize, chemical crystallization studies have found that mass transport in hydrogel-based materials is relatively slow and controlled because the mobility of ions in the solution is restricted by the polymer network and supersaturation concentrations can be more difficult to achieve. Ultimately, these changes in transport and

chemical activity can slow the overall rate of crystallization and change the size and morphology of the resulting products. In the present work, such changes likely contributed to the reduced void-filling that was observed in pastes cured with the high crosslink density, small mesh size hydrogel particles.

In addition to crosslink density, the presence of silica within the hydrogel particles directly impacted the cement microstructure. For both the high and low crosslink density hydrogel particles, silica resulted in increased void-filling as illustrated in Figure 18 and Figure 19. Thus, silica appeared to have increased the formation of hydrated product in the hydrogel-induced void. This result was most likely due to silica acting as a filler material [54] in addition to fostering pozzolanic reactions. Furthermore, the high surface area of NS may have promoted nucleation of C-S-H over the surface [55]. The presence of silica inside the composite hydrogels along with the unrestricted space for nucleation and growth provided by the deswollen hydrogel void was also expected to contribute towards enhancement of hydration product growth.

Lastly, when considering the impact of the silica-containing hydrogels on the internally cured pastes, it is important to note that the relatively small dosage of the silica in the system did not result in detectible increases in global pozzolanic activity (results and details will be discussed in Section 4.5). In a previous study with spherical hydrogel particles, it was relatively straight-forward to distinguish CH growth by its typical morphology and confirm with EDX measurements [46]. However, for the present study with irregular shaped hydrogel particles, the growth observed in the hydrogel-induced voids was more complex and likely composed of CH intermixed with C-S-H. As such, EDX measurements were likely to be inaccurate and not performed.

The acrylamide-based composite hydrogel particles studied here displayed much greater void-filling ability after 3 days of hydration compared with particles containing a high concentration of acrylic acid with and without NS [67], [112]. However, even in acrylic acid-based hydrogel particles, addition of silica resulted in a measurable increase in the formation of hydration product within the hydrogel-induced voids [67], consistent with present results. Significant void-filling behavior was also observed in pastes containing suspension polymerized (spherical) polyacrylamide hydrogel particles not containing silica [46]. In this prior work, hydrogel particles that had low crosslink density (0.5 wt.% MBAM) and thus higher absorption capacity also displayed greater void-filling ability compared to particles with higher crosslink density (2 wt.% MBAM) and lower absorption capacity which was consistent with the present study results.

Together, these comparisons with prior work indicate that the presence of silica in the hydrogel particles as well as the organic chemistry of the polymer network jointly impact the void-filling ability of these particles and thus corresponding paste properties. Specifically, pozzolanic reactions and corresponding strength gains appear to be more extensive for pastes containing composite hydrogel particles that retain fluid in the presence of silica for a greater length of time, even if the overall absorption capacity of these particles is relatively low. That is, compared to high-capacity, fast-desorbing hydrogel particles composed of acrylic acid, acrylamide-based composite hydrogel particles swell less in pore solution but have increased void-filling abilities such that incorporation of these low-swelling yet highly retentive particles in cement allows for microstructural refinement and gains in compressive strength by pozzolanic reactions to be realized.

4.4 Compressive strength of cement paste

The changes in compressive strength of the cement paste samples at various ages are shown in Figure 22, including the results for three hydrogel-free control samples, C.30, C.35, and C.40, which have w/c of 0.30, 0.35, and 0.40, respectively (Figure 22a). The results for cement pastes containing high and low crosslink density hydrogel particles are shown in Figure 22b and Figure 22c, respectively. After 28 days of curing, increases in strength beyond all control samples were observed for pastes containing high crosslink density hydrogel particles with the highest dosage of silica fume, i.e. SF-10-2 in Figure 22b (p-value <0.05, all t-tests were two-sample, two-tailed hypothesis tests conducted at the 95% confidence level). In comparison, the 28-day compressive strength values for pastes containing low crosslink density hydrogels with SF were either reduced or comparable to the hydrogel free control pastes (Figure 22c).

Reduced early-age (3 days) strength was observed for almost all paste samples containing composite hydrogel particles compared with the respective control pastes containing silica-free particles, i.e. C.35-AM-2 in Figure 10b and C.35-AM-0.5 in Figure 22c. Among internally cured samples, pastes containing hydrogels with the highest dosage of silica fume (SF-10-2) had the lowest early-age strength. Interestingly, a statistically significant 3- to 28-days strength gain (with a confidence of 95%) was observed in internally cured pastes, especially the ones with composite silica-containing hydrogel particles. For instance, a higher strength gain was observed in pastes

containing SF-10-2 (+135%, p-value =0) and NS-10-2 (+95%, p-value = 0) when compared to the control paste C.35-AM-2 (+46%, p-value = 0.011).

Reductions in early-age strength may be explained by considering the desorption behavior of the different hydrogel particles. As shown in Figure 22, the 3 days strength of paste containing composite hydrogel particles was reduced compared to silica-free hydrogel particles. This reduction could indicate that that the composite hydrogel particles were desorbing more fluid at earlier ages compared with the silica-free hydrogel particles, leading to a cement matrix that has a local w/c greater than 0.35 and thus reduced strength. This idea is perhaps consistent with other published results [113], showing that the presence of SF in OPC-SCM systems increased the desorption rate of SAP hydrogel particles; as SF typically creates a finer pore structure, the authors suggested that the presence of SF facilitates hydrogel desorption by increasing the capillary pressure of the matrix. Here, the silica confined within the composite hydrogel was not released from the particle; however, the silica may still increase the local capillary pressure, leading to accelerated desorption at early ages.

It is important to note that fluid desorption from the hydrogel particles into the cement matrix was not directly observed or measured in this study. The results from the 24-hours free "*ex situ*" swelling experiments shown in Figure 13 and Figure 14 did not display any signatures of fluid desorption. Additionally, swelling tests conducted for up to 3 days did not show any significant change in absorption capacity compared with the 24-hours absorption values in Figure 13 and Figure 14 (see Figure 15). While *ex situ* swelling tests are useful to determine the equilibrium absorption of a particular SAP formulation, it is well known that these tests are not completely accurate representations of the environment that a SAP particle experiences when confined in a cement matrix [43]. Specifically, in *ex situ* swelling tests, there are no significant chemical or physical driving forces that evolve over time to encourage fluid desorption from the hydrogel particles. For example, Montanari et al. [44] recently showed that the sorption behavior of SAP was dependent on the concentration of ions in the pore solution which of course changes over time during hydration.

To better understand the relationship between longer term (28 days) compressive strength and microstructure, Table 13 summarizes the relative changes of hydration product growth, void size, and compressive strength for select hydrogel compositions. From Table 13, for silica-free hydrogels, a decrease in crosslink density corresponded to a 33% increase in void-filling, a small

(6%) increase in void size. However, a 22% decrease in 28 days compressive strength was observed for a decrease in crosslink density of the silica-free hydrogels (p-value = 0.026). The negative correlation between void-filling and compressive strength was unexpected as it was assumed that the compressive strength of the paste would increase if more of the SAP-induced voids were filled with hydrated product. This unexpected observation may instead indicate that at the relatively low hydrogel dosages used in this study, any strength gains which resulted from SAP-induced void-filling were local and did not contribute towards the global compressive strength.

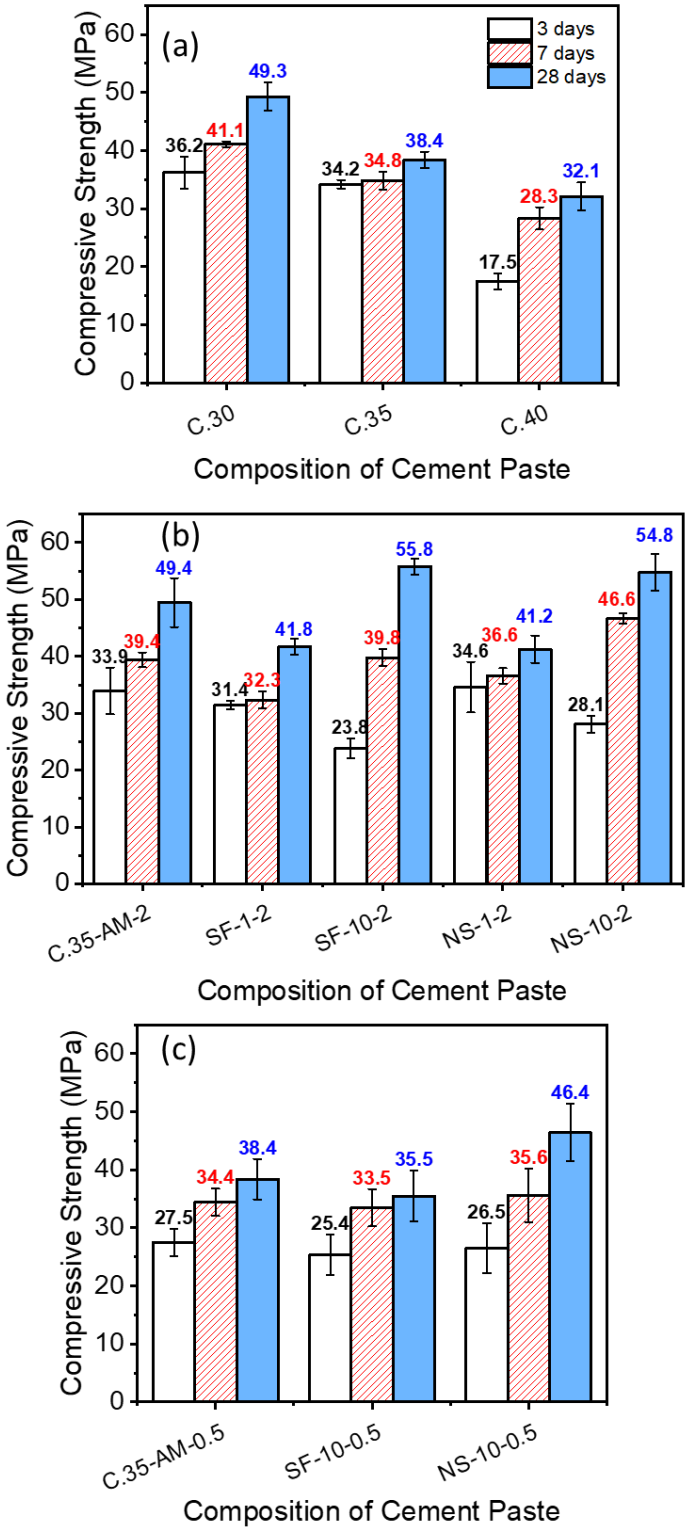

Figure 22: Compressive strength of cement pastes at various ages. (a) Control pastes at different w/c without hydrogel particles; (b) pastes internally cured with high crosslink density hydrogel particles; and (c) pastes internally cured with low crosslink density hydrogel particles.

Table 13: Impact of crosslink density decrease on hydration product growth in hydrogel-induced voids, void size, and 28 days compressive strength.

Comparison Samples	Average area of hydration product in hydrogel voids	Average diameter of hydrogel-induced void	Compressive Strength of cement paste
C.35-AM-2 to C.35-AM-0.5	33% ↑	6% ↑	22% ↓
SF-10-2 to SF-10-0.5	12% ↑	23% ↑	36% ↓
NS-10-2 to NS-10-0.5	28% ↑	49% ↑	15% ↓

For the SF-containing hydrogel samples compared in Table 13, a decrease in crosslink density corresponded to a moderate increase (12%) in void-filling and a statistically significant 36% decrease (p-value = 0.002) in 28 days compressive strength. So again, the expected benefits of void-filling were not observed at the global scale. In this case, the dramatic strength reduction between the samples have resulted from the substantial increase in size (23%) of the hydrogel-induced voids, which could increase the likelihood for crack initiation and propagation during compression testing and result in failure at reduced loads. For the NS-containing hydrogel samples compared in Table 13, a decrease in crosslink density corresponded to a 28% increase in void-filling, a large increase (49%) in void size, and a moderate decrease (15%, p=0.069) in 28 days compressive strength. So, despite the fact that the low crosslinked NS-containing hydrogels created relatively large voids in the cement paste, the compressive strength reduction was not statistically significant, unlike the SF-containing samples, perhaps due to the increased void-filling abilities of these NS-containing hydrogels.

Overall, the comparisons illustrated in Table 13 and the results shown in Figure 22 clearly indicate that the compressive strength of cement paste containing hydrogel particles was dependent on the crosslink density of the particles, as the higher-swelling low crosslink density hydrogel particles resulted in reduced long term compressive strengths. Table 13 also shows that there was not one dominant feature of the microstructure that completely explained the strength reductions, as both a hydrogel's void-filling ability as well as its total void size appeared to play important roles.

In one final experimental attempt to better understand the relationship between hydrogel-induced microstructure features and paste compressive strength, another set of compressive strength tests was conducted on paste samples containing dried and sieved low crosslink density hydrogels with different particle sizes (Figure 23). Samples denoted in Figure 23 as "-75" contained low crosslink density particles with dry sizes of 45-75 µm; samples denoted as "-114" contained low crosslink density particles with dry sizes of 75-114 µm. Paste samples containing composite silica-containing hydrogels with larger particle size resulted in small strength reductions at all ages (3, 7, 28 days). For instance, compared to the NS-10-0.5-75 sample, there was a 16% reduction in 28 days strength for NS-10-0.5-114, which was not statistically significant at 95% confidence level (p-value = 0.065). Such reductions were expected as larger particles will swell to greater dimensions in the cement paste and result in larger hydrogel-induced voids. Although hydration product growth in these voids might offset some of the loss in strength, larger voids will lead to reduced overall strength.

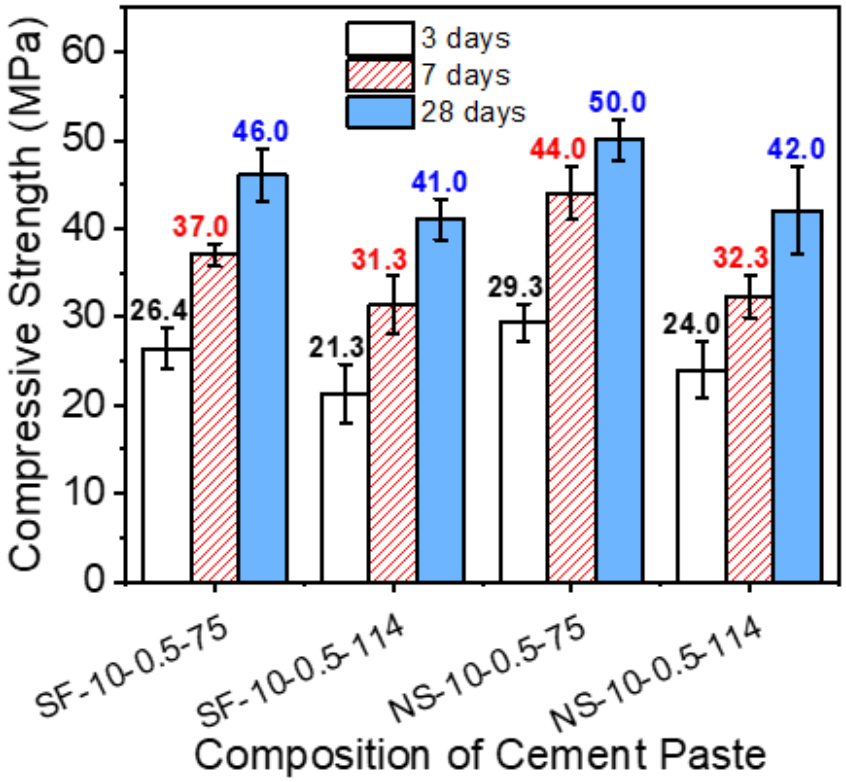

Figure 23: Compressive strength of cement pastes at various ages internally cured with 0.5% crosslinked hydrogel particles of different size ranges: "-75" denotes dry particles within 45-75 µm and "-114" denotes dry particles within 75-114 µm.

To summarize, considering the comparisons in Table 13 and data in Figure 22 and Figure 23, increased hydrogel-induced void size in the cement paste microstructure due to either larger hydrogel particles or hydrogel particles with lower crosslink density (and thus greater swelling) resulted in compressive strength reductions. However, as illustrated by the NS-containing hydrogels, these void-size-dependent strength reductions were at least partially off-set by the growth of hydrated product within the voids.

4.5 Thermogravimetric Analysis

The CH content in the cement paste samples at two hydration ages is shown in Figure 24. As hydration proceeded, the amount of CH increased in the samples. CH content further increased with silica dosage in the hydrogel; for example, at 28 days, a 14% increase in CH within the NS-10-2 paste sample was observed compared to the internally cured control (C.35-AM-2) sample.

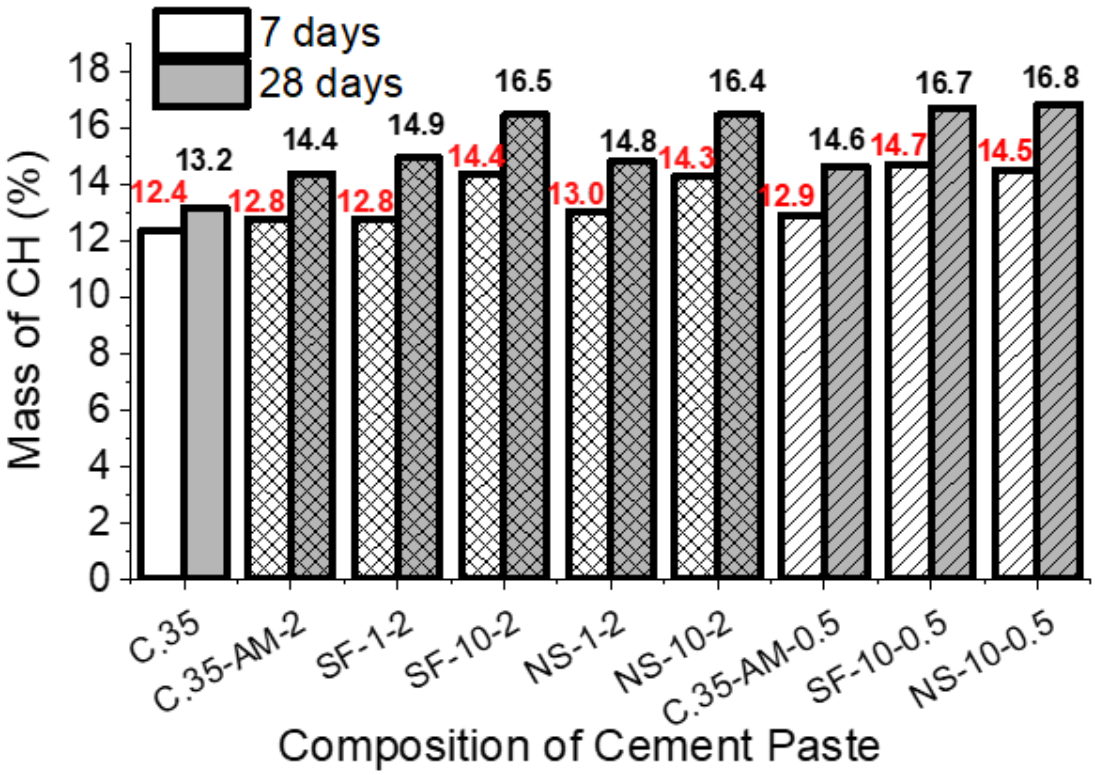

Figure 24: Calcium hydroxide content (%) of cement paste at 7 and 28 days. For clarity, cross-hatched bars represent samples containing high crosslink density hydrogel particles and hatched bars represent samples containing low crosslink density hydrogel particles.

In systems containing SCMs, the conversion of CH to C-S-H should decrease the CH content when compared to samples without any SCM. Here, the observed increases in CH in Figure 24 in samples containing composite hydrogels indicate that the presence of silica in the hydrogel particles did not impact the global CH content inside the paste matrix. While unexpected, this was not a surprising outcome as even at the highest dosage of silica in the hydrogel particles (10 wt.% of monomer), silica was less than 0.005 wt.% of the cement used in fresh paste mixture. The silica concentration in a single swollen SF-10-2 or NS-10-2 particle was estimated to be approximately 0.5-1.5 vol.% based on starting reagent concentrations in Table 2, average silica, and dry hydrogel particle size, and swelling dimensions from micrographs. To put these dosages into context, typical NS dosages in conventional OPC-SCM mixtures range from 0.2 to 12 wt.% of cement [114]. Thus, the dosage of silica in the paste mixtures of this study was most likely insufficient to decrease global CH content as C-S-H is created, as measured by TGA. Instead, the measured increase in CH in Figure 24 was consistent with the results from the non-evaporable water measurements (Figure 17), indicating that pastes internally cured with composite hydrogel particles had increased degree of hydrations.

No significant changes in CH content were observed in Figure 24 for samples cured with low crosslink density hydrogels compared with high crosslink density hydrogels, despite the increases in void-filling observed in pastes containing low crosslink density particles (see Table 13). For instance, in Figure 24, the increase in CH content was 15% in NS-10-0.5 sample, when compared to C.35-AM-0.5. As aforementioned, the increase in CH content for NS-10-2 sample was 14%, when compared to C.35-AM-2. This observation again supports the idea that at these relatively low dosages of hydrogel particles in cement pastes, any local microstructural or compositional changes related to the hydrogel particles may be difficult to quantify directly using global characterization techniques, like macroscale compression testing or TGA.

4.6 Electrical Resistivity of Cement Paste

Resistivity is related to the volume and connectivity of pores inside the paste samples, and conductivity is primarily due to pore solution [98]. In general, as paste hydrates over time, pore volume decreases, causing a corresponding increase in resistivity. As shown in Figure 25, there was a prominent increase in resistivity for paste samples containing composite silica-containing high crosslinked hydrogel particles after 21 days when compared to all other paste samples.

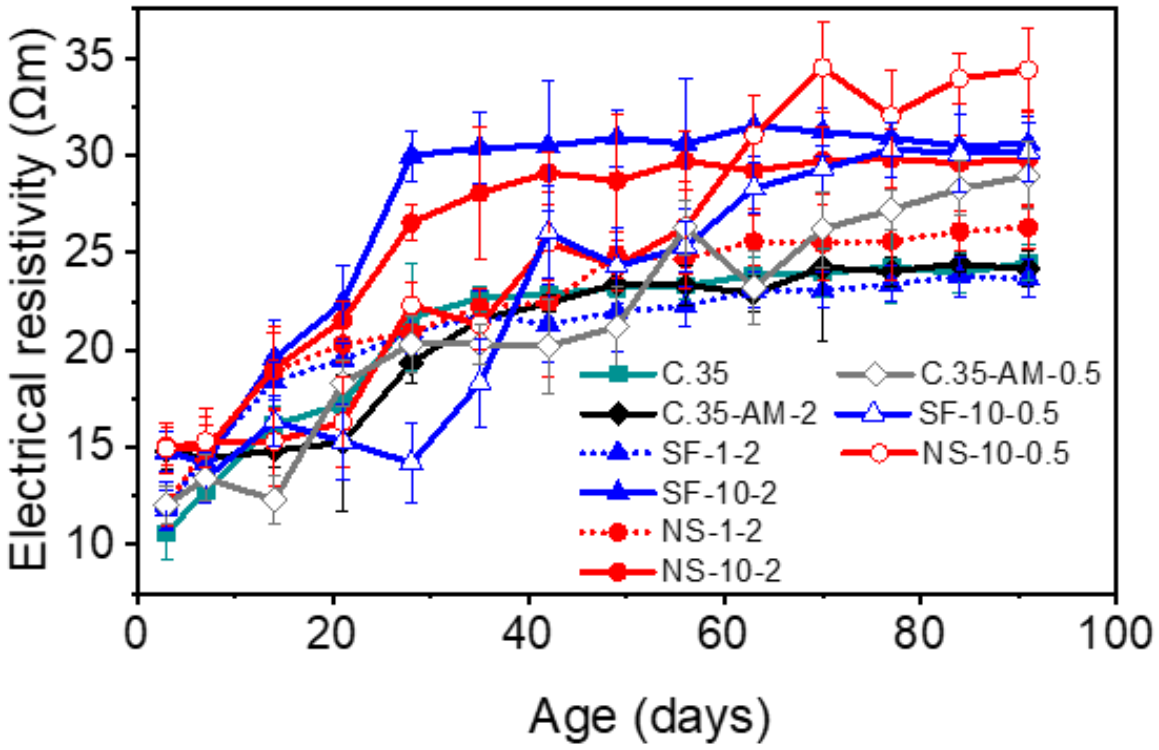

Figure 25: Variation of electrical resistivity of cement paste samples with the age of the sample.

Similar trends have been seen in another study with SAPs [97] which suggested that the electrical resistivity of cementitious composites containing SAP was dependent on two competing factors: increased amount of macrovoids (including SAP-induced voids) and densification of the pore structure in the vicinity of SAP-induced voids as a result of enhanced water replenishment. The results in Figure 25 suggest that the dominant factor for pastes internally cured with high crosslink density hydrogels was the latter – an increased degree of hydration due to the presence of hydrogel particles. The SF-10-0.5 did not show any marked improvement when compared to the SF-10-2 samples, which might be because the larger macrovoids played a more important role in the resistivity of the lower crosslinked hydrogels.

The increase in resistivity of samples containing SF-10-0.5 and NS-10-0.5 composite hydrogel particles when compared to other control samples suggest that the dosage and size range of composite hydrogel particles was insufficient to cause a connected pore structure that would increase conductivity of ions. This was confirmed by the images of the hydrogel-induced voids

(Figure 18 and Figure 19) showing that the internally cured cement paste did not have an interconnected pore system. Growth of hydration product inside the hydrogel-induced voids decreases the porosity and hence causes a gradual increase in resistivity over time. Similar decrease in porosity in the micro- and mesopore range have been observed in cement paste containing SAP by previous researchers [115].

4.7 Isothermal Calorimetry of Cement Paste

Figure 26 represents the rate of heat of hydration release from cement paste containing different compositions of composite polyacrylamide hydrogels synthesized for this study. The presence of low crosslinked Si-containing hydrogel particles accelerated the main hydration peak, when compared to the reference paste without hydrogels in it. Additionally, for pastes internally cured with high crosslinked hydrogel particles, a slight retardation in main hydration peak was observed, when compared to the reference paste containing no hydrogel particles (C.35).

An acceleration in main hydration peak was observed for paste containing lower crosslinked Si- containing hydrogel particles, in comparison to the reference paste without any hydrogel particles in it. For instance, there was an acceleration of occurrence of main hydration peak by approximately 2 hours for NS-10-0.5, when compared to C.35. In fact, as can be seen in the inset figure in Figure 26, the transition from induction to acceleration period was fastened for pastes internally cured with low crosslinked composite Si-containing hydrogels. A possible explanation for this behavior might be a decrease in w/c, as suggested by previous researchers [116], [117]. The NS-10-0.5 and SF-10-0.5 are the hydrogel formulations with the highest equilibrium absorption capacity (see Figure 13 and Figure 14). This along with the fact that no additional “curing” water was added to the mixtures to account for SAP absorption, it is expected that these two formulations would cause the largest reduction in effective w/c of the paste. This in turn would increase the overall concentration of alkali ions in the pore solution as the rate of dissolution of alkali ions eventually would exceed the absorption of alkali ions into the polymer network. The overall increase in alkali ions would manifest as acceleration of hydration reactions. As such, an acceleration in occurrence of main hydration peak was observed for NS-10-0.5 and SF-10-0.5, when compared to C.35 or C.35-AM-0.5. This is also an indication that the NS-10-0.5 and SF-10-0.5 hydrogel particles did not release the absorbed water during the initial acceleration period. The longer retention of water in the hydrogel particles might explain the greater hydration

products growth observed in the vicinity of the voids of NS-10-0.5 and SF-10-0.5 containing pastes (see Figure 19).

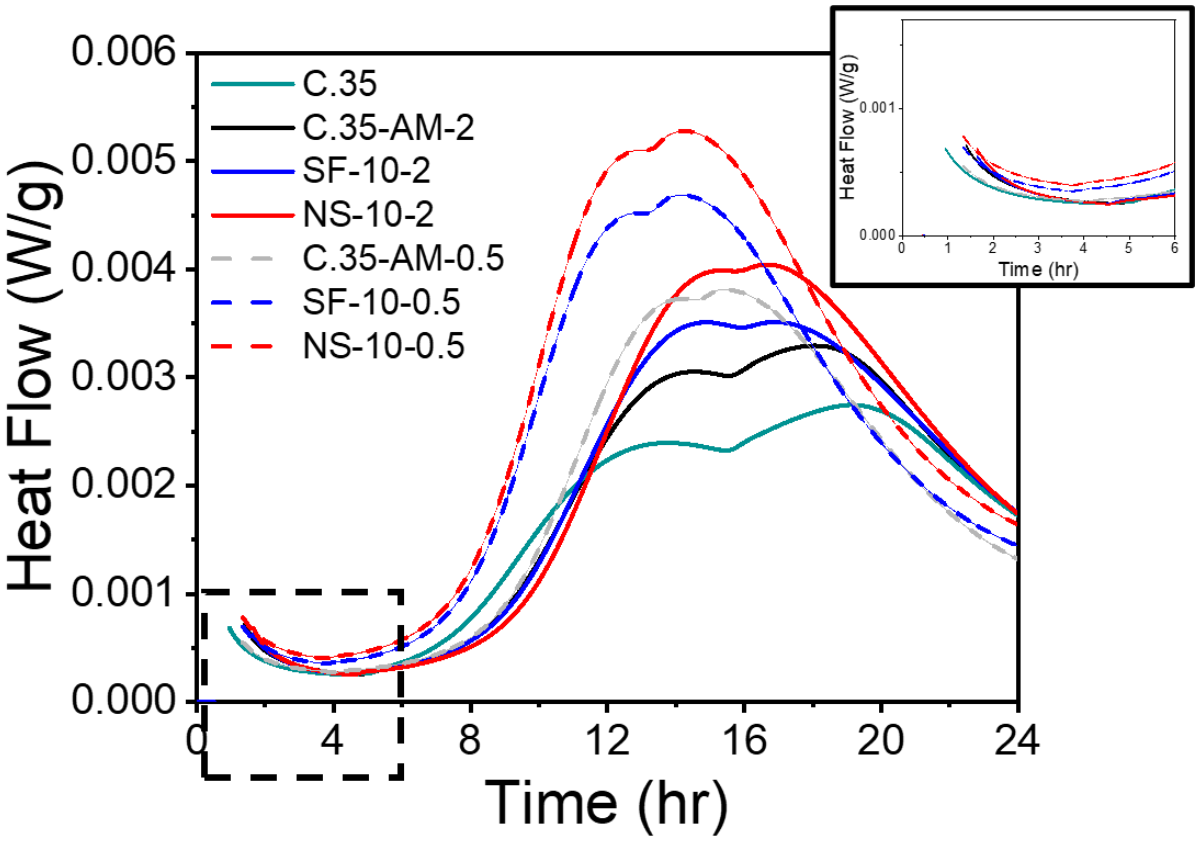

Figure 26: Hydration heat release rate from cement paste (24 hours) with composite silica-containing polyacrylamide hydrogel. For clarity, dashed lines represent cement paste with low crosslinked hydrogel particles while solid lines represent cement paste with high crosslinked hydrogel particles. For easier visualization, the first 6 hours after mixing are zoomed in.

The presence of high crosslinked hydrogel particles caused a slight delay in occurrence of main hydration peak, when compared to C.35. This behavior, although contradictory to the behavior of the lower crosslinked hydrogel particles used in this study, has been observed by previous researchers conducting isothermal calorimetry of SAP-cured pastes [118]. The delay in hydration peak that they observed in pastes containing SAP was attributed to SAP desorption kinetics and absorption of the alkali ions into the SAP. While the complexation of alkali ions from pore solution might retard hydration during early age, especially in pastes containing polyacrylic acid-rich SAPs, this is not expected to be a major concern for the present study. This is because

this study consisted of polyacrylamide hydrogels, which are less prone to complexation with cations present in pore solution. However, even if complexation with cation was not a major concern, there would still be some amount of alkali ions that enters the hydrogel particle due to the osmotic gradient. This would reduce the alkali ions in pore solution, though not by a significant amount as the rate of dissolution of ions in pore solution would eventually exceed the rate at which SAP particles absorb fluid. As such, a less prominent delay in hydration was observed when compared to previous literature on isothermal calorimetry of SAP [118]. This also seems to suggest that for the low crosslinked hydrogel particles, the acceleration of the hydration peak would imply that the lowering of the effective w/c due to the hydrogel's higher absorption capacity played a more important role than the removal of alkali ions from the pore solution. Again, this is unsurprising due to the composition of the hydrogel particles. Since the higher crosslinked hydrogels had a lower equilibrium absorption capacity, their effect at reducing w/c, and thus potential acceleration of the hydration peak was probably not as marked as the lower crosslinked hydrogels.

The presence of hydrogels caused an increase in height of the main hydration peak, when compared to the paste containing no hydrogel particles. Just et al. [118] observed that the height of the main peak increases with increasing w/c. This would imply that hydrogel particles had started releasing water at the end of acceleration period, thus increasing height of main peak. Water released by the hydrogels increased internal RH in paste to promote hydration. The height of the peak is indicative of the absorption capacity of the hydrogels, with the highest height observed for the two formulations with highest absorption capacity (NS-10-0.5 and SF-10-0.5). The release of the higher amount of stored water from the NS-10-0.5 hydrogel particles would cause a greater rise in height of peak.

Figure 27 shows the cumulative heat of cement paste for the duration of the experiment (48 hours). The pastes containing hydrogel particles reached a higher cumulative heat when compared to the reference paste (C.35) after 2 days. In fact, all the hydrogel containing paste samples displayed higher cumulative heat after 16 hours, when compared to the C.35 paste. Pastes with low crosslinked composite Si-containing hydrogel particles displayed the greatest cumulative heat, which is indicative of a greater total hydration. This result is consistent with the non-evaporable water content results obtained for this study (see Figure 17).

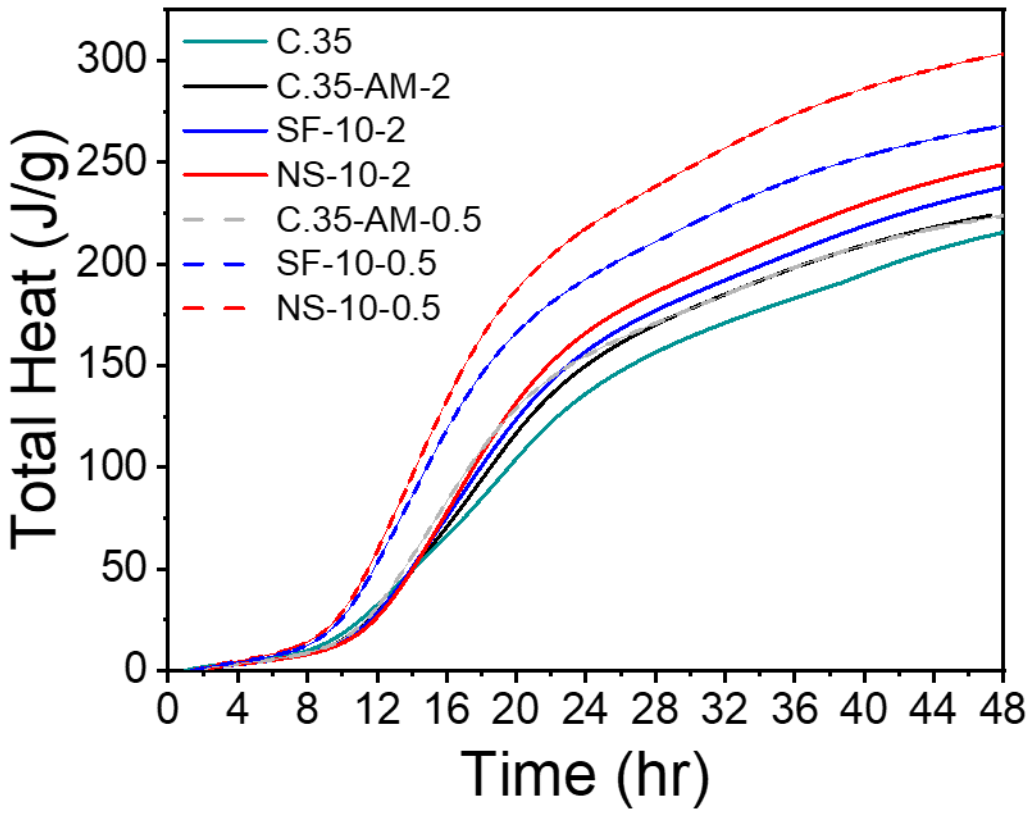

Figure 27: Cumulative heat of cement paste (48 hours) with composite silica-containing polyacrylamide hydrogel. For clarity, blue and red dashed curves represent cement paste with low crosslinked hydrogel particles while solid blue and red curves represent cement paste with high crosslinked hydrogel particles.

4.8 Compressive and Flexural Strength of Mortar

The evolution of compressive strength of mortar mixtures at various ages are shown in Figure 28. At early age (1 day), an improvement in strength was observed in mortars containing hydrogel particles, when compared to the reference mortar without any hydrogel particles in it (C.35), with the higher crosslinked hydrogels containing mortar undergoing statistically significant strength gain at a 95% confidence level. After 28 days, compressive strengths of all mortar mixtures were comparable to the reference mortar.

As shown in Figure 28, an initial strength gain was observed in internally cured samples, when compared to the reference mortar. For instance, the mortar mixture containing pure polyacrylamide hydrogel particles at 2% crosslink density (C.35-AM-2) displayed a statistically significant 32% increase in strength (p-value = 0.022), when compared to the reference mortar (C.35). This initial strength gain could be attributed to the lower effective w/c brought about by

the absorption of mixing water by the hydrogel particles (as no extra water was added to compensative for SAP absorption). The reduction in effective w/c would contribute to a lower capillary porosity and thus a higher strength. It is evident that the lowering of the effective w/c plays a more important role in influencing strength than the retardation effect due to higher dosage of WRA or the presence of macrovoids from hydrogel particles. Similar trends were observed in a study by Wyrzykowski et al. [119].

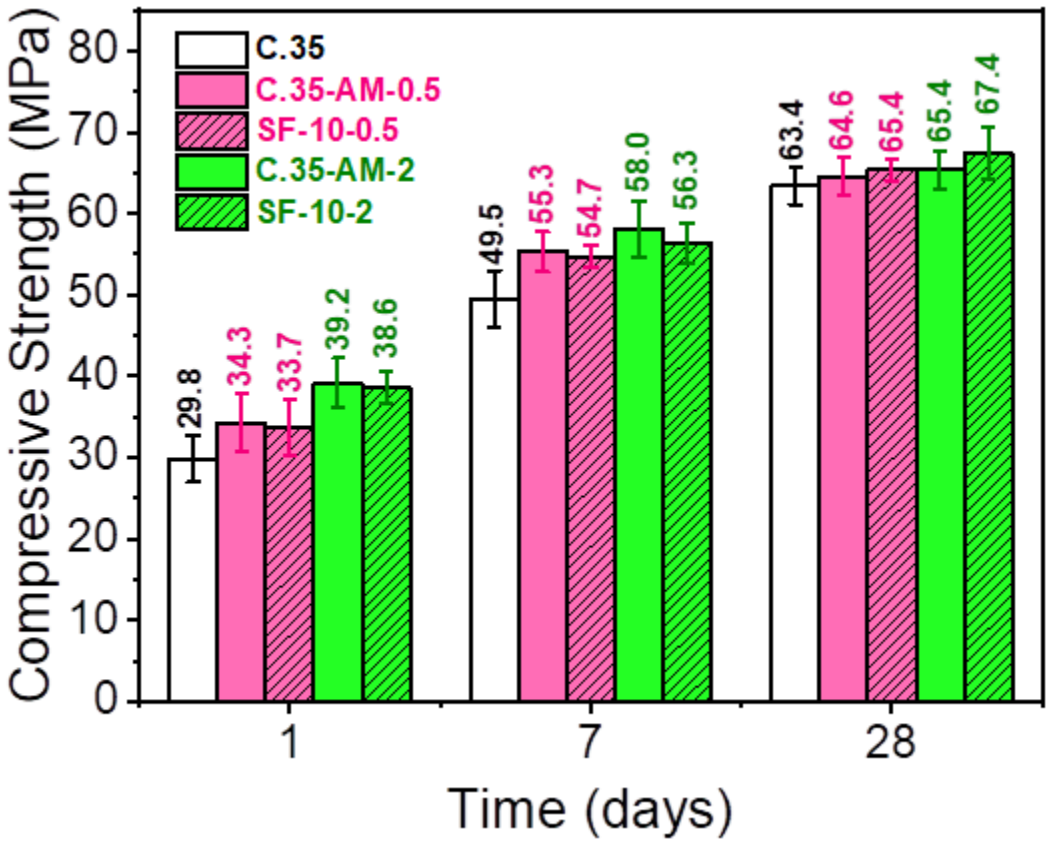

Figure 28: Compressive strength of mortar at 1, 7 and 28 days. The hatched bars denote mortars with composite silica-containing polyacrylamide hydrogel particles. The pink and green bars denote mortars with hydrogel particles with a crosslink density of 0.5% and 2% by weight of monomer, respectively.

A slightly higher strengths at 1 day were observed for mortar mixtures containing hydrogel particles with 2% crosslink density, than mortar mixtures containing hydrogel particles with 0.5% crosslink density. For instance, a 14% increase in 1 day strength was observed for C.35-AM-2,

when compared to C.35-AM-0.5. This increase in strength, although not statistically significant (p-value = 0.161), still gives useful insights to the strength development mechanisms of mortars containing different SAP formulations. As the equilibrium absorption capacity of AM-0.5 hydrogel particles were greater than that of AM-2, it is expected that the presence of AM-0.5 hydrogel particles would initially lower the effective w/c of mortars more than AM-2 would. However, AM-0.5 hydrogel particles are also expected to leave larger macrovoids (as seen in Table 12). It is possible that the presence of larger macrovoids voids plays a role in diminishing the strength gain due to lowering of effective w/c in the presence of hydrogel particles.

The addition of hydrogel particles did not have any significant impact on 28 days compressive strength. It implies that the improvement in hydration of the internally cured mortar mixtures balances out the negative effect on strength due to the presence of hydrogel-induced voids. Additionally, there were no major difference observed in strength at later ages due to the incorporation of different compositions of mortar mixtures.

Figure 29 shows the effect of presence of composite silica-containing polyacrylamide hydrogels on the flexural strength of mortar mixtures. Similar to compressive strength trends, higher early flexural strengths were observed in mortar mixtures containing hydrogel particles, although the standard deviations of flexural strength were larger. This is probably due to the fact that flexural strength is more sensitive to flaws in the sample due to the presence of hydrogel-induced voids.

The presence of hydrogel particles with higher crosslink density displayed a comparable flexural strength at both 1 and 28 days, when compared to mortars containing hydrogel particles with lower crosslink density. For instance, SF-10-2 displayed a 12% increase in 28-days flexural strength, when compared to SF-10-0.5, which is not statistically significant strength gain at 95% confidence level (p-value = 0.381). The number and size of macrovoids play an important role in the tensile fracture of cementitious systems. However, it seems that the extent of void-filling also plays a major role in influencing flexural strength. It is evident that the greater void filling observed in the microstructural analysis at least partially offset the larger size of the macrovoids in the hydrogel particles with lower crosslink density, and thus the flexural strength is comparable to mortars containing high crosslinked hydrogels.

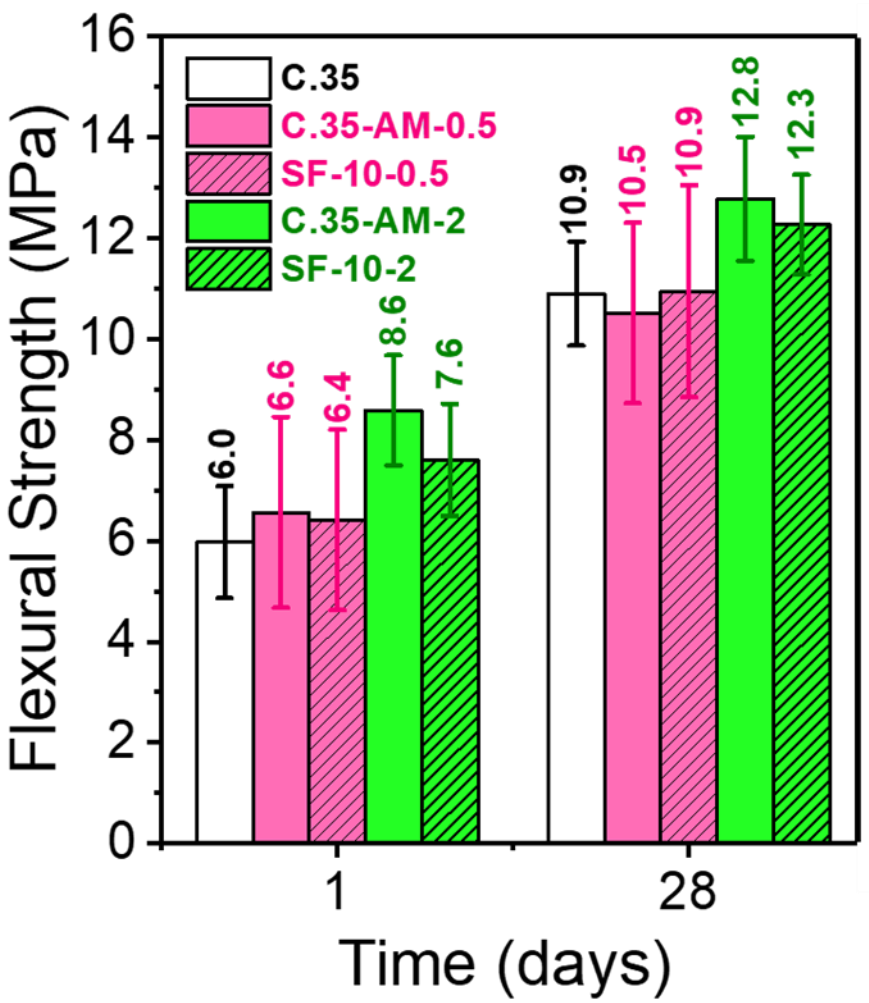

Figure 29: Flexural strength of mortar at 1 and 28 days. The hatched bars denote mortar containing composite silica-containing polyacrylamide hydrogel particles. The pink and green bars denote mortars with hydrogel particles with a crosslink density of 0.5% and 2% by weight of monomer, respectively.

From the compressive and flexural strength results, it can be concluded that addition of the hydrogel particles did not have any significant impact on 28-days mortar strength, although there was some improvement in 1 day strength. The presence of hydrogel particles influences evolution of strength over time in two ways: by improving hydration and thus refining the capillary pore structure, and by creation of hydrogel related voids as the water leaves the hydrogel particles. From the results obtained, it can be surmised that the composition of the synthesized hydrogels is such that the two factors mentioned above balances each other out, so that there is no significant impact on long term strength, when compared to the reference sample. Also, although a greater total hydration was expected from isothermal calorimetry analysis of cement paste with lower

crosslinked hydrogel particles at 1 day, the effect did not translate to an improvement in mechanical strength of mortars. This seems to suggest that the size of the macrovoids due to SAP's presence influences mechanical strength to a greater extent than the improvement in hydration due to the greater absorption capacity of the lower crosslinked hydrogels.

4.9 Autogenous shrinkage of mortar

The autogenous shrinkage results for mortar specimens are shown in Figure 30. Addition of hydrogel particles resulted in reduction of the autogenous shrinkage strains of the mortars, when compared to the reference mortar without any hydrogels in it. A higher reduction was observed in low crosslinked hydrogel particles, when compared to the high crosslinked hydrogel particles.

Mortars with low crosslinked composite Si-containing hydrogels underwent the least amount of autogenous shrinkage strain, during the duration of the experiment. This could be due to the fact that of the hydrogels used for this study, SF-10-0.5 had the highest equilibrium absorption capacity and thus the capability to retain and release higher amount of water as the matrix began experiencing autogenous shrinkage. This is consistent with the results obtained for autogenous shrinkage of mortars with the high crosslinked hydrogels, which displayed some amount of mitigation of the shrinkage strains, though not quite as effectively as the low crosslinked hydrogels.

The presence of SF in the composite hydrogels did not impact the ability of the hydrogels to reduce autogenous shrinkage strains. For instance, SF-10-2 was more effective in reducing autogenous shrinkage of the mortar, when compared to AM-2. If the SF from the composite hydrogels were able to cause a global pozzolanic activity, this would have resulted in an increase in autogenous shrinkage of the silica-containing hydrogels, when compared to the same composition silica free polyacrylamide hydrogels. Use of SF in the mortar mixing (instead of in the hydrogel synthesis as was done in the present study) has been seen to cause an increased autogenous shrinkage of mortars by previous researchers [120]. In the present study, the silica dosage used in the composite hydrogel amounts to less than 0.005% by weight of cement, and thus it is not surprising that the SF-containing hydrogels do not impart any global pozzolanic effect. This result is consistent with the thermogravimetric analysis data obtained for this study (see Figure 24). Additionally, just after setting, there is a small expansion observed in some mortars.

Previous researchers have hypothesized that this could be due to several different mechanisms including crystallization pressure of portlandite [121].

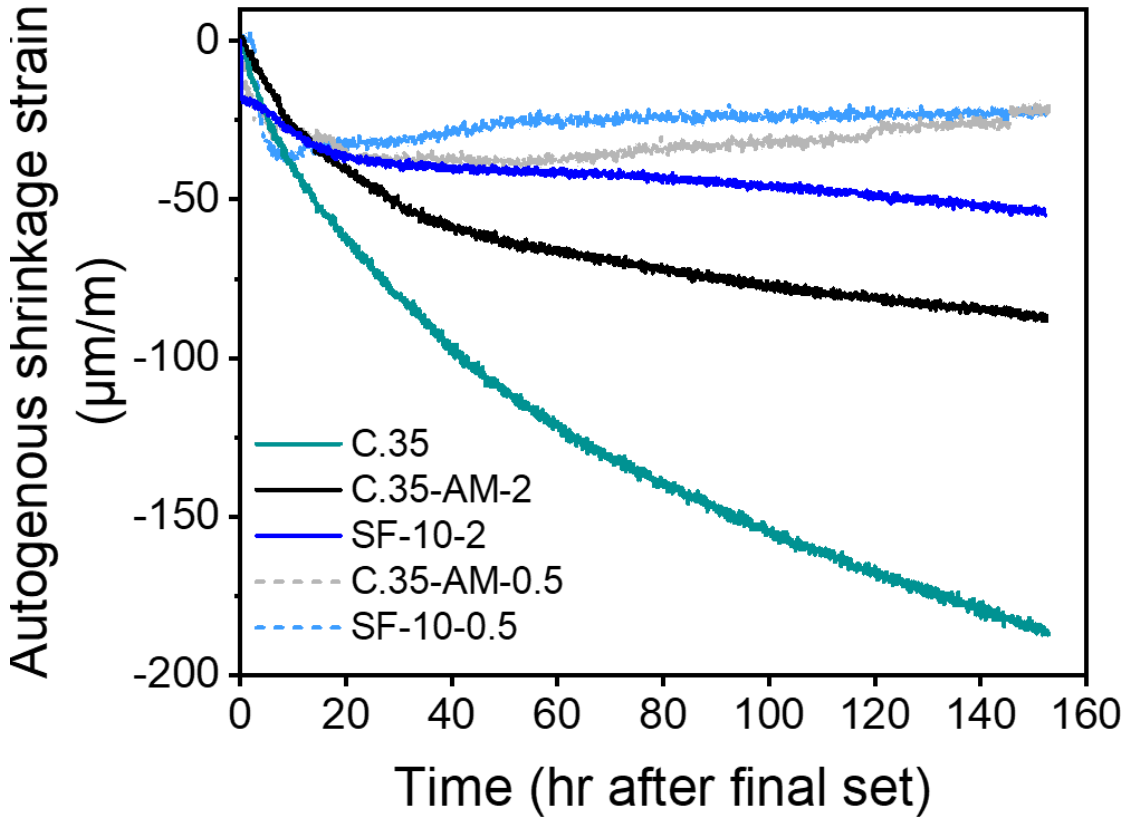

Figure 30: Autogenous shrinkage of mortar internally cured with composite Si-containing hydrogel particles.

4.10 Conclusion

Composite polyacrylamide hydrogel particles containing silica led to better hydration of internally cured cement paste compared to silica-free hydrogel particles. The main findings were as follows:

- Equilibrium free absorption capacities of composite hydrogels with low crosslink density and higher silica dosage were greatest among the hydrogels studied. This was attributed to the silica facilitating water absorption and the lower crosslink density allowing the polymer molecules more degrees of freedom, leading to increased swelling.

- For pastes including composite hydrogel particles with higher dosage of silica and higher crosslink density, the compressive strength and electrical resistivity increased substantially at later ages compared to hydrogel-free pastes and pastes containing silica-free hydrogel particles, also consistent with the increase in non-evaporable water content.
- The microstructure analysis of internally cured cement paste showed that some of the hydrogel-induced voids were filled with hydration products after 3 days. This "void-filling" phenomenon was more extensive in pastes cured with composite hydrogel particles with low crosslink density and higher dosage of silica. These samples also displayed the largest average diameter of hydrogel-induced voids.
- The size of the hydrogel-induced void appeared to play a more important role in determining compressive strength at later ages than the local microstructure refinement due to void-filling. However, results indicated that strength reductions due to larger void sizes may be at least partially off-set by the growth of hydrated product within the voids, which was enhanced by the presence of silica in the hydrogel particles.
- An improvement in total cumulative heat was observed in paste containing hydrogel particles, indicating greater hydration of the cement paste cured with the synthesized hydrogels. Greater amount of hydration was observed for pastes with low crosslinked composite Si-containing hydrogel particles using both isothermal calorimetry and non-evaporable water content studies.
- Presence of hydrogel particles had no significant impact on 28 days compressive and flexural strength of mortars, although an improvement in early age strength was observed in mortar mixtures internally cured with the composite Si-containing hydrogel particles.
- Autogenous shrinkage of mortars was significantly reduced in presence of the hydrogel particles. Mitigation of autogenous shrinkage was more prominent in samples containing hydrogel particles with low crosslink density.
- Overall, for the acrylamide-based hydrogels that were synthesized in this study, the selection of silica type – nanosilica or silica fume – did not play as strong a role in defining hydrogel absorption behavior (and thus internal curing performance) as the magnitude of crosslink density within the polymer network.

From this study, it is clear that the relationship between extent of hydration, void size, and void-filling activity will strongly influence long-term strength and is thus an important structure-property relationship to consider when selecting SAPs for internal curing purposes. From a practical perspective, the incorporation of silica within the hydrogel's polymer network allows for supplementary cementitious materials to be incorporated in a novel manner without undue health hazards associated with nanomaterials. And a greater dosage of silica may be used in the future to enhance pozzolanic reactions and further increase the quality of the concrete internally cured with composite hydrogel particles. This research also found that the crosslink density of polyacrylamide networks can be specifically manipulated to ensure that acrylamide-rich SAPs achieve sufficient absorption capacities and can thus be effective internal curing agents.

5. INFLUENCE OF COMPOSITE RETARDING ADMIXTURE-CONTAINING HYDROGEL PARTICLES ON CEMENTITIOUS SYSTEMS

5.1 Characterization of composite retarding admixture-containing hydrogel particles

5.1.1 Absorption capacity of hydrogel particles

Figure 31 shows the absorption capacity of the hydrogel particles synthesized for this study in RO water. Compared to the pure AM particles, the addition of CA resulted in greater absorption in RO water. At equilibrium (3 days), the presence of CA caused an increase of 10% and 12%, respectively for the washed and unwashed hydrogel particles. Presence of sucrose resulted in greater increase in absorption capacity of the hydrogel particles, when compared to AM particles. Addition of sucrose increased the absorption capacity by 39% and 42% for washed and unwashed hydrogel particles, respectively.

As depicted in Figure 31, the S-20-2-unwashed hydrogel particles displayed the greatest absorption capacity in RO water. The presence of eight hydroxyl groups (O-H), along with hydrogen atoms and hydrophilic oxygen atoms present in sucrose will contribute towards hydrogen bonding with water molecules, thus enhancing the intake of water into the AM network. This idea is consistent with the lower absorption capacity observed for the CA-containing hydrogel particles, since the number of hydroxyl groups present in CA is less than the number present in sucrose, which decreases the potential sites for formation of hydrogen bonds with water. The total number of hydrophilic groups present in both CA and sucrose are greater than the number of hydrophilic functional groups in AM, which might explain why both the composite hydrogel particles have higher swelling capacity than that of pure PAM hydrogels.

The unwashed hydrogel particles displayed slightly higher equilibrium absorption capacity than the unwashed hydrogels. For instance, S-20-2-unwashed had 2% higher absorption capacity when compared to S-20-2-washed. This could be due to the fact that during the “washing” step in the post-synthesis process, some of the retarding admixture got dissolved in the DI water and was able to escape the AM network. More detailed insights into this phenomenon could be obtained from comparing peak intensities of the “washed” and “unwashed” hydrogel particles during FTIR analysis. However, since the changes in equilibrium absorption capacity of the washed and

unwashed hydrogel particles of each composition was less than 3%, it was assumed that a significant amount of the retarding admixture remained within the network even after undergoing the "washing" step during post-synthesis procedure.

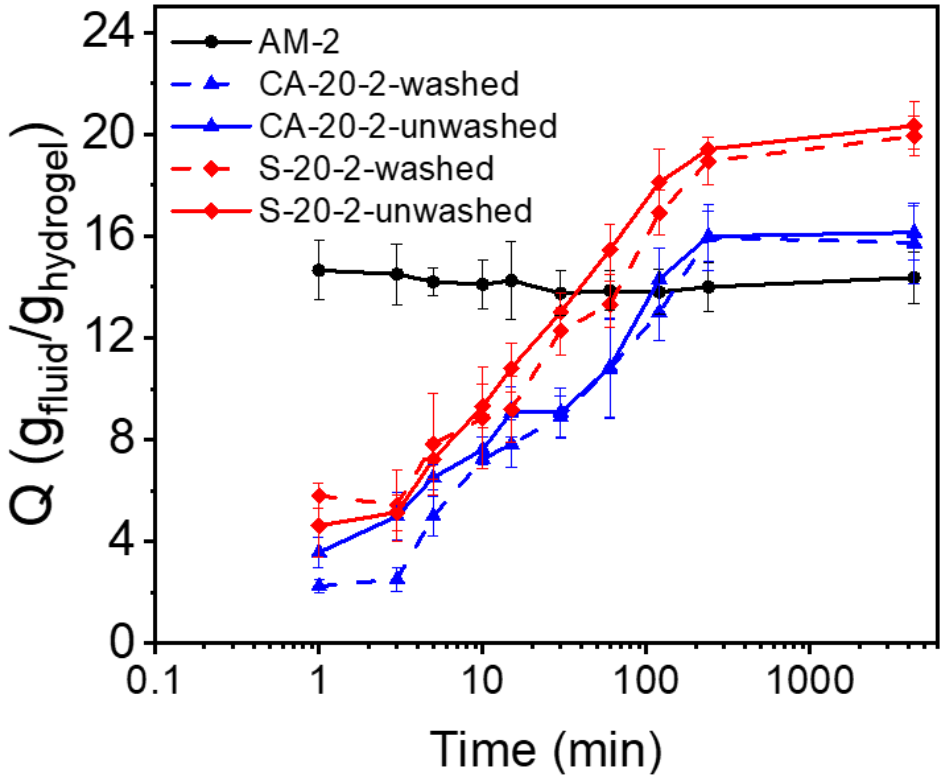

Figure 31: Absorption capacity of hydrogel particles as a function of immersion time in RO water.

5.1.2 Thermogravimetric analysis of hydrogel particles

Figure 32 shows the curves obtained for thermogravimetric analysis of S-20-2-washed and AM-2 hydrogel particles. The AM-2 sample displayed significant weight loss in three separate regions, which are well documented in literature on TGA of polyacrylamide [105], [106]. At temperatures less than 220°C, the weight loss observed was attributed to evaporation of water. Although the hydrogel particles were kept in sealed conditions until the time of testing, there were still some water molecules that adsorbed onto the hydrogels. The second region of weight loss corresponded with the decomposition of the amide group from 220-340°C. The third region of

weight loss was in the range 340-430°C, which previous researchers attributed to PAM chain scission.

The composite hydrogel particles also displayed weight loss peaks in the same three regions that are characteristic of PAM. Based on thermogravimetric analysis of sucrose, thermal decomposition of sucrose is expected to occur mainly in the 220°C to 324°C range, which is where the gradient of the S-20-2-washed hydrogels start a sharp decline, indicating greater weight loss than the AM-2 sample. By calculating the difference in weight loss between the S-20-2-washed and AM-2 curves in the 220°C to 324°C is 7.5%. The expected amount of sucrose in the polymer is 5.66%.

From previous literature on thermogravimetric analysis of citric acid, it was seen that major decomposition occurs in the 150–220°C range [122].. Although a sharp decline in weight loss was observed in the CA-20-2-washed sample in the 200-340°C range, this was probably due to decomposition of both CA and amide group. The difference in weight loss of the CA-20-2-washed and AM-2 in the 150-220°C range is 7.0%, which might probably account for the dosage of CA present in the composite hydrogels. The expected dosage of CA based on the yield of the polymer after synthesis is 6%. The 1% difference might be caused by some impurities or other reagents used during the synthesis process that might have decomposed in the same temperature range (initiators, crosslinkers, impurities in CA).

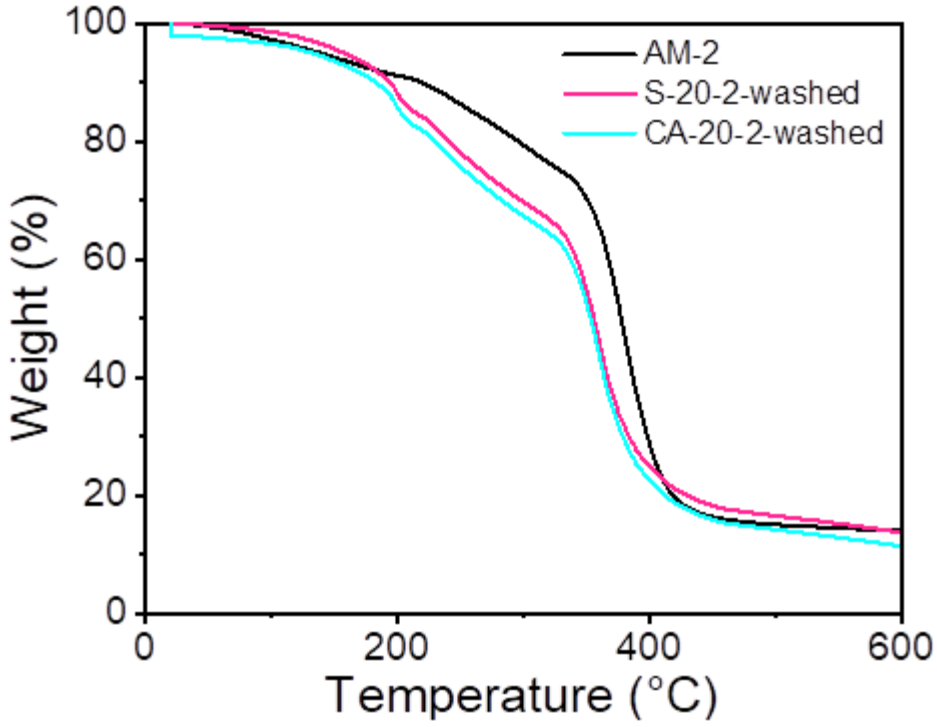

Figure 32: Thermogravimetric analysis of composite retarding admixture-containing hydrogel particles.

5.1.3 FTIR analysis of hydrogel particles

During the infrared spectroscopy analysis, absorption of energy at particular wavelengths is caused by the presence of specific functional groups. The re-transmission of the energy gives rise to the peaks seen in the spectra. The FTIR spectra of AM-2 synthesized for this study is shown in Figure 33. The peak seen at 3340 cm^{-1} is attributed due to the N-H asymmetric stretching. Additionally, the absorption band observed at 1602 cm^{-1} corresponds to the N-H bending. These, along with N-H symmetric stretching observed at 3187 cm^{-1} is characteristic of the amide group in the polyacrylamide hydrogel particles used for the analysis [123]. The peaks at 1646 cm^{-1} was assigned to the vibration of the C=O stretching [124]. Similar peaks were observed in a previous study of FTIR spectra of polyacrylamide in pure water [125]. The narrow and weak absorption band at 2926 cm^{-1} was attributed to the stretching vibrations of C-H [124], [126]. This peak has been seen in previous researches on polyacrylamide-based hydrogels [127].

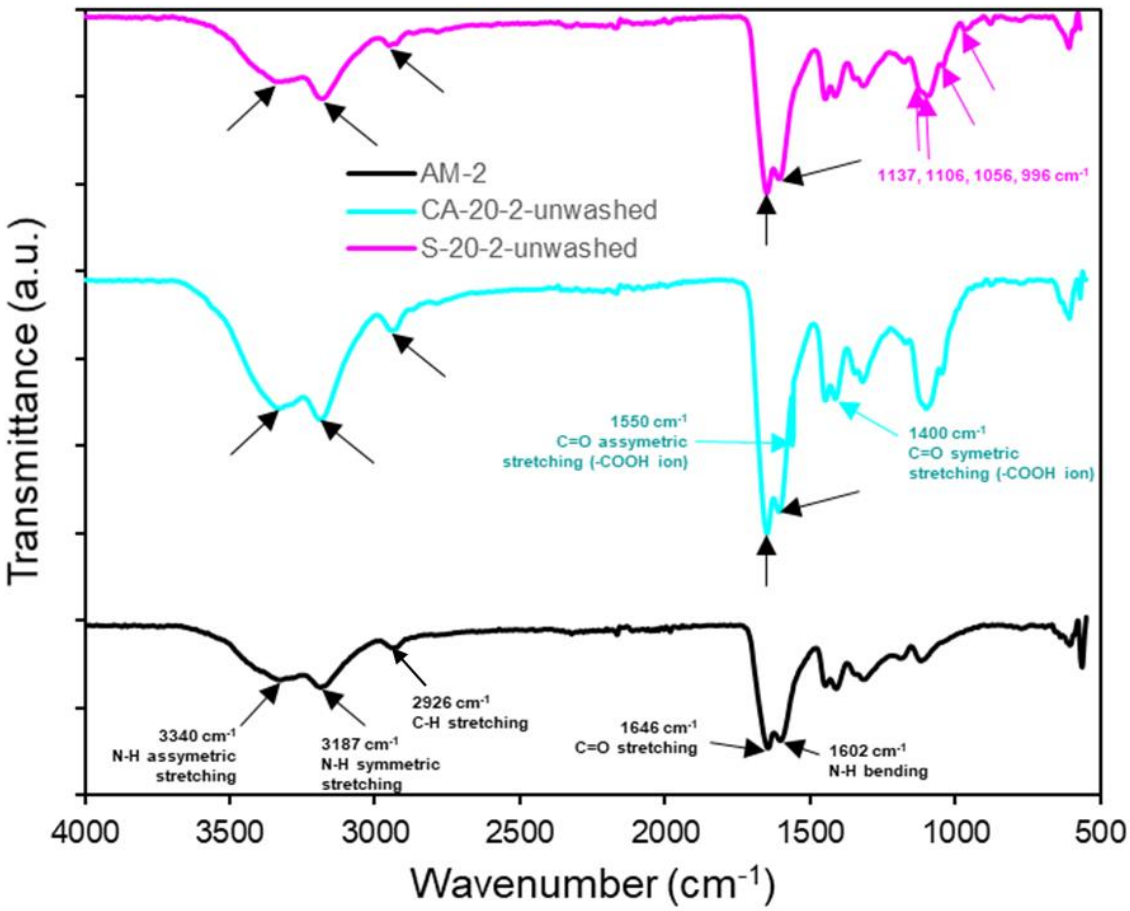

Figure 33: FTIR spectra of synthesized hydrogel particles. Black arrows show peaks due to functional groups associated with acrylamides. Teal and pink arrows show peaks due to the presence of functional groups characteristic of CA and sucrose, respectively..

The FTIR spectra obtained from the composite CA-containing polyacrylamide hydrogel particles is also shown in Figure 33. The absorption bands detected at 1649, 1602 and 3325 cm^{-1} are due to the C=O stretching, N-H bending, N-H stretching of the amide group, respectively. These are typical peaks due to the presence of the $–CONH_2$ group in acrylamide [125]. These peaks are similar to the characteristic bands observed for the AM hydrogel particles. The sharp peak obtained at 1550 and 1400 cm^{-1} are attributes of the asymmetric and symmetric stretching of C=O in the carboxylate anion [124], [128]. These peaks are probably indications of the successful incorporation of citric acid to the hydrogel synthesis procedure.

FTIR spectra for composite sucrose-containing hydrogel particles are shown in Figure 33 in pink. The spectral bands observed at 1650, 1602 and 3325 cm^{-1} are characteristic of the presence of amide group, as has already been discussed in the previous paragraphs. Additionally, peaks at

1137, 1106, 1056 and 996 cm^{-1} were observed, which are documented in literature as characteristic bands due to the presence of sucrose [129]. The bands at 996, 1056 and 1137 cm^{-1} were not observed in the AM sample that was analyzed using FTIR (see Figure 33)

5.2 Isothermal calorimetry of cement paste containing composite hydrogel particles

Results obtained from isothermal calorimetry analysis of cement paste with composite CA-containing admixtures are presented in Figure 34. Compared to the reference paste containing no hydrogel particles (C.35), all other paste samples displayed a delay in the main hydration peak, although the delay observed in the CA-20-2 pastes were in similar amount to that observed for C.35-AM-2 (Figure 34a). The total heat curves indicate that all the pastes containing hydrogel particles underwent a comparable amount of total hydration to that of the reference paste without any hydrogel particles in it.

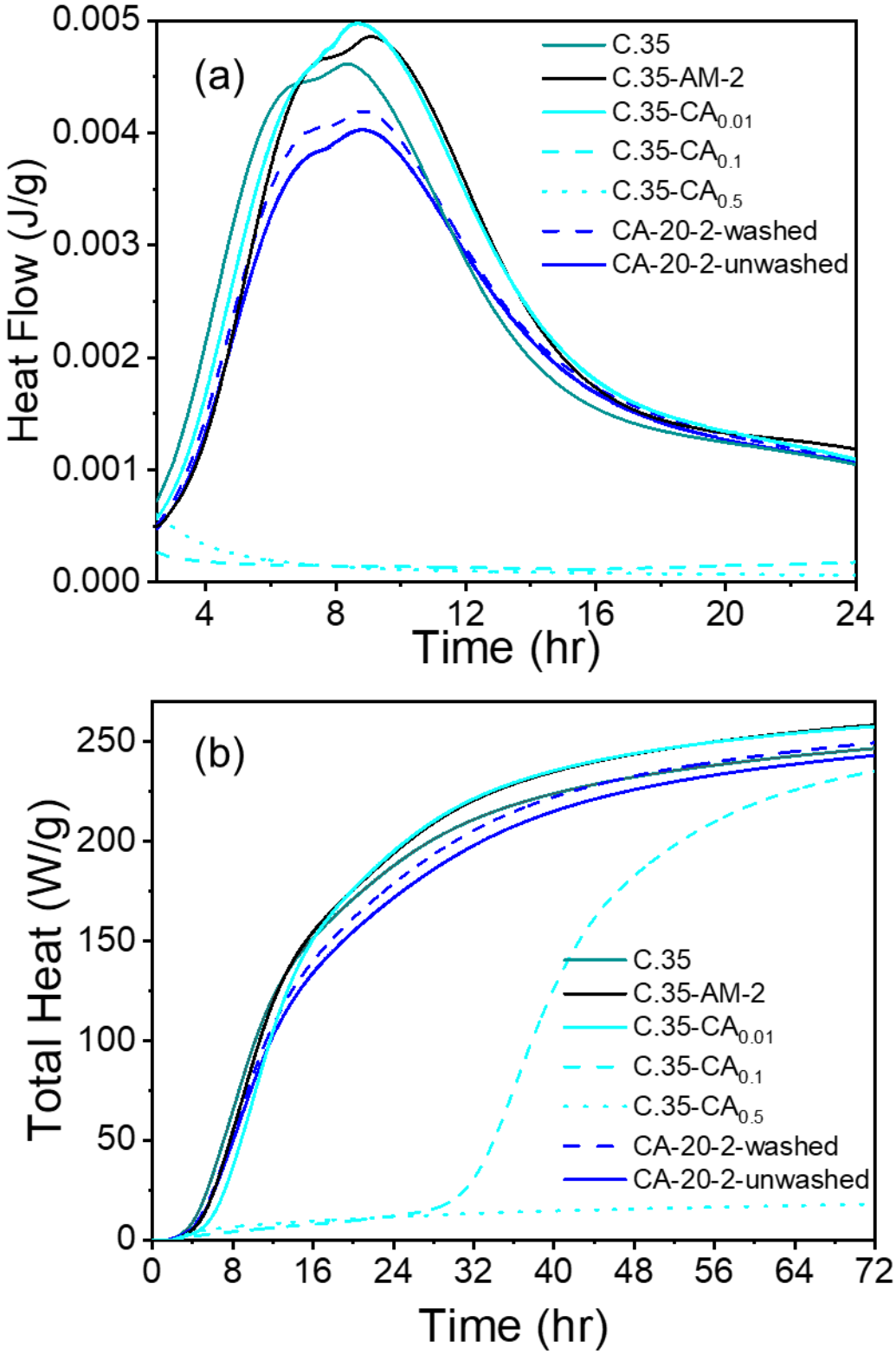

Figure 34: Isothermal calorimetry of cement paste showing the effect of CA and PAM (a) Hydration heat release rate (until 24 hours) and (b) cumulative heat (until 72 hours).

A small delay of the main peak of hydration for paste containing hydrogel particles were observed when compared to the reference paste (~1 hour). Similar results were obtained by previous researchers conducting isothermal calorimetry analysis on SAP-containing pastes [118], [130]. Addition of CA delayed the main hydration peak, with the delay becoming more prominent with increasing dosage of CA. In fact, the main hydration peak was not observed within 24 hours for the pastes containing CA dosages of 0.1% and 0.5% by weight of cement. CA has been observed to retard the hydration peaks in previous researches too, although a 0.1% dosage has been seen to accelerate hydration [80].

The delay in main hydration peak observed for the two CA-20-2 paste samples were comparable to the C.35-AM-2 paste sample. This implies that presence of citric acid did not significantly impact the ability of the composite hydrogel to retard cement hydration. The C.35-$CA_{0.01}$ paste also displayed the main hydration peak to approximately the same time as that of the paste containing composite hydrogels. It is possible that while presence of same dosage of CA in the paste delayed the hydration slightly, the presence of CA in the hydrogel network could only impact hydration kinetics around the hydrogel particles.

The presence of CA in the hydrogel network is expected to influence hydration through two separate mechanisms. First, the composite CA-containing hydrogel's increased swelling capacity when compared to the AM-2 hydrogels would cause an acceleration in the hydration. This is because with higher absorption capacity of the hydrogels, more water is removed from the system. High alkali concentration accelerate hydration of cement, and this effect is enhanced at lower w/c [130]. However, the presence of CA in the hydrogel particles would delay the hydration by adsorption onto the cement grains. This effect would negate any potential acceleration caused by the increased absorption capacity of the hydrogel, thus the paste containing composite hydrogels displayed peaks at similar times to that of C.35-AM-2. Also, no significant difference in observance of main peak of hydration was observed due to the utilization of washed composite hydrogels instead of unwashed hydrogels. This is not surprising since the absorption capacity of the two composite hydrogels were similar.

Isothermal calorimetry analysis of cement paste with composite sucrose-containing admixtures are presented in Figure 35. Compared to the reference paste containing no hydrogel particles (C.35), all other paste samples displayed a delay in the main hydration peak. Pastes containing composite hydrogels displayed a slightly greater delay in main hydration peak, when

compared to the C.35-AM-2 and C.35 paste. Addition of sucrose delayed the main hydration peak, with the delay becoming more prominent with increasing dosage of sucrose. Similar to the pastes containing CA, the main hydration peak was not observed within 24 hours for the pastes containing sucrose dosages of 0.1% and 0.5% by weight of cement.

Presence of sucrose in the composite hydrogels were successfully able to delay the hydration peak by a greater amount, when compared to the C.35-AM-2 paste. This implies that the presence of sucrose was successfully able to further retard the hydration of the cement paste, beyond the capabilities of the pure AM-2 alone. In fact, the delays in hydration peak of the composite sucrose-containing hydrogels are similar to that obtained for the C.35-$S_{0.01}$ paste, which had the same dosage of sucrose as that incorporated in the composite hydrogels synthesized for this study. Another interesting observation was that exotherm of the main hydration peak dropped proportionally to the extension of the induction period when comparing the two pastes with composite sucrose-containing hydrogels to C.35-AM-2 pastes. Similar observations were made by Juenger et al. when utilizing higher dosage of sucrose to cement paste [73]. Thus, even at the low dosage of sucrose used in the composite hydrogel synthesis of this study, they were successfully able to retard the main hydration peaks. Total heat of hydration curves indicate that all the pastes containing hydrogels underwent similar total hydration and were comparable to that of the reference without hydrogel particles (Figure 35b).

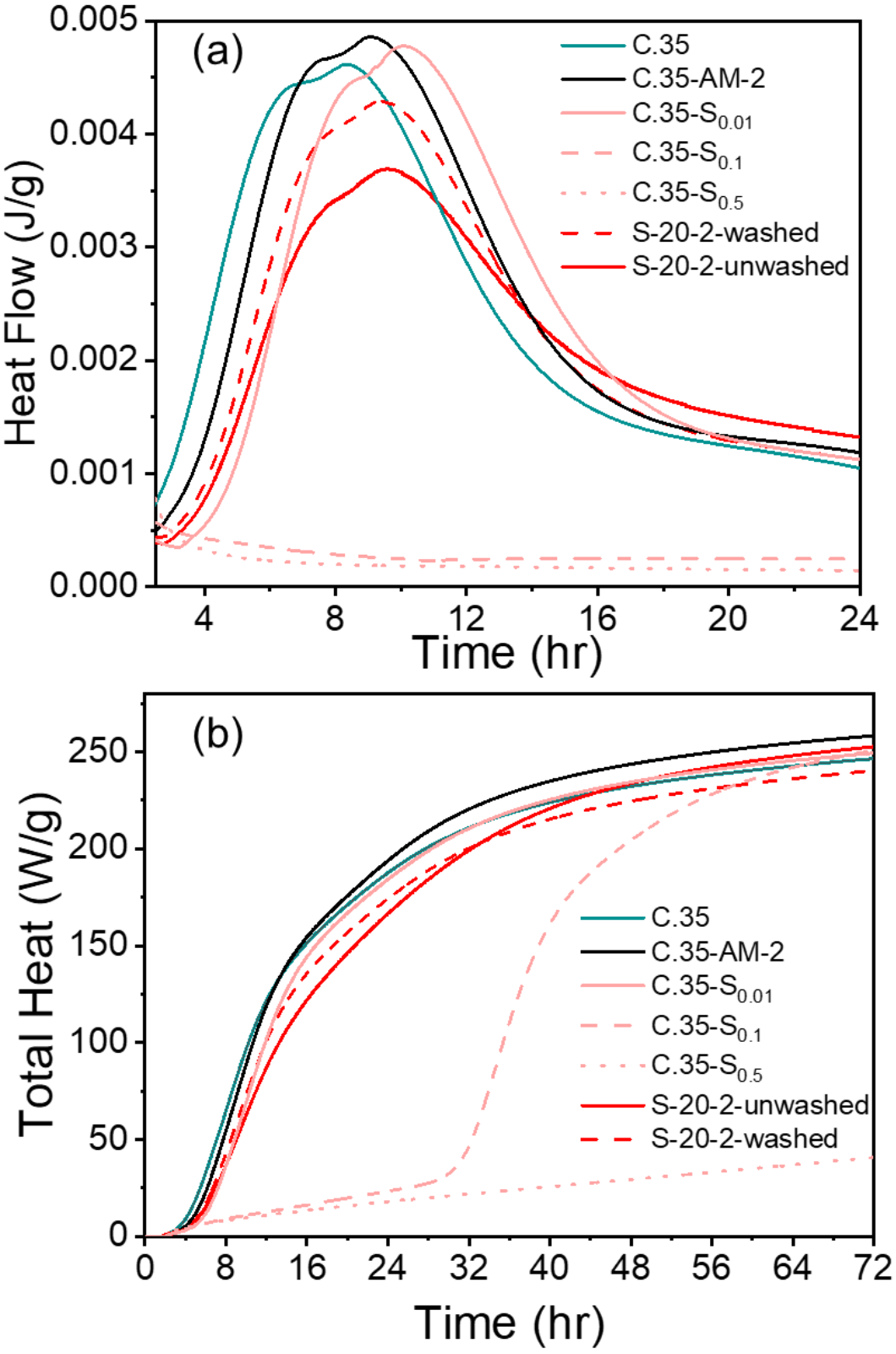

Figure 35: Isothermal calorimetry of cement paste showing the effect of sucrose and PAM (a) Hydration heat release rate (until 24 hours) and (b) cumulative heat (until 72 hours).

5.3 Conclusion

Composite polyacrylamide hydrogel particles containing retarding admixtures were synthesized for this study to investigate their potential influence on retarding the hydration of cement paste. The main findings were as follows:

- Free equilibrium absorption capacities of composite hydrogels with sucrose was the greatest among the hydrogels studied. This was attributed to the functional groups present in sucrose that would facilitate hydrogen bonding, leading to increased absorption of fluid when compared to pure polyacrylamide hydrogel particles.
- FTIR analysis of the composite hydrogels revealed the presence of CA and sucrose in the composite CA- and sucrose-containing polyacrylamide hydrogels, respectively. Thermogravimetric analysis was utilized to estimate the retarding admixture present in the dry composite hydrogels after synthesis.
- Isothermal calorimetry analysis of cement paste containing the composite hydrogels revealed that presence of sucrose in the hydrogel particles successfully delayed the main hydration peak, beyond the retardation capabilities of pure polyacrylamide hydrogels alone.
- Overall, washing the composite hydrogels during post-synthesis processing did not have a significant impact on the absorption capacity of the hydrogel particles, indicating that the retarding admixtures did not leave the network during this step.

From this study, it was seen that it is possible to custom synthesize SAPs to fine tune their ability to alter hydration peaks and thus setting time of cement paste. This would allow for specific formulations to be utilized in areas where there is a need for increased amount of transportation or placement times. In future, a higher dosage of sucrose could be utilized in the hydrogel synthesis process to further enhance the delay in main hydration peaks observed. Also, utilization of accelerating admixtures (such as calcium chloride or sodium nitrite etc.) in the composite PAM synthesis could be explored to investigate synergistic effect of early hydration due to presence of SAPs and the accelerating admixture dosage in the composite hydrogels.

6. EARLY AGE PERFORMANCE OF COMMERCIALLY AVAILABLE SAPS IN CEMENTITIOUS MATERIALS

6.1 Characterization of SAP particles

Scanning electron microscopy (SEM) images of dry SAP particles are shown in Figure 36. Here, the expression "dry SAP particles" refers to the state of SAP as received and stored in a sealed container at room temperature until testing. Both SAPs were composed of particles with irregular shapes. The dry particle size of the LA and HA SAP were calculated to be 116.0 ± 70.0 μm and 48.9 ± 21.9 μm, respectively. These average sizes were obtained by analyzing the SEM images of about 100 particles using ImageJ software.

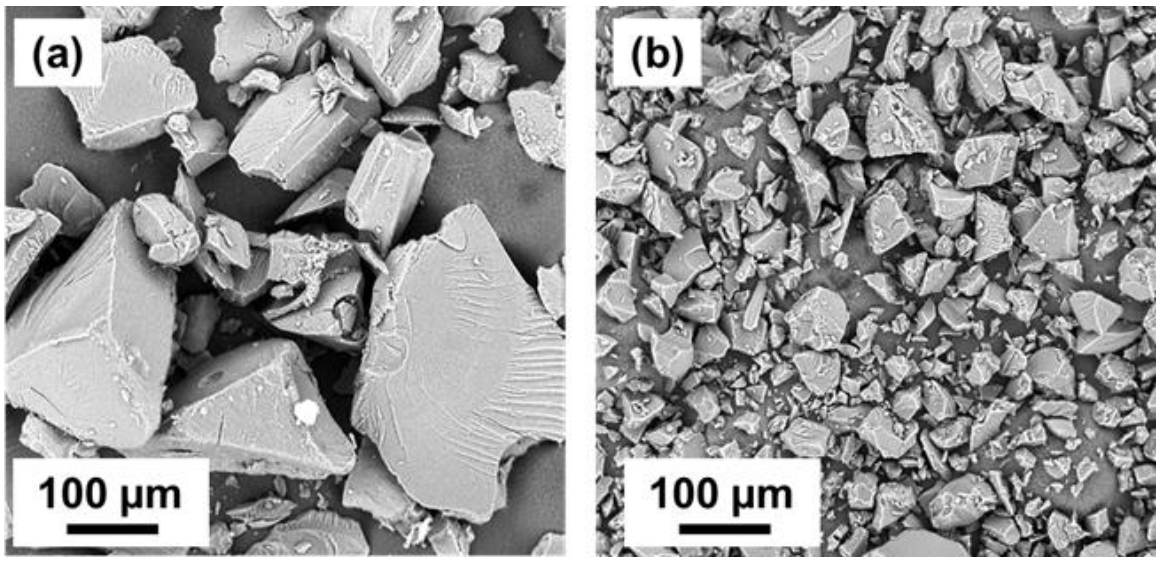

Figure 36: SEM images of the (a) LA and (b) HA dry SAP particles used in the experiments.

The absorption capacity of the LA and HA SAP particles in pore solutions of different compositions are shown in Figure 37. The tests were denoted as X+Y where X and Y represents the binder used to create the pore solution and type of SAP particles, respectively. For instance, B Type I+Slag+LA represents absorption capacity tests conducted using LA SAP particles in pore solution comprising of Buzzi Type I cement and slag. The absorption capacity tests indicate that pore solution composition had less influence on the LA SAP particles, when compared to the HA SAP particles.

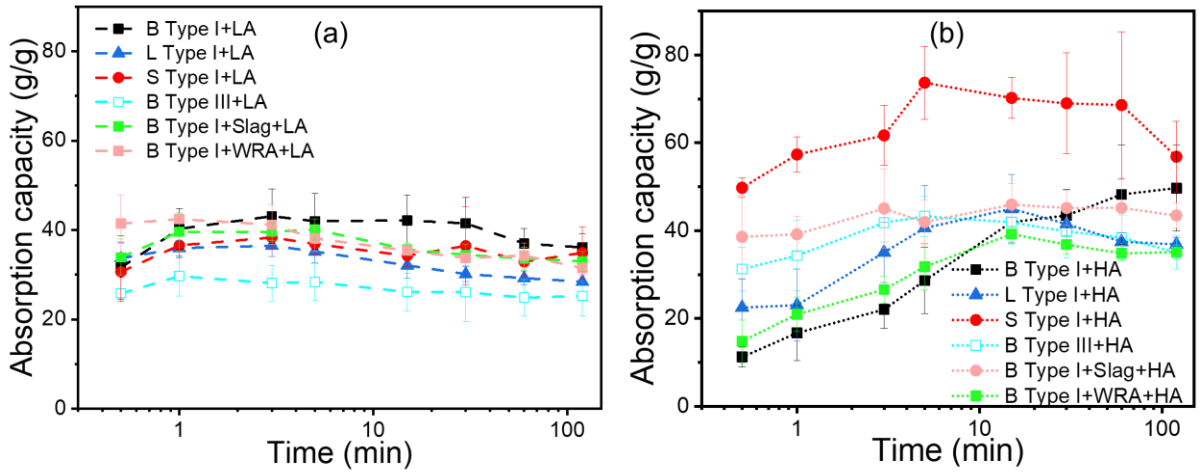

Figure 37: Absorption capacity of (a) LA and (b) HA SAP particles as a function of immersion time in pore solution. For clarity, square, triangle, and round symbols denote Buzzi Unicem, Lehigh and St. Mary's Type I cement, respectively. Absorption capacity of the LA and HA SAP particles are plotted using dashed and dotted lines, respectively.

After the first 30 minutes of exposure to the B-Type I pore solution, the LA SAP particles had a significantly (~30%) lower equilibrium absorption capacity compared to HA SAP particles. While SAP compositions are unknown, it has been demonstrated previously that either an increase in anionicity [25] or increase in crosslinking density will decrease the equilibrium absorption capacity of SAP [40], [46]. In addition, the initial absorption kinetics for the first few minutes indicate that the LA SAP particles absorbed fluid more rapidly than the HA SAP particles even though the HA SAP particles were of smaller average size. While insights into this phenomenon are not possible without information regarding SAP composition, it has been seen in the past that smaller particles generally absorb more quickly [40]. However, it is also possible that the smaller average size of the HA SAP particles gave rise to a phenomenon known as "gel blocking" where the flow of water into the teabag is physically blocked as the small particles aggregate and swell [131].

The varying composition of the pore solution had less impact on the absorption capacities of LA SAP particles, when compared to the HA SAP particles. In fact, a closer look at the equilibrium absorption capacities (at 2 hour) indicates that the upper and lower equilibrium absorption capacities obtained for LA SAP particles only differs by a 30%. It has been shown by previous Erk group research that the increase in acrylamide content in the SAP composition would result in lesser vulnerability to pore solution composition [25], [43], [104]. The lowest absorption

capacities of LA SAP particles obtained for the B Type III pore solution can easily be explained by the fineness of Type III cement, which was highest of the four different cement compositions used in this study. The higher fineness of the cement grains would allow dissolution more quickly, and thus the pore solution would contain greater concentrations of alkali ions. Greater amount of alkali ions present in the pore solution of the gravimetric test would result in greater complexation with the polymer backbone, thus resulting in overall lower absorption capacities.

The difference in pore solution composition had a greater effect on HA SAP particles, when compared to the LA SAP particles. First, a desorption behavior was observed for HA SAP particles in some compositions of the pore solution after 5 minutes. For instance, a 23% reduction in equilibrium absorption capacity (at 2 hours) was observed for the S Type I+HA sample, when compared to the absorption capacity at 5 minutes. This could be due to the presence of higher amount of acrylic acid in HA SAP particles, when compared to LA SAP particles. Second, it was seen that HA SAP particles in S Type I pore solution displayed the highest absorption capacities, of the pore solution compositions studied. This could be because St. Mary's cement had the lowest fineness of the different cements used in this study.

6.2 Characterization of mortar

6.2.1 Autogenous shrinkage of mortar

Autogenous shrinkage of mortars at 0.42 w/c is shown in Figure 38. The presence of SAP particles reduced autogenous shrinkage of SAP-cured mortars, when compared to the reference mortar (B Type III_No SAP_0.5_0.42). Type I mortars did not experience any significant autogenous shrinkage strains. Also, it was interesting to note that HA SAP particles were more successful in mitigating autogenous shrinkage of mortars, and this effect is particularly pronounced in Type III cement mortars.

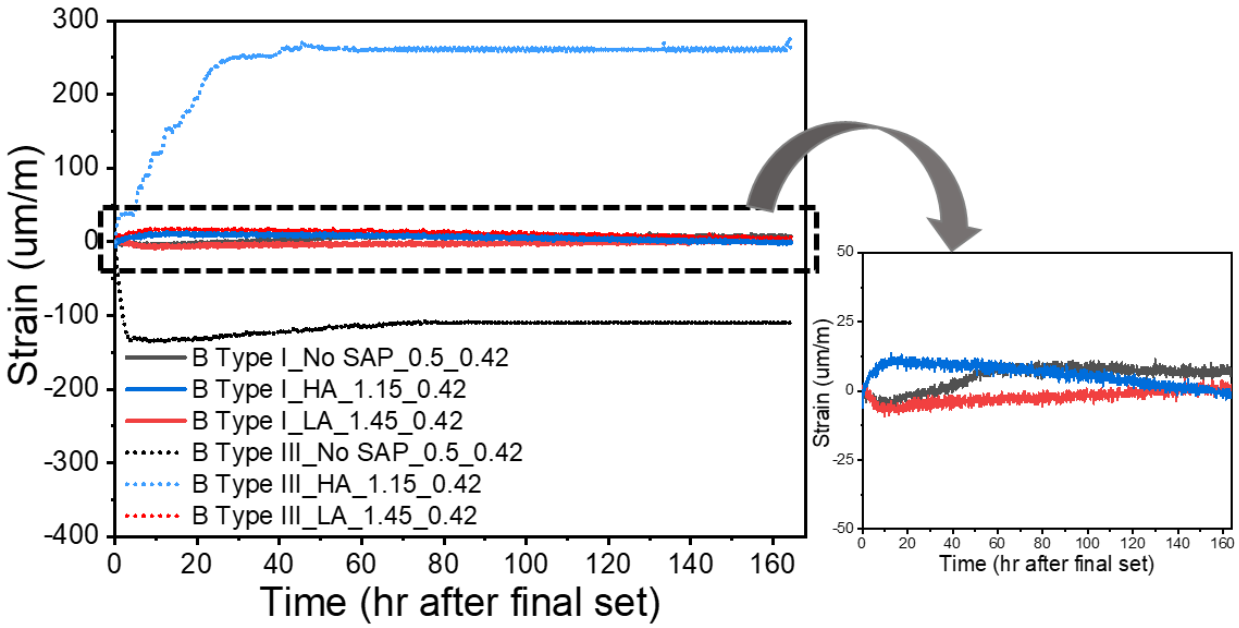

Figure 38: Autogenous shrinkage of Buzzi Type I and Type III mortars with a w/c of 0.42. For easier visualization of the Type I mortars, the right-side plot is zoomed in.

The addition of HA SAP particles induced an early age expansion in the mortars. This effect was particularly prominent in the Type III mortar mixture. Bentz et al. [132] reported similar expansive strains due to addition of SAP to mortars and indicated that this might be due to the formation of ettringite in early stages of hydration. The needle-like morphology of ettringite would result in expansive strains development in the microstructure. Although this phenomenon would be prevalent in the reference mortar too, however it is suppressed by the autogenous shrinkage and chemical shrinkage of the reference mortars. The measured autogenous shrinkage is a reflection of the self-desiccation of the mortar and any expansion produced due to formation of hydration products (such as ettringite). Since most of the self-desiccation was mitigated due to the presence of HA SAP particles, the expansive strains became the dominant factor in determining autogenous shrinkage strains of B Type III_HA_1.15_0.42_mortar. The slightly higher amount of sulfate ions presents in the Type III cement used, when compared to Type I cement might result in greater formation of ettringite in the Type III mortars. Other researchers have reported this expansive strain to be the result of thermal expansion and abrupt desorption of the retained water in the SAP after final set [133].

To further investigate the effect of internal curing on autogenous shrinkage of Type I mortars, a set of experiments were carried out at a lower w/c (w/c=0.35) for 5 days. Figure 39 shows the autogenous shrinkage of mortars at a w/c of 0.35. As seen in the figure, presence of SAP particles reduced the shrinkage strains, and this effect was particularly significant in the mortars containing HA SAP particles.

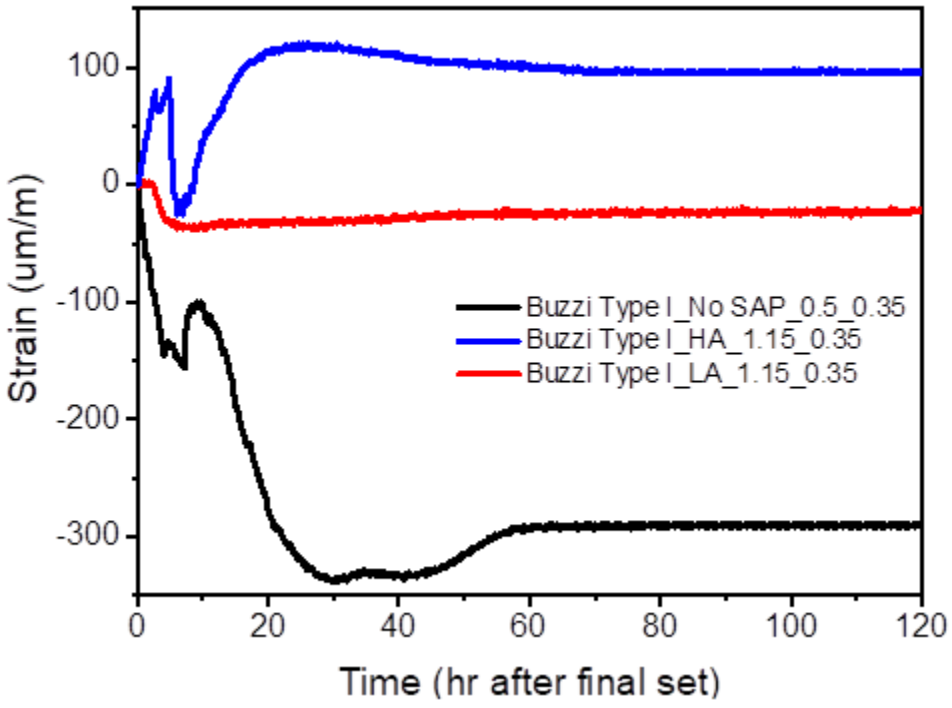

Figure 39: Autogenous shrinkage of Buzzi Type I mortars with a w/c of 0.35.

6.2.2 Backscattered electron microscopy of mortar

SEM micrographs of select w/c 0.42 mortars (Mix Designs ID 1, 2 and 3, see Table 9) are shown in Figure 40. In the B Type I_No SAP_0.5_0.42 sample (Figure 40a), microcracks were clearly visible throughout the cement paste matrix of the mortar. Microcracks were notably absent in the matrices of the corresponding SAP-containing samples (Figure 40b and Figure 40c). The lack of microcracks in these SAP-containing samples may potentially help them to achieve the later-age levels of compressive and flexural strengths which are either comparable to or improved compared to the levels of strengths in the reference specimens.

Analysis of the average diameter of the SAP-induced voids in mortars with SAP particles revealed that their average sizes were 302 μm and 127 μm, in samples containing LA and HA SAP particles respectively. This relative size relationship was expected as the average dry particle size of the LA SAP particles was larger than that of the HA SAP particles (see Section 6.1). However, the presence of larger SAP-induced voids does not necessarily mean that mechanical strength will be compromised. Other factors, such as SAP absorption kinetics and the subsequent release of water during hydration of cement might also play a role in determining the values of mechanical strength.

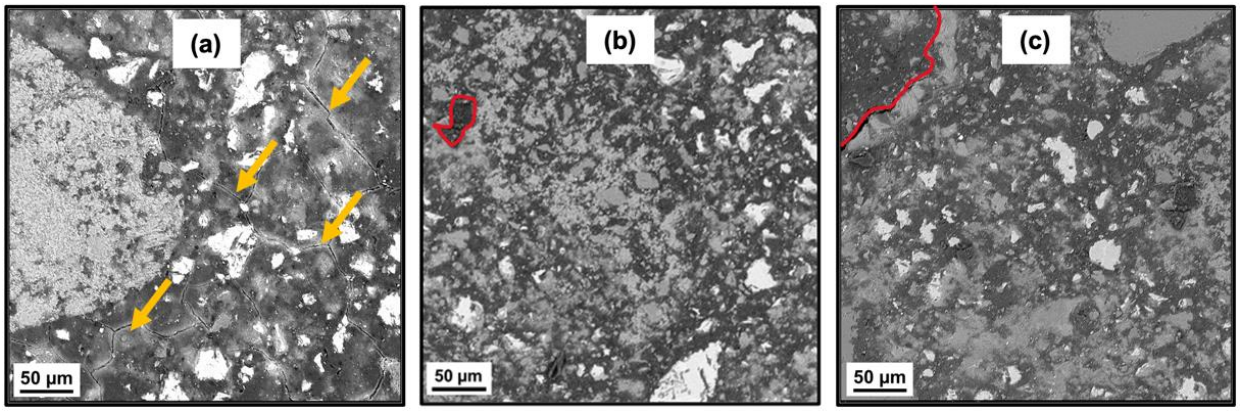

Figure 40: Representative SEM images of 28-day mortar samples (w/c 0.42): (a) B Type I_No SAP_0.5_0.42, (b) B Type I_LA_0.5_0.42, (c) B Type I_HA_0.5_0.42. The arrows in (a) indicate microcracks formed in the matrix of the mortar. The red outlines in in (b) and (c) indicate the outer edges of deswollen SAP particles.

Some of the SAP-induced voids in the sample with HA SAP-particles contained growths of identifiable hydration products. Figure 41a shows a SAP-induced void in a B Type I_HA_0.5_0.42 specimen with two spots (1 and 2) where energy-dispersive x-ray (EDX) analysis was conducted. In instances where there was substantial growth of hydration products around the vicinity of the SAP-induced voids, the perimeter of the SAP particle in the hardened matrix was difficult to distinguish as the significant growth of hydration product partially obscured the original dimensions of the swollen SAP particles. Figure 41b illustrates the relevant features of the SAP void: original perimeter of the SAP particle at the time of final set outlined in red and hydration product growth highlighted in cyan. Remnants of the dehydrated SAP, along with other intermixed

hydration products were also present (region inside the SAP void that is not highlighted in Figure 41b). The EDX analysis of the locations shown in Figure 41a yielded the following atomic percentages (Ca: 27.4±0.1%, O: 66±1%, others (Na, Si, K, Al, Mg, S, Na): 6±1%). Based on the EDX analysis and the morphology of the growth inside the SAP-induced voids it is postulated that it is most likely a portlandite. Previous studies have also found portlandite in SAP-induced voids [104], [130]. The growth of hydration products inside the SAP-induced voids was not observed in the LA SAP-cured samples.

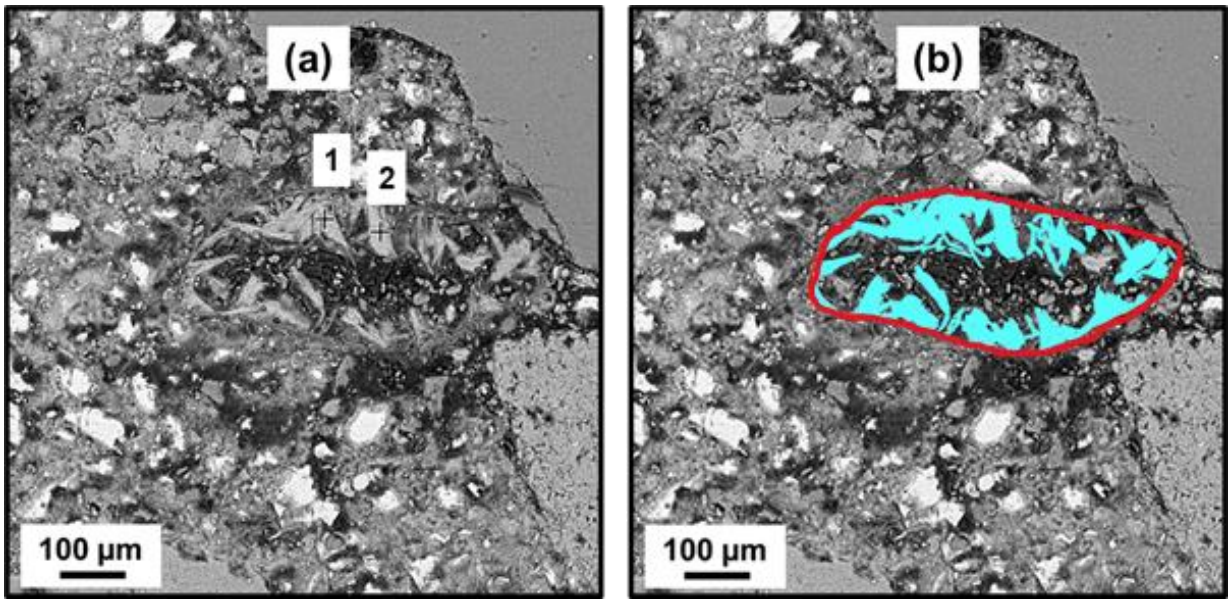

Figure 41: SEM image of a SAP-induced void in 28-day mortar sample B Type I_HA_0.5_0.42 (a) with two spots highlighted for EDX analysis (1 and 2); (b) the SAP void outlined in red and the portlandite growth inside the void highlighted in cyan.

6.3 Characterization of cement paste

6.3.1 Isothermal calorimetry analysis

Isothermal calorimetry analysis of cement paste was studied to investigate the effect of the two SAP formulations on the early age hydration of cement paste. The variables were: SAP type, cement type and source, presence of slag and presence of WRA. Figure 42 shows the isothermal calorimetry analysis of cement paste with two different types of cement from the same source

(Buzzi Unicem, Greencastle, IN). Presence of HA SAP particles caused a higher amount of cumulative heat in both Type I and Type III pastes, which is an indication of greater amount of hydration when compared to the respective Type I and Type III pastes without any SAP in it. For both Type I and Type III cement pastes, presence of LA SAP particles did not significantly impact time and height of peak hydration, and also cumulative heat attained, when compared to their respective references without any SAP.

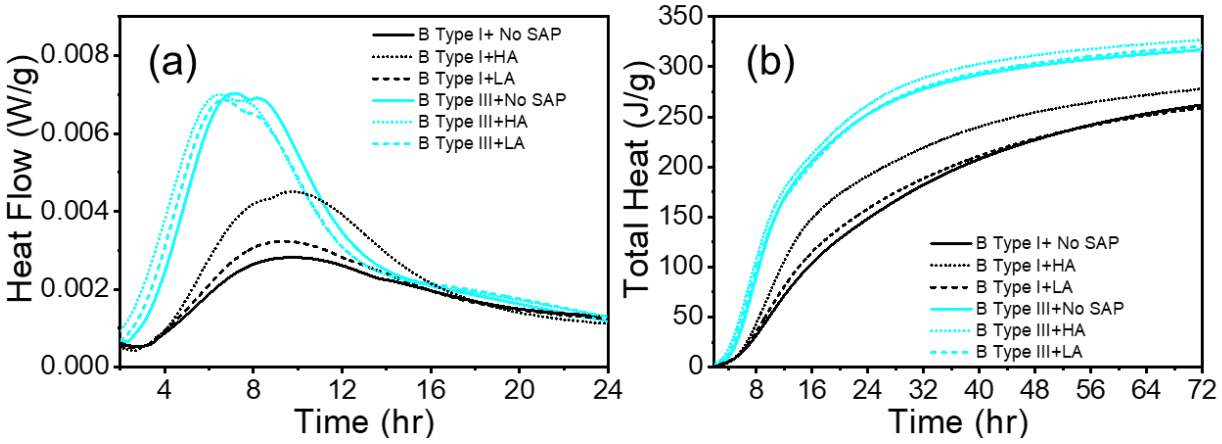

Figure 42: Isothermal calorimetry analysis of cement paste showing the effect of Type I and Type III cement from the same source on (a) heat flow (24 hours) and (b) total heat (72 hours).

The presence of HA SAP particles increased the height of main hydration peak and total heat generated substantially in Buzzi Type I cement paste, when compared to B Type I+No SAP. The increase in height of main peak is an indication of the increase in w/c [118] Thus this implies that majority of the HA SAP particles released their stored water by the end of the acceleration period, thus facilitating hydration reactions of C_3S. The greater amount of total heat observed in the B Type I+HA paste, when compared to B Type I+No SAP is also another indication that throughout the entire duration of the experiment, the HA SAP-containing paste underwent greater hydration. A similar trend in improvement in total heat was also observed for B Type III+HA paste, when compared to B Type III+No SAP, though not as drastic a difference.

The presence of LA SAP particles did not seem to significantly impact both the heat flow and the total heat curves obtained for B Type I and Type III pastes. A slight increase in height of main hydration peak was recorded for B Type I+LA, when compared to B Type I+No SAP. Again,

this is consistent with the assumption that this might indicate that the SAP particles released the water during the acceleration period. Since LA SAP particles' absorption capacity was lower than that of HA SAP particles, it is possible that the lesser amount of water stored and thus released by the LA SAP would result in lesser increase in effective w/c, when compared to HA SAP-containing pastes. No major difference in total heat attained was observed for the LA SAP-containing pastes, when compared to the reference pastes. The LA SAP absorption capacity from Figure 37 seemed to suggest that it is composed of majority polyacrylamide. Thus, it is possible that the water retained in the LA SAP was either insufficient and/or retained too long to fully explore the potential of internal curing on hydration reactions during the duration of the isothermal calorimetry experiment (3 days).

For the pastes with Type III cement, faster early-strength development was observed when compared to Type I cement pastes. This could be deduced since the slope of the curves during the acceleration period is higher for the pastes containing Type III cement, when compared to Type I cement pastes. Additionally, higher cumulative heat at the end of 3 days was observed for Type III pastes, when compared to Type I pastes. This is unsurprising as the Type III cement contains a much finer particle size (a 44% increase in Blaine fineness) when compared to Type I cement grains, which would result in faster hydration and strength development reactions to occur.

Figure 43 shows the effect of different sources of Type I cement on the isothermal calorimetry analysis of internally cured cement pastes. The total heat curves indicate S Type I pastes underwent higher total hydration with/without SAP, when compared to the B Type I or L Type I pastes without SAP. Also, presence of HA SAP particles caused slightly higher total hydration in pastes from all three cement sources.

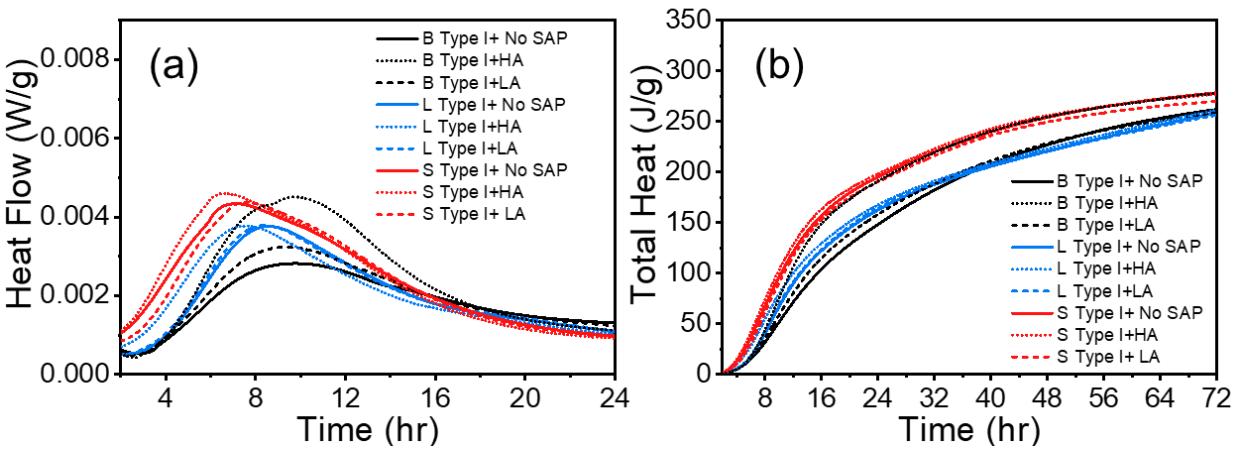

Figure 43: Isothermal calorimetry analysis of cement paste showing the effect of three different sources of Type I cement on (a) heat flow (24 hours) and (b) total heat (72 hours).

From Figure 43a, it was seen that regardless of the source of cement, the HA SAP containing pastes increased the rate of hydration (as indicated by the steeper gradient of the curve) during the acceleration period when compared to the corresponding reference paste without SAP, which is indicative of greater amount of strength development reactions. This is also reflected in Figure 43b, where the HA SAP containing pastes displayed greater total hydration compared to the reference paste without SAP, with the highest improvement observed in B Type I+HA, when compared to B Type I+No SAP.

The S Type I cement pastes displayed earlier setting time when compared to B Type I and L Type I cement pastes, which follows the trend expected based on the initial setting time reported in the mill certificates of the three cements. The S Type I+HA paste indicated a faster attainment of the acceleration period, along with a slightly higher main hydration peak, when compared to S Type I+No SAP. This could be due to HA SAP displaying a larger absorption capacity in S Type I pore solution (Figure 37b) and thus the release of the retained water from the SAP after the induction period caused a quicker rate of acceleration period and higher peak of main hydration.

All three S Type I cement pastes displayed total hydration comparable to the B Type I+HA paste sample. This could be due to the fact that of the three cement sources studied, S Type I had the highest total amount of alkali oxide content. This would result in dissolution of the greater amount of alkali ions in the pore solution and contribute towards earlier attainment of higher hydration. Similar to the results obtained for B Type I pastes discussed above, presence of LA SAP

particles had no prominent impact on hydration peak, or the total heat accumulated in both S Type I and L Type I cement, when compared to the corresponding reference paste without SAP.

Figure 44 displays the effect of partial replacement of cement with slag on the isothermal calorimetry analysis of internally cured pastes. A lower amount of total hydration was observed for all three pastes containing slag, as indicated by the total heat curve (Figure 44b). This is expected due to the presence of slag in the binder system, and have been reported by previous researchers too [134]. To understand the full extent of the benefit of internal curing in slag-containing mixtures, a longer duration of isothermal calorimetry analysis might be more beneficial. Additionally, no significant impact of internal curing with HA SAP particles was observed in the pastes containing 30% slag. Previous researchers have reported a reduction in main hydration peak and a delay in hydration kinetics in slag containing pastes without any SAP [135]. It is possible that this effect negated the greater hydration promoted due to the presence of HA SAP particles.

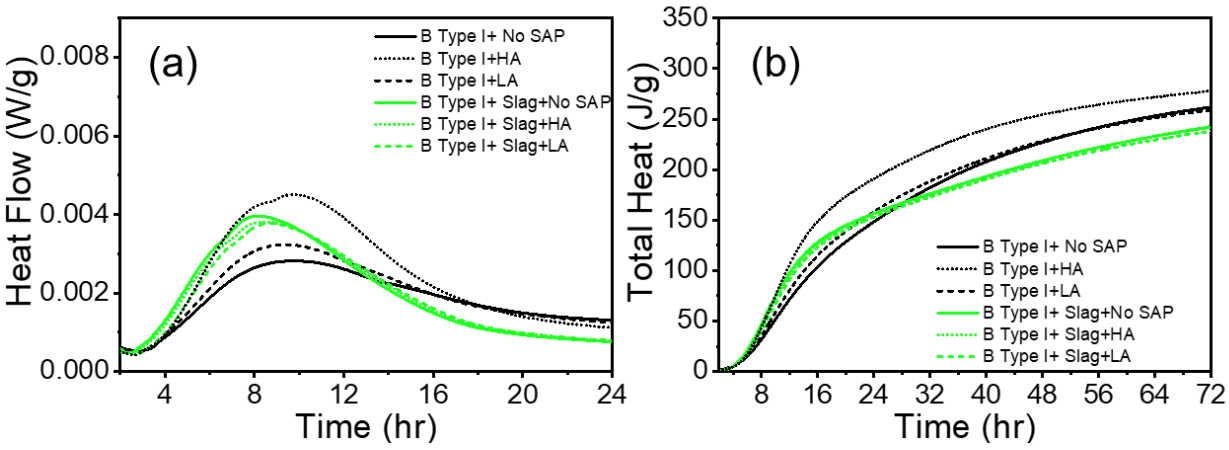

Figure 44: Isothermal calorimetry analysis of cement paste showing the effect of partial replacement of cement by slag on (a) heat flow (24 hours) and (b) total heat (72 hours).

Effect of the presence of WRA dosage on internally cured Type I and Type III pastes are shown in Figure 45. It is clear that although the presence of WRA retarded the main hydration peak for both Type I and Type III pastes (Figure 45a), the eventual total hydration reached was comparable to the pastes of same composition without WRA (Figure 45b). For the pastes containing WRA, an overlap of the calcium aluminate reaction peak with the main hydration peak was observed. This effect was more prominent for the Type III cement pastes with WRA, and this

is probably indication of the pastes being potentially sensitive to high admixture dosages. Also, it was interesting to note that HA containing B Type I pastes underwent higher hydration when compared to the reference paste without SAP, even with the presence of WRA. In summary, the results indicate that the dosage of WRA used in the study had no impact on total hydration, and only retarded attainment of main peak of hydration of the cement pastes.

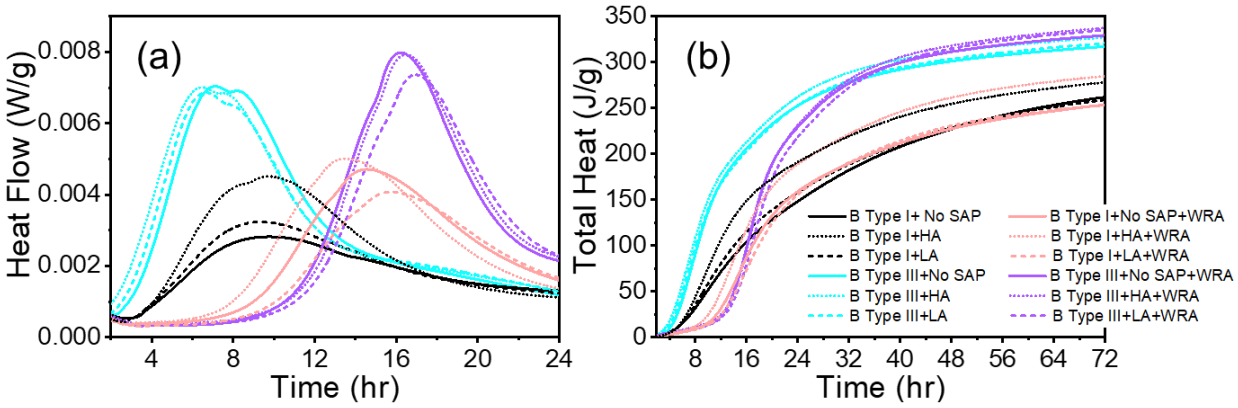

Figure 45: Isothermal calorimetry analysis of cement paste showing the effect of WRA on cement paste (a) heat flow (24 hours) and (b) total heat (72 hours).

6.3.2 Non-evaporable water content

The non-evaporable water content (W_n) at 7 days is shown in Figure 46. It was evident that the addition of HA SAP particles increased the hydration of the cement paste samples, which is in agreement with previous research performed on cement paste containing hydrogel particles [96]. A higher improvement in hydration was observed for Type III cement paste, when compared to Type I cement paste from same source (Buzzi Unicem, Greencastle, IN). No significant improvement of hydration was observed when comparing paste containing LA SAP particles and the corresponding reference pastes without SAP.

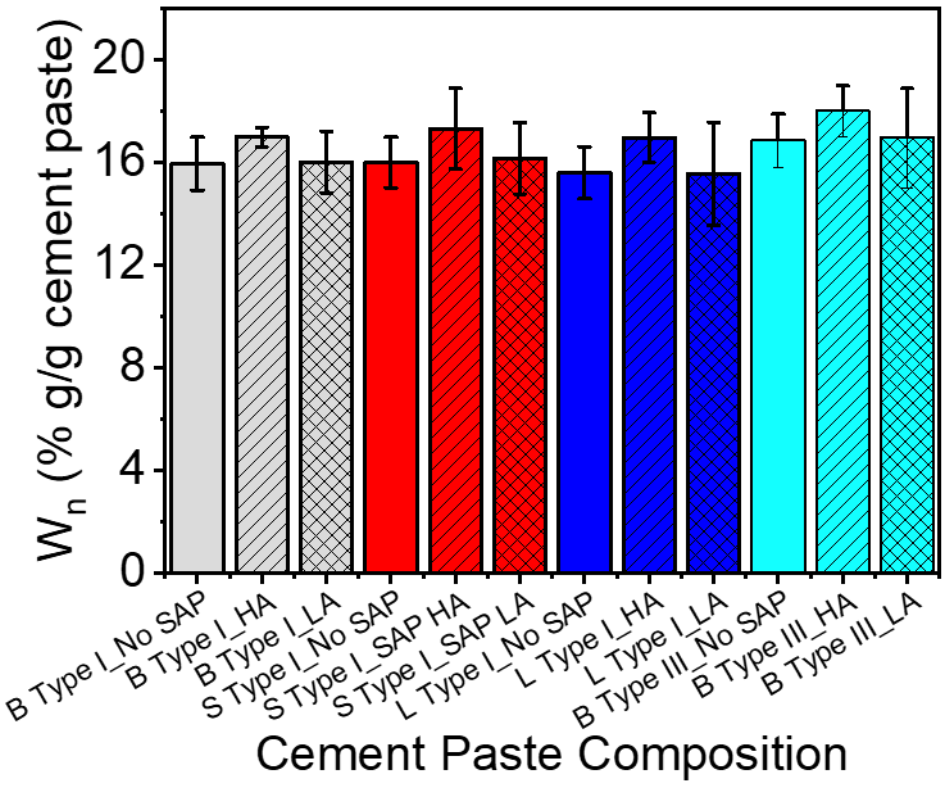

Figure 46: Non-evaporable water content (Wn) of the cement pastes at 7 days at a w/c of 0.42. For clarity, hatched bars represent samples containing HA SAP particles and cross-hatched bars represent samples containing LA SAP particles.

6.3.3 Backscattered electron microscopy

Scanning electron micrographs of reference and internally cured cement pastes are shown in Figure 47. For each internally cured paste sample, the amounts of hydration product observed within the SAP voids were measured (Figure 48) and are described below to ultimately determine the effects of the two compositions of SAP particles and cement source on the cement paste microstructure.

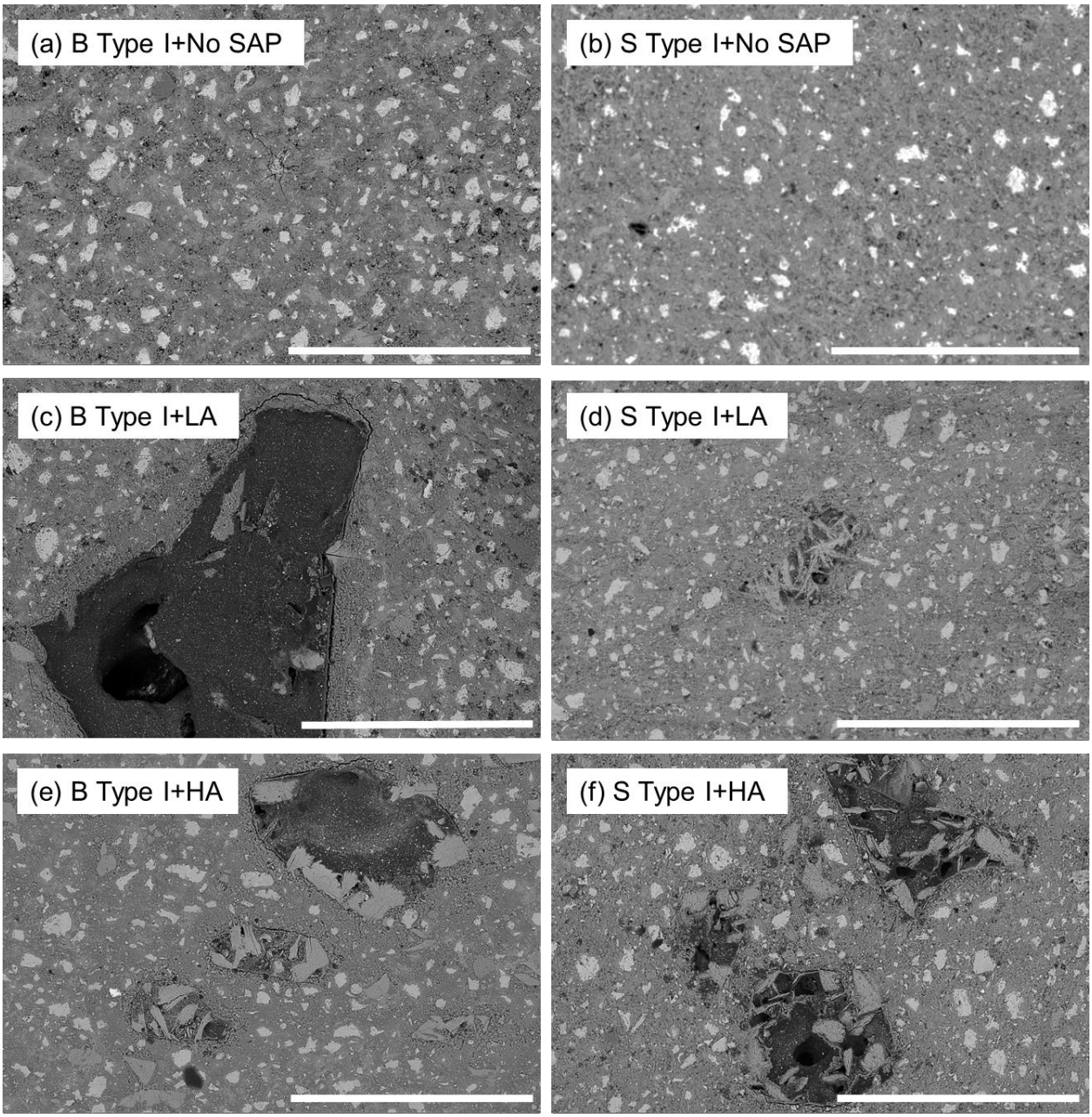

Figure 47: Microstructure analysis of 7-days old pastes cured with LA and HA SAP particles. Buzzi Type I cement was used for (a), (c) and (e), while St. Mary's Type I cement was used for (b), (d) and (f). Scale bar in each micrograph represents 400 μm. 4% and 83% of the SAP voids are filled with hydration products in (c) and (d), respectively, while 14% and 18% of the SAP void are filled with hydration products in the upper-right SAP voids in (e) and (f), respectively.

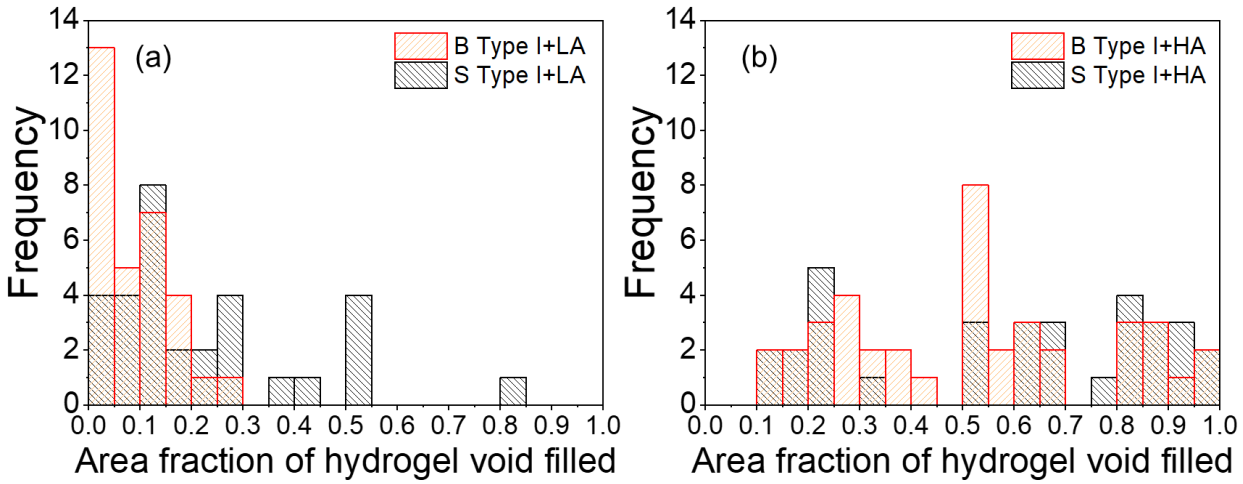

Figure 48: Microstructure analysis of pastes cured with LA and HA SAP particles. (a) and (b) Area of SAP particle voids filled with hydration products as a function of cement paste composition.

As seen in the micrographs in Figure 47 (d), (e) and (f), one of the features of the cement microstructures was the observed "filling" of the SAP voids with hydration product. Based on elemental analysis conducted in mortar specimen (see Figure 41), the hydration products are believed to be mostly CH with some amount of intermixed C-S-H.

To determine how the hydrogel particle composition affected the observed void-filling, the amounts (by area fraction) of hydration product observed within the SAP voids were quantified for each internally cured paste. Of the 30 or more SAP voids that were analyzed for paste containing LA SAP particles (see histogram in Figure 48a), the following numbers of voids were more than 50% filled: 0 void in B Type I+LA and 5 voids in S Type I+LA. By comparison, of the 31 hydrogel voids analyzed for paste containing HA SAP particles (see Figure 48b), the following numbers of voids were more than 50% filled: 24 voids in B Type I+HA and 22 voids in S Type I+HA. Thus, more voids resulting from HA SAP particles were filled with hydration products compared to voids resulting from LA SAP particles.

A greater filling of SAP voids in B Type I+HA and S Type I+HA observed when compared to corresponding pastes containing LA SAP particles. This greater filling might partly contribute to the higher total hydration observed in the isothermal calorimetry (see Figure 43) and non-evaporable water content experiments (see Figure 46). While details regarding composition of the HA SAP is unknown, some conclusions can be drawn from the free absorption capacity experiments conducted (Figure 37b). HA displayed greater absorption capacity in the gravimetric

absorption experiments, thus a larger amount of water is expected to be absorbed by the SAP particles, which would fuel hydration reactions in the vicinity of the void. Additionally the crosslinker amount, desorption kinetics of the SAP particles are also expected to play a role in influencing the growth of hydration products in the vicinity of the SAP voids.

In addition to SAP type, the cement source also played a role in impacting the cement microstructure. The voids in LA SAP particles, although displaying minimal hydration product growth in B Type I cement paste, displayed some hydration product growth in some of the SAP voids analyzed in S Type I cement. The higher alkali content of S Type I cement when compared to B Type I cement, might have resulted in overall increase in alkali ion concentrations even withing the LA-SAP voids. This would result in accelerated hydration even within the SAP voids and thus formation of hydration products in the vicinity of the voids.

6.4 Conclusion

The effect of two SAP formulations in influencing autogenous shrinkage, microstructure and hydration of cementitious systems were investigated. Some of the major findings were:

- Presence of SAP particles were successfully able to reduce autogenous shrinkage of mortars. This effect was particularly pronounced when using the HA SAP particles.
- Total heat plot from isothermal calorimetry analysis and non-evaporable water content measurements of cement pastes indicate that presence of HA SAP particles contributed to greater hydration of the cement paste.
- Microstructural analysis of cement paste with HA SAP particles revealed significant formation of hydration products in the SAP voids. Additionally, microstructural refinement typically associated with SAP internal curing of lower w/c mixtures, namely the absence of microcracks compared to SAP-free samples, was observed in mortars at a w/c of 0.42.

REFERENCES

[1] E. M. Gartner, "Potential improvements in cement sustainability," in *31st Cement and Concrete Science Conference - Novel Developments and Innovation in Cementitious Materials*, 2011.

[2] P. K. Mehta and P. J. M. Monteiro, *Concrete: Microstructure, Properties, and Materials*, 4th ed. McGraw-Hill Education, 2014.

[3] W. Booth, "In earthquake, Haiti's concrete buildings proved anything but.," *The Washington Post*, p. A.6, 27-Mar-2010.

[4] IEA, "Technology Roadmap - Low-Carbon Transition in the Cement Industry – Analysis - IEA," Paris, 2018.

[5] K. Van Vliet *et al.*, "Set in stone? A perspective on the concrete sustainability challenge," *MRS Bull.*, vol. 37, no. 04, pp. 395–402, Apr. 2012.

[6] J. Walraven, "High Performance Concrete: a Material with a Large Potential," *J. Adv. Concr. Technol.*, vol. 7, no. 2, pp. 145–156, 2009.

[7] C. Shi, Z. Wu, J. Xiao, D. Wang, Z. Huang, and Z. Fang, "A review on ultra high performance concrete: Part I. Raw materials and mixture design," *Constr. Build. Mater.*, vol. 101, pp. 741–751, 2015.

[8] G. Habert, D. Arribe, T. Dehove, L. Espinasse, and R. Le Roy, "Reducing environmental impact by increasing the strength of concrete: quantification of the improvement to concrete bridges," *J. Clean. Prod.*, vol. 35, pp. 250–262, Nov. 2012.

[9] W. J. Weiss, W. Yang, and S. P. Shah, "Shrinkage Cracking of Restrained Concrete Slabs," *J. Eng. Mech.*, vol. 124, no. 7, pp. 765–774, 1998.

[10] O. M. Jensen and P. F. Hansen, "Water-entrained cement-based materials: I. Principles and theoretical background," *Cem. Concr. Res.*, vol. 31, no. 4, pp. 647–654, 2001.

[11] H. J. H. Brouwers, "Paste models for hydrating calcium sulfates, using the approach by Powers and Brownyard," *Constr. Build. Mater.*, vol. 36, pp. 1044–1047, Nov. 2012.

[12] P. Lura, O. M. Jensen, and K. van Breugel, "Autogenous shrinkage in high-performance cement paste: An evaluation of basic mechanisms," *Cem. Concr. Res.*, vol. 33, no. 2, pp. 223–232, Feb. 2003.

[13] ACI Committee 231, “ACI 231R-10 - Report on Early-Age Cracking: Causes, Measurement, and Mitigation,” 2010.

[14] T. Barrett, A. Miller, and W. J. Weiss, “Documentation of the INDOT Experience and Construction of the Bridge Decks Containing Internal Curing in 2013,” Joint Transportation Research Program, West Lafayette, IN, Nov. 2015.

[15] V. H. Villarreal, “Internal curing - Real world ready mix production and applications: A practical approach to lightweight modified concrete,” in *American Concrete Institute, ACI Special Publication*, 2008, vol. 256, no. 256 SP, pp. 44–54.

[16] American Concrete Institute, *ACI 213R-14: Guide for Structural Lightweight-Aggregate Concrete*. Farmington Hills: American Concrete Institute, 2014.

[17] O. M. Jensen and P. F. Hansen, “Water-entrained cement-based materials : II. Experimental observations,” *Cem. Concr. Res.*, vol. 32, no. 6, pp. 973–978, 2002.

[18] M. Wyrzykowski, P. Lura, F. Pesavento, and D. Gawin, “Modeling of water migration during internal curing with superabsorbent polymers,” *J. Mater. Civ. Eng.*, vol. 24, no. 8, pp. 1006–1016, 2012.

[19] C. Schröfl, V. Mechtcherine, and M. Gorges, “Relation between the molecular structure and the efficiency of superabsorbent polymers (SAP) as concrete admixture to mitigate autogenous shrinkage,” *Cem. Concr. Res.*, vol. 42, no. 6, pp. 865–873, 2012.

[20] O. M. Jensen and P. Lura, “Techniques and materials for internal water curing of concrete,” *Mater. Struct.*, vol. 39, no. 9, pp. 817–825, 2006.

[21] S. Mönning, “Superabsorbing Additions in Concrete – Applications, Modeling and Comparison of Different Internal Water Sources,” University of Stuttgart, 2009.

[22] P. Lura, O. M. Jensen, and J. Weiss, “Cracking in cement paste induced by autogenous shrinkage,” *Mater. Struct.*, vol. 42, no. 8, pp. 1089–1099, 2009.

[23] H. Beushausen, M. Gillmer, and M. Alexander, “The influence of superabsorbent polymers on strength and durability properties of blended cement mortars,” *Cem. Concr. Compos.*, vol. 52, pp. 73–80, 2014.

[24] S. Oh and Y. C. Choi, “Superabsorbent polymers as internal curing agents in alkali activated slag mortars,” *Constr. Build. Mater.*, vol. 159, pp. 1–8, 2018.

[25] M. J. Krafcik and K. A. Erk, “Characterization of superabsorbent poly(sodium-acrylate acrylamide) hydrogels and influence of chemical structure on internally cured mortar,” *Mater. Struct.*, vol. 49, no. 11, pp. 4765–4778, 2016.

[26] D. Snoeck, O. M. Jensen, and N. De Belie, “The influence of superabsorbent polymers on the autogenous shrinkage properties of cement pastes with supplementary cementitious materials,” *Cem. Concr. Res.*, vol. 74, pp. 59–67, 2015.

[27] L. Montanari, P. Suraneni, and W. J. Weiss, “Accounting for Water Stored in Superabsorbent Polymers in Increasing the Degree of Hydration and Reducing the Shrinkage of Internally Cured Cementitious Mixtures,” *Adv. Civ. Eng. Mater.*, vol. 6, no. 1, pp. 583–599, 2017.

[28] V. Mechtcherine *et al.*, “Effect of internal curing by using superabsorbent polymers (SAP) on autogenous shrinkage and other properties of a high-performance fine-grained concrete: results of a RILEM round-robin test,” *Mater. Struct.*, vol. 47, no. 3, pp. 541–562, Mar. 2014.

[29] L. De Meyst, J. Kheir, J. R. Tenório Filho, K. Van Tittelboom, and N. De Belie, “The Use of Superabsorbent Polymers in High Performance Concrete to Mitigate Autogenous Shrinkage in a Large-Scale Demonstrator,” *Sustainability*, vol. 12, no. 11, p. 4741, Jun. 2020.

[30] A. Mignon *et al.*, “pH-responsive superabsorbent polymers: A pathway to self-healing of mortar,” *React. Funct. Polym.*, vol. 93, pp. 68–76, 2015.

[31] D. Snoeck, S. Steuperaert, K. Van Tittelboom, P. Dubruel, and N. De Belie, “Visualization of water penetration in cementitious materials with superabsorbent polymers by means of neutron radiography,” *Cem. Concr. Res.*, vol. 42, no. 8, pp. 1113–1121, 2012.

[32] H. X. D. Lee, H. S. Wong, and N. R. Buenfeld, “Self-sealing of cracks in concrete using superabsorbent polymers,” *Cem. Concr. Res.*, vol. 79, pp. 194–208, 2016.

[33] V. Mechtcherine, C. Schrofl, M. Reichardt, A. J. Klemm, and K. H. Khayat, “Recommendations of RILEM TC 260-RSC for using superabsorbent polymers (SAP) for improving freeze–thaw resistance of cement-based materials,” *Mater. Struct.*, vol. 52, no. 75, 2019.

[34] V. Mechtcherine *et al.*, “Effect of superabsorbent polymers (SAP) on the freeze–thaw resistance of concrete: results of a RILEM interlaboratory study,” *Mater. Struct.*, vol. 50, no. 1, p. 14, Feb. 2017.

[35] M. Krafcik, N. Macke, and K. A. Erk, “Improved Concrete Materials with Hydrogel-Based Internal Curing Agents,” *Gels*, vol. 3, no. 4, pp. 46–64, 2017.

[36] S. Mönnig and P. Lura, “Superabsorbent Polymers — An Additive to Increase the Freeze-Thaw Resistance of High Strength Concrete,” in *Advances in Construction Materials 2007*, Berlin, Heidelberg: Springer Berlin Heidelberg, 2007, pp. 351–358.

[37] V. Mechtcherine, E. Secrieru, and C. Schröfl, “Effect of superabsorbent polymers (SAPs) on rheological properties of fresh cement-based mortars — Development of yield stress and plastic viscosity over time,” *Cem. Concr. Res.*, vol. 67, pp. 52–65, 2015.

[38] C. Schroefl, V. Mechtcherine, P. Vontobel, J. Hovind, and E. Lehmann, “Sorption kinetics of superabsorbent polymers (SAPs) in fresh Portland cement-based pastes visualized and quantified by neutron radiography and correlated to the progress of cement hydration,” *Cem. Concr. Res.*, vol. 75, pp. 1–13, 2015.

[39] L. P. Esteves, “Superabsorbent polymers: On their interaction with water and pore fluid,” *Cem. Concr. Compos.*, vol. 33, no. 7, pp. 717–724, 2011.

[40] Q. Zhu, C. W. Barney, and K. A. Erk, “Effect of ionic crosslinking on the swelling and mechanical response of model superabsorbent polymer hydrogels for internally cured concrete,” *Mater. Struct.*, vol. 48, no. 7, pp. 2261–2276, 2015.

[41] S.-H. Kang, S.-G. Hong, and J. Moon, “Importance of monovalent ions on water retention capacity of superabsorbent polymer in cement-based solutions,” *Cem. Concr. Compos.*, vol. 88, pp. 64–72, 2018.

[42] P. Zhong, M. Wyrzykowski, N. Toropovs, L. Li, J. Liu, and P. Lura, “Internal curing with superabsorbent polymers of different chemical structures,” *Cem. Concr. Res.*, vol. 123, p. 105789, 2019.

[43] K. A. Erk and B. Bose, “Using Polymer Science To Improve Concrete: Superabsorbent Polymer Hydrogels in Highly Alkaline Environments,” in *Gels and Other Soft Amorphous Solids*, American Chemical Society, 2018, pp. 333–356.

[44] L. Montanari, P. Suraneni, M. T. Chang, C. Villani, and J. Weiss, “Absorption and Desorption of Superabsorbent Polymers for Use in Internally Cured Concrete,” *Adv. Civ. Eng. Mater.*, vol. 7, no. 4, pp. 547–566, 2018.

[45] J. Siramanont, W. Vichit-Vadakan, and W. Siriwatwechakul, “The Impact of SAP Structure on the Effectiveness of Internal Curing,” in *International RILEM conference on Use of superabsorbent polymers and other new additives in concrete*, 2010, pp. 243–252.

[46] C. R. Davis, B. Bose, A. Alcaraz, C. J. Martinez, and K. A. Erk, “Altering the Crosslinking Density of Polyacrylamide Hydrogels to Increase Swelling Capacity and Promote Calcium Hydroxide Growth in Cement Voids,” in *Third International RILEM Conference on the Application of Superabsorbent Polymers and Other New Admixtures Towards Smart Concrete*, 2019.

[47] K. Farzanian and A. Ghahremaninezhad, “Desorption of superabsorbent hydrogels with varied chemical compositions in cementitious materials,” *Mater. Struct.*, vol. 51, no. 3, pp. 1–15, 2018.

[48] K. Farzanian and A. Ghahremaninezhad, “On the Effect of Chemical Composition on the Desorption of Superabsorbent Hydrogels in Contact with a Porous Cementitious Material,” *Gels*, vol. 4, no. 3 70, pp. 1–13, 2018.

[49] O. A. Mohamed and O. F. Najm, “Compressive strength and stability of sustainable self-consolidating concrete containing fly ash, silica fume, and GGBS,” *Front. Struct. Civ. Eng.*, vol. 11, no. 4, pp. 406–411, 2017.

[50] W. Aquino, D. A. Lange, and J. Olek, “The influence of metakaolin and silica fume on the chemistry of alkali–silica reaction products,” *Cem. Concr. Compos.*, vol. 23, no. 6, pp. 485–493, 2001.

[51] L. P. Singh, S. R. Karade, S. K. Bhattacharyya, M. M. Yousuf, and S. Ahalawat, “Beneficial role of nanosilica in cement based materials – A review,” *Constr. Build. Mater.*, vol. 47, pp. 1069–1077, 2013.

[52] L. Senff, J. A. Labrincha, V. M. Ferreira, D. Hotza, and W. L. Repette, “Effect of nano-silica on rheology and fresh properties of cement pastes and mortars,” *Constr. Build. Mater.*, vol. 23, no. 7, pp. 2487–2491, 2009.

[53] J. Björnström, A. Martinelli, A. Matic, L. Börjesson, and I. Panas, “Accelerating effects of colloidal nano-silica for beneficial calcium–silicate–hydrate formation in cement,” *Chem. Phys. Lett.*, vol. 392, no. 1–3, pp. 242–248, 2004.

[54] B.-W. Jo, C.-H. Kim, G. Tae, and J.-B. Park, “Characteristics of cement mortar with nano-SiO2 particles,” *Constr. Build. Mater.*, vol. 21, no. 6, pp. 1351–1355, 2007.

[55] H. Biricik and N. Sarier, “Comparative study of the characteristics of nano silica - , silica fume - and fly ash - incorporated cement mortars,” *Mater. Res.*, vol. 17, no. 3, pp. 570–582, 2014.

[56] R. Merget *et al.*, “Health hazards due to the inhalation of amorphous silica,” *Arch. Toxicol.*, vol. 75, no. 11–12, pp. 625–634, 2002.

[57] L. B. Agostinho, de C. P. Alexandre, E. F. da Silva, and R. D. Toledo Filho, “Rheological study of Portland cement pastes modified with superabsorbent polymer and nanosilica,” *J. Build. Eng.*, vol. 34, p. 102024, Feb. 2021.

[58] A. Pourjavadi, S. M. Fakoorpoor, P. Hosseini, and A. Khaloo, “Interactions between superabsorbent polymers and cement-based composites incorporating colloidal silica nanoparticles,” *Cem. Concr. Compos.*, vol. 37, pp. 196–204, Mar. 2013.

[59] A. Pourjavadi, S. M. Fakoorpoor, A. Khaloo, and P. Hosseini, “Improving the performance of cement-based composites containing superabsorbent polymers by utilization of nano-SiO2 particles,” *Mater. Des.*, vol. 42, no. 2012, pp. 94–101, Dec. 2012.

[60] T. A. Cunha, L. B. Agostinho, and E. F. Silva, “Application of Nano-silica Particles to Improve the Mechanical Properties of High Performance Concrete Containing Superabsorbent Polymers,” in *3rd International Conference on the Application of Superabsorbent Polymers (SAP) and Other New Admixtures Towards Smart Concrete.*, vol. 24, Boshoff W., Combrinck R., Mechtcherine V., and Wyrzykowski M., Eds. Springer Cham, 2020, pp. 211–221.

[61] T. A. Cunha, P. Francinete, M. A. Manzano, L. A. Aidar, J. G. Borges, and E. F. Silva, “Determination of time zero in high strength concrete containing superabsorbent polymer and nano-silica,” *J. Build. Pathol. Rehabil.*, vol. 1, no. 1, pp. 1–12, Dec. 2016.

[62] G. Lefever *et al.*, “Combined use of superabsorbent polymers and nanosilica for reduction of restrained shrinkage and strength compensation in cementitious mortars,” *Constr. Build. Mater.*, vol. 251, p. 118966, Aug. 2020.

[63] G. Lefever, D. Snoeck, D. G. Aggelis, N. De Belie, S. Van Vlierberghe, and D. Van Hemelrijck, “Evaluation of the self-healing ability of mortar mixtures containing superabsorbent polymers and nanosilica,” *Materials (Basel).*, vol. 13, no. 2, Jan. 2020.

[64] G. Lefever *et al.*, “The Influence of Superabsorbent Polymers and Nanosilica on the Hydration Process and Microstructure of Cementitious Mixtures,” *Materials (Basel).*, vol. 13, no. 22, p. 5194, Nov. 2020.

[65] G. Olivier, R. Combrinck, M. Kayondo, and W. P. Boshoff, “Combined effect of nano-silica, super absorbent polymers, and synthetic fibres on plastic shrinkage cracking in concrete,” *Constr. Build. Mater.*, vol. 192, pp. 85–98, Dec. 2018.

[66] J. Justs, M. Wyrzykowski, D. Bajare, and P. Lura, “Internal curing by superabsorbent polymers in ultra-high performance concrete,” *Cem. Concr. Res.*, vol. 76, pp. 82–90, 2015.

[67] M. J. Krafcik, B. Bose, and K. A. Erk, “Synthesis and Characterization of Polymer-Silica Composite Hydrogel Particles and Influence of Hydrogel Composition on Cement Paste Microstructure,” *Adv. Civ. Eng. Mater.*, vol. 7, no. 4, pp. 590–613, 2018.

[68] K. A. Erk, “Cementitious Mixtures, Compositions for Use in Cementitious Mixtures, and Methods of Producing Cementitious Mixtures,” 16/138339, 2019.

[69] J. F. Young, “A review of the mechanisms of set-retardation in portland cement pastes containing organic admixtures,” *Cem. Concr. Res.*, vol. 2, no. 4, pp. 415–433, Jul. 1972.

[70] J. Cheung, A. Jeknavorian, L. Roberts, and D. Silva, “Impact of admixtures on the hydration kinetics of Portland cement,” *Cement and Concrete Research*, vol. 41, no. 12. Pergamon, pp. 1289–1309, 01-Dec-2011.

[71] J. J. Thomas, H. M. Jennings, and J. J. Chen, “Influence of nucleation seeding on the hydration mechanisms of tricalcium silicate and cement,” *J. Phys. Chem. C*, vol. 113, no. 11, pp. 4327–4334, Mar. 2009.

[72] V. K. Peterson and M. C. Garci Juenger, “Hydration of tricalcium silicate: Effects of CaCl 2 and sucrose on reaction kinetics and product formation,” *Chem. Mater.*, vol. 18, no. 24, pp. 5798–5804, Nov. 2006.

[73] M. C. Garci Juenger and H. M. Jennings, “New insights into the effects of sugar on the hydration and microstructure of cement pastes,” *Cem. Concr. Res.*, vol. 32, no. 3, pp. 393–399, Mar. 2002.

[74] N. L. Thomas and J. D. Birchall, “The retarding action of sugars on cement hydration,” *Cem. Concr. Res.*, vol. 13, no. 6, pp. 830–842, Nov. 1983.

[75] F. F. Ataie, M. C. G. Juenger, S. C. Taylor-Lange, and K. A. Riding, "Comparison of the retarding mechanisms of zinc oxide and sucrose on cement hydration and interactions with supplementary cementitious materials," *Cem. Concr. Res.*, vol. 72, pp. 128–136, Jun. 2015.

[76] B. Na, Z. Wang, H. Wang, and X. Lu, "WOOD-cement compatibility review," *Wood Res.*, vol. 59, no. 5, pp. 813–825, 2014.

[77] K. Kochova, K. Schollbach, F. Gauvin, and H. J. H. Brouwers, "Effect of saccharides on the hydration of ordinary Portland cement," *Constr. Build. Mater.*, vol. 150, pp. 268–275, Sep. 2017.

[78] M. Bishop, S. G. Bott, and A. R. Barron, "A new mechanism for cement hydration inhibition: Solid-state chemistry of calcium nitrilotris(methylene)triphosphonate," *Chem. Mater.*, vol. 15, no. 16, pp. 3074–3088, Aug. 2003.

[79] Y. Zuo, J. Zi, and X. Wei, "Hydration of cement with retarder characterized via electrical resistivity measurements and computer simulation," *Constr. Build. Mater.*, vol. 53, pp. 411–418, Feb. 2014.

[80] N. B. Singh, A. K. Singh, and S. Prabha Singh, "Effect of citric acid on the hydration of portland cement," *Cem. Concr. Res.*, vol. 16, no. 6, pp. 911–920, Nov. 1986.

[81] D. Li, B. Chen, X. Chen, B. Fu, H. Wei, and X. Xiang, "Synergetic effect of superabsorbent polymer (SAP) and crystalline admixture (CA) on mortar macro-crack healing," *Constr. Build. Mater.*, vol. 247, p. 118521, Jun. 2020.

[82] E. Karadag, D. Saraydin, N. Sahiner, and O. Güven, "Radiation induced acrylamide/citric acid hydrogels and their swelling behaviors," *J. Macromol. Sci. Part A - Pure Appl. Chem.*, vol. 38, no. 11, pp. 1105–1121, 2001.

[83] V. Mechtcherine, C. Schroefl, and M. Gorges, "Effectiveness of various superabsorbent polymers (SAP) in mitigating autogenous shrinkage of cement-based materials," in *Ninth International Conference on Creep, Shrinkage, and Durability Mechanics (CONCREEP-9)*, 2013, pp. 324–331.

[84] K. Arroudj, A. Zenati, M. N. Oudjit, A. Bali, and A. Tagnit-Hamou, "Reactivity of Fine Quartz in Presence of Silica Fume and Slag," *Engineering*, vol. 3, pp. 569–576, 2011.

[85] J. Chisholm, "Comparison of quartz standards for X-ray diffraction analysis: HSE A9950 (Sikron F600) and NIST SRM 1878," *Ann. Occup. Hyg.*, vol. 49, no. 4, pp. 351–358, 2005.

[86] S. H. Behrens and D. G. Grier, “The Charge of Glass and Silica Surfaces,” *J. Chem. Phys.*, vol. 115, pp. 6716–6721, 2001.

[87] J. Jiang, G. Oberdörster, and P. Biswas, “Characterization of size, surface charge, and agglomeration state of nanoparticle dispersions for toxicological studies,” *J. Nanoparticle Res.*, vol. 11, no. 1, pp. 77–89, 2009.

[88] M. Rubinstein and R. H. Colby, *Polymer physics*, 1st ed. Oxford University Press, 2003.

[89] V. Mechtcherine *et al.*, “Testing superabsorbent polymer (SAP) sorption properties prior to implementation in concrete: results of a RILEM Round-Robin Test,” *Mater. Struct.*, vol. 51, no. 28, pp. 1–16, 2018.

[90] D. Snoeck, C. Schröfl, and V. Mechtcherine, “Recommendation of RILEM TC 260-RSC: testing sorption by superabsorbent polymers (SAP) prior to implementation in cement-based materials,” *Mater. Struct. Constr.*, vol. 51, no. 5, pp. 1–7, Oct. 2018.

[91] C. Schröfl, D. Snoeck, and V. Mechtcherine, “A review of characterisation methods for superabsorbent polymer (SAP) samples to be used in cement-based construction materials: report of the RILEM TC 260-RSC,” *Mater. Struct.*, vol. 50, no. 197, pp. 1–19, 2017.

[92] W. Siriwatwechakul, J. Siramanont, and W. Vichit-Vadakan, “Behavior of Superabsorbent Polymers in Calcium- and Sodium-Rich Solutions,” *J. Mater. Civ. Eng.*, vol. 24, no. 8, pp. 976–980, 2012.

[93] M. Wyrzykowski, A. Assmann, C. Hesse, and P. Lura, “Microstructure development and autogenous shrinkage of mortars with C-S-H seeding and internal curing,” *Cem. Concr. Res.*, vol. 129, p. 105967, Mar. 2020.

[94] C. R. Davis, S. L. Kelly, and K. A. Erk, “Comparing laser diffraction and optical microscopy for characterizing superabsorbent polymer particle morphology, size, and swelling capacity,” *J. Appl. Polym. Sci.*, vol. 135, no. 14, pp. 1–10, Apr. 2018.

[95] M. T. Hasholt and O. M. Jensen, “Chloride migration in concrete with superabsorbent polymers,” *Cem. Concr. Compos.*, vol. 55, pp. 290–297, 2015.

[96] Y. Wehbe and A. Ghahremaninezhad, “Combined effect of shrinkage reducing admixtures (SRA) and superabsorbent polymers (SAP) on the autogenous shrinkage, hydration and properties of cementitious materials,” *Constr. Build. Mater.*, vol. 138, pp. 151–162, 2017.

[97] K. Farzanian, K. Pimenta Teixeira, I. Perdigão Rocha, L. De Sa Carneiro, and A. Ghahremaninezhad, "The mechanical strength, degree of hydration, and electrical resistivity of cement pastes modified with superabsorbent polymers," *Constr. Build. Mater.*, vol. 109, pp. 156–165, 2016.

[98] R. Spragg, C. Villani, K. Snyder, D. Bentz, J. W. Bullard, and J. Weiss, "Factors that Influence Electrical Resistivity Measurements in Cementitious Systems," *Transp. Res. Rec. J. Transp. Res. Board*, vol. 2342, no. 1, pp. 90–98, 2013.

[99] "ASTM C128 - 15 Standard Test Method for Relative Density (Specific Gravity) and Absorption of Fine Aggregate," 2015.

[100] "ASTM C1437 - 20 Standard Test Method for Flow of Hydraulic Cement Mortar," 2020.

[101] "ASTM C109 / C109M - 20b Standard Test Method for Compressive Strength of Hydraulic Cement Mortars (Using 2-in. or [50 mm] Cube Specimens)," 2020.

[102] "ASTM C348 - 20 Standard Test Method for Flexural Strength of Hydraulic-Cement Mortars," 2020.

[103] "ASTM C1698 - 09(2014) Standard Test Method for Autogenous Strain of Cement Paste and Mortar," 2014.

[104] B. Bose, C. R. Davis, and K. A. Erk, "Microstructural refinement of cement paste internally cured by polyacrylamide composite hydrogel particles containing silica fume and nanosilica," *Cem. Concr. Res.*, vol. 143, p. 106400, May 2021.

[105] T. L. Thornell, "Synthesis and Characterization of Model Acrylic-based Polymer Gels," Purdue University, 2018.

[106] M. E. S. R. Silva *et al.*, "Miscibility Behavior of Polyacrylamides Poly(Ethylene Glycol) Blends: Flory Huggins Interaction Parameter Determined by Thermal Analysis," *J. Mod. Phys.*, vol. 4, no. 7, pp. 45–51, Jul. 2013.

[107] J. Yang, S. Meng, L. Xu, and E. G. Wang, "Water adsorption on hydroxylated silica surfaces studied using the density functional theory," *Phys. Rev. B*, vol. 71, no. 3, p. 035413, 2005.

[108] E. Asenath-Smith, H. Li, E. C. Keene, Z. W. Seh, and L. A. Estroff, "Crystal growth of calcium carbonate in hydrogels as a model of biomineralization," *Adv. Funct. Mater.*, vol. 22, no. 14, pp. 2891–2914, Jul. 2012.

[109] F. Nindiyasari, L. Fernández-Díaz, E. Griesshaber, J. M. Astilleros, N. Sánchez-Pastor, and W. W. Schmahl, "Influence of gelatin hydrogel porosity on the crystallization of CaCO 3," *Cryst. Growth Des.*, vol. 14, no. 4, pp. 1531–1542, Apr. 2014.

[110] J. A. Lopez-Berganza, S. Chen, and R. M. Espinosa-Marzal, "Tailoring Calcite Growth through an Amorphous Precursor in a Hydrogel Environment," *Cryst. Growth Des.*, vol. 19, no. 6, pp. 3192–3205, Jun. 2019.

[111] M. K. Jo, Y. Oh, H. J. Kim, H. L. Kim, and S. H. Yang, "Diffusion-Controlled Crystallization of Calcium Carbonate in a Hydrogel," *Cryst. Growth Des.*, vol. 20, no. 2, pp. 560–567, Feb. 2020.

[112] S. L. Kelly, M. J. Krafcik, and K. A. Erk, "Synthesis and Characterization of Superabsorbent Polymer Hydrogels Used as Internal Curing Agents in High-Performance Concrete : Impact of Particle Shape on Mortar Compressive Strength," in *International Congress on Polymers in Concrete (ICPIC 2018): Polymers for Resilient and Sustainable Concrete Infrastructure*, M. M. R. Taha, Ed. Springer International Publishing AG, 2018, pp. 91–97.

[113] K. Farzanian and A. Ghahremaninezhad, "On the Interaction between Superabsorbent Hydrogels and Blended Mixtures with Supplementary Cementitious Materials," *Adv. Civ. Eng. Mater.*, vol. 7, no. 4, pp. 567–589, 2018.

[114] M. Berra, F. Carassiti, T. Mangialardi, A. E. Paolini, and M. Sebastiani, "Effects of nanosilica addition on workability and compressive strength of Portland cement pastes," *Constr. Build. Mater.*, vol. 35, pp. 666–675, 2012.

[115] D. Snoeck *et al.*, "The effects of superabsorbent polymers on the microstructure of cementitious materials studied by means of sorption experiments," *Cem. Concr. Res.*, vol. 77, pp. 26–35, 2015.

[116] C. Schroefl, V. Mechtcherine, P. Vontobel, J. Hovind, and E. Lehmann, "Sorption kinetics of superabsorbent polymers (SAPs) in fresh Portland cement-based pastes visualized and quantified by neutron radiography and correlated to the progress of cement hydration," *Cem. Concr. Res.*, vol. 75, pp. 1–13, Sep. 2015.

[117] J. W. Bullard *et al.*, "Mechanisms of cement hydration," *Cem. Concr. Res.*, vol. 41, no. 12, pp. 1208–1223, Dec. 2011.

[118] J. Justs, M. Wyrzykowski, F. Winnefeld, D. Bajare, and P. Lura, “Influence of superabsorbent polymers on hydration of cement pastes with low water-to-binder ratio,” *J. Therm. Anal. Calorim. 2013 1151*, vol. 115, no. 1, pp. 425–432, Aug. 2013.

[119] M. Wyrzykowski, A. Assmann, C. Hesse, and P. Lura, “Microstructure development and autogenous shrinkage of mortars with C-S-H seeding and internal curing,” *Cem. Concr. Res.*, vol. 129, p. 105967, Mar. 2020.

[120] M. H. Zhang, C. T. Tam, and M. P. Leow, “Effect of water-to-cementitious materials ratio and silica fume on the autogenous shrinkage of concrete,” *Cem. Concr. Res.*, vol. 33, no. 10, pp. 1687–1694, Oct. 2003.

[121] G. Sant, B. Lothenbach, P. Juilland, G. Le Saout, J. Weiss, and K. Scrivener, “The origin of early age expansions induced in cementitious materials containing shrinkage reducing admixtures,” *Cem. Concr. Res.*, vol. 41, no. 3, pp. 218–229, Mar. 2011.

[122] N. T. Silva, N. F. Nascimento, L. S. Cividanes, C. A. Bertran, and G. P. Thim, “Kinetics of cordierite crystallization from diphasic gels,” *J. Sol-Gel Sci. Technol.*, vol. 47, no. 2, pp. 140–147, Aug. 2008.

[123] A. Mignon *et al.*, “pH-sensitive superabsorbent polymers: a potential candidate material for self-healing concrete,” *J. Mater. Sci.*, vol. 50, no. 2, pp. 970–979, Nov. 2014.

[124] M. Said, Y. Atassi, M. Tally, and H. Khatib, “Environmentally Friendly Chitosan-g-poly(acrylic acid-co-acrylamide)/Ground Basalt Superabsorbent Composite for Agricultural Applications,” *J. Polym. Environ.*, vol. 26, no. 9, pp. 3937–3948, Sep. 2018.

[125] K. G. Uranta, S. Rezaei-Gomari, P. Russell, and F. Hamad, “Studying the Effectiveness of Polyacrylamide (PAM) application in hydrocarbon reservoirs at different operational conditions,” *Energies*, vol. 11, no. 9, 2018.

[126] M. Chi, C. Liu, J. Shen, Z. Dong, Z. Yang, and L. Wang, “Antibacterial superabsorbent polymers from tara gum grafted poly(acrylic acid) embedded silver particles,” *Polymers (Basel).*, vol. 10, no. 9, p. 945, Aug. 2018.

[127] A. M. Dumitrescu *et al.*, “Ni ferrite highly organized as humidity sensors,” *Mater. Chem. Phys.*, vol. 156, no. March, pp. 170–179, 2015.

[128] I. Anil, S. T. Gunday, O. Alagha, and A. Bozkurt, “Synthesis, Characterization, and Swelling Behaviors of Poly(acrylic acid-co-acrylamide)/Pozzolan Superabsorbent Polymers,” *J. Polym. Environ.*, vol. 27, no. 5, pp. 1086–1095, May 2019.

[129] S. Armenta, S. Garrigues, M. De La Guardia, and P. Rondeau, “Attenuated Total Reflection-Fourier transform infrared analysis of the fermentation process of pineapple,” *Anal. Chim. Acta*, vol. 545, no. 1, pp. 99–106, Jul. 2005.

[130] P. Zhong, Z. Hu, M. Griffa, M. Wyrzykowski, J. Liu, and P. Lura, “Mechanisms of internal curing water release from retentive and non-retentive superabsorbent polymers in cement paste,” *Cem. Concr. Res.*, vol. 147, p. 106494, Sep. 2021.

[131] S. L. Kelly, “Inverse Suspension Polymerization of Superabsorbent Polymer (SAP) Hydrogels for Internally Cured Concrete,” Purdue University, 2017.

[132] D. P. Bentz, S. Z. Jones, M. A. Peltz, and P. E. Stutzman, “Mitigation of autogenous shrinkage in repair mortars via internal curing,” *Concr. Aust.*, vol. 41, no. 4, pp. 35–39, 2015.

[133] L. Montanari, P. Suraneni, and W. J. Weiss, “Accounting for water stored in superabsorbent polymers in increasing the degree of hydration and reducing the shrinkage of internally cured cementitious mixtures,” *Adv. Civ. Eng. Mater.*, vol. 6, no. 1, pp. 583–599, Dec. 2017.

[134] E. Gruyaert, N. Robeyst, and N. De Belie, “Study of the hydration of Portland cement blended with blast-furnace slag by calorimetry and thermogravimetry,” *J. Therm. Anal. Calorim. 2010 1023*, vol. 102, no. 3, pp. 941–951, May 2010.

[135] H. Moon, S. Ramanathan, P. Suraneni, C.-S. Shon, C.-J. Lee, and C.-W. Chung, “Revisiting the Effect of Slag in Reducing Heat of Hydration in Concrete in Comparison to Other Supplementary Cementitious Materials,” *Materials (Basel).*, vol. 11, no. 10, Sep. 2018.